Australian Government
Department of Defence
Defence Science and
Technology Organisation

Assembly and Initial Analysis of a Database of the Characteristics of Fixed-Wing Unmanned Aircraft Systems

Jennifer L Palmer

Aerospace Division
Defence Science and Technology Organisation

DSTO-TR-2952

ABSTRACT

The *DSTO UAS Database* contains geometric, aerodynamic, and performance data for nearly nine hundred semi-autonomous and remotely piloted unmanned aircraft systems (UAS) utilising fixed-wing unmanned aerial vehicles (UAVs). The *Database* has been created using information from a variety of public sources and is intended to serve as a repository and as a source of data for analysis of the various systems. Here, the characteristics of fixed-wing UAVs are examined as functions of their mass. Where appropriate, fixed-wing UAVs are compared with manned aircraft and birds to provide the reader with an overview of the contents of the *Database* and to indicate some of its possible uses. Other demonstrated applications include historical analyses.

Produced by

Aerospace Division
DSTO Defence Science and Technology Organisation
506 Lorimer St
Fishermans Bend, Victoria 3207 Australia

Telephone: 1300 333 362
Fax: (03) 9626 7999

AR-015-904
November 2014

APPROVED FOR PUBLIC RELEASE

Assembly and Initial Analysis of a Database of the Characteristics of Fixed-Wing Unmanned Aircraft Systems

Executive Summary

Unmanned aircraft systems (UAS) are expected to fulfil the majority of future military intelligence, surveillance, and reconnaissance missions and eventually to replace most manned air-combat and strike aircraft. Thus, they have become an important topic of study for DSTO. This has motivated the creation of a database of UAS based on fixed-wing unmanned aerial vehicles (UAVs), termed the *DSTO UAS Database*. It serves as a repository of information about the various systems in development or use worldwide and as a source of data for analyses of individual systems and groups. Geometric, aerodynamic, and performance data for semi-autonomous and remotely piloted UAS are available from a wide range of public sources; however, collation of a database was found to be necessary because the existing sources do not provide the information in a form that permits detailed mathematical and historical or developmental analyses.

Nearly nine hundred UAS are included in the *Database* both for completeness and, where possible, to permit systematic analyses of UAS characteristics. In this report, the geometric and aerodynamic parameters of UAVs are examined as functions of UAV operating mass and compared with those of manned aircraft and birds, through the use of scaling laws derived under the assumptions of geometric and aerodynamic similarity. These scaling laws are shown to apply equally well to manned transport aircraft and most classes of UAVs; however, there are some significant exceptions, including the smallest UAVs (*i.e.* 'micro' air vehicles or MAVs) and those with strict power limitations (*e.g.* solar-powered UAVs). Several performance characteristics are explored, and it is shown that the data loosely correlate with power laws. Thus, estimates of the range and endurance of a UAV can be inferred from its mean mass.

The *Database* permits comparisons amongst different classes of UAS (*e.g.* medium-altitude, long-endurance *vs.* high-altitude, long-endurance). Demonstrated applications include comparisons of fixed- and flapping-wing MAVs with birds and comparisons of long-endurance UAS with ultra-efficient manned aircraft and natural flyers. The aim is to explore the extremes made possible by the absence of a human pilot, beginning with the most obvious: small size and long endurance. Similarly, one could compare and contrast manned tactical fighter aircraft with unmanned combat air vehicles (UCAVs) to examine how design has changed with the removal of the aircrew.

The *Database* has recently been converted by members of The Technical Cooperation Program (TTCP) from its original Microsoft Excel® spreadsheet format to a structured database format to make it more widely available to and searchable by potential users. Periodic maintenance, further validation of the data, and on-going additions are planned. This report describes the state of the *Database* prior to its transmittal to TTCP.

Author

Dr Jennifer L Palmer
Aerospace Division

The author joined the Defence Science & Technology Organisation in 2007. Her work focuses on autonomous aircraft, including research on hybrid-propulsion and mission-management technologies for small surveillance aircraft, 'micro' air vehicles, and flapping-wing flight. Prior to immigrating to Australia from the US in 2004, she was employed at Lockheed Martin Missiles & Space in Sunnyvale, California, where her work involved analyses of missile systems and test failures. She earned a Ph.D. in Mechanical Engineering from Stanford University in 1997, with a thesis on the demonstration of advanced laser-based diagnostic techniques for hypersonic flows.

Contents

GLOSSARY

LIST OF FIGURES

LIST OF TABLES

1 INTRODUCTION 1

2 *DATABASE* POPULATION 3

3 AGGREGATED UAS DATA 8
3.1 Geometric and Aerodynamic Characteristics 9
3.1.1 Wingspan 9
3.1.2 Length and Fuselage Dimensions 13
3.1.3 Wing Area, Chord, and Aspect Ratio 13
3.1.4 Wing Loading 19
3.2 Performance Characteristics 21
3.2.1 Best-Range and Operating Airspeeds and Reynolds Numbers 21
3.2.2 Endurance and Range 27
3.2.3 Ceiling 29
3.3 Power Requirements 29
3.3.1 Supplied Power and Power-to-Weight Ratio 29
3.3.2 Power Required at Best-Range Conditions 33
3.3.3 Flight Efficiency and Maximum Lift-to-Drag Ratio 35
3.3.4 Available Thrust and Thrust-to-Weight Ratio 38
3.4 Load Capacity and Usage 40
3.4.1 Load Capacity 40
3.4.2 Payload, Battery or Fuel, and Useful-Load Masses 43
3.4.3 Payload–Range Product 49
3.4.4 Payload Types 49
3.5 Launch and Recovery Methods 53

4 COMPARATIVE UAS ANALYSIS 57
4.1 MAVs and NAVs 57
4.2 HALE UAVs and Other Efficient Flyers 59

5 CONCLUSIONS AND RECOMMENDATIONS 62

REFERENCES 63

ACKNOWLEDGEMENTS 69

APPENDIX A DETAILED DESCRIPTION OF UAS DATA ENTRY 70

A.1 Masses and Weights 70
A.2 Geometric and Aerodynamic Characteristics 70
A.3 Performance Characteristics 70
A.4 Propulsion System and Power Requirements 72

APPENDIX B ESTIMATION OF BEST-RANGE POWER FOR PROPELLER-DRIVEN AIRCRAFT 74

APPENDIX C SCALING LAWS FOR THE CHARACTERISTICS OF MANNED AIRCRAFT AND BIRDS 76

Glossary

Acronyms

AER TP-6	TTCP Aerospace Group Technical Panel 6 (Unmanned Aerial Systems)
AUVSI	Association for Unmanned Vehicle Systems International
CBRN	chemical, biological, radiological, and nuclear
CFL	confidence level
DARPA	Defense Advanced Research Projects Agency
ELINT	electronic intelligence (payload)
EO	electro-optical (sensor)
EW	electronic warfare (payload)
ERAST	Environmental Research Aircraft and Sensor Technology
H_2	hydrogen
HALE	high-altitude, long-endurance
HC	hydrocarbon
ICE	internal combustion engine
IR	infra-red (sensor)
ISA	International Standard Atmosphere
ISR	intelligence, surveillance, and reconnaissance
ISTAR	intelligence, surveillance, target acquisition, and reconnaissance
LOS	line-of-sight
MALE	medium-altitude, long-endurance
MAV	'micro' air vehicle
MTOM	maximum take-off mass
N/A	not available
NAV	'nano' air vehicle
RMS	root-mean-squared
RPV	remotely piloted vehicle
TTCP	The Technical Cooperation Program
UAS	unmanned aerial system or systems
UAV	unmanned aerial vehicle
UCAV	unmanned combat air vehicle
VTOL	vertical take-off and landing

Symbols

AR	wing aspect ratio
b	wingspan (m)
b_{fore}	fore-plane wingspan (m)
b_{tail}	tail-unit wingspan (m)
$\bar{c}$	mean wing chord (m)
C_D	drag coefficient
$C_{D,0}$	parasitic drag coefficient
$C_{D,(R/C)_{\max}}$	drag coefficient at speed of maximum climb rate
$C_{D,V_{\max\text{-}\mathcal{R}}}$	drag coefficient at best-range airspeed
C_L	lift coefficient

$C_{L,(R/C)_{\max}}$	lift coefficient at speed of maximum climb rate
$C_{L,V_{\max\text{-}\mathcal{R}}}$	lift coefficient at best-range airspeed
d_{fuse}	maximum fuselage diameter (m)
e	Oswald's span efficiency
f_{frame}	airframe mass fraction
f_{batt}	battery mass fraction
f_{fuel}	maximum fuel-mass fraction
f_{pay}	maximum payload-mass fraction
f_{propul}	propulsion-system (*e.g.* battery, fuel-cell, and solar-cell plus motor or engine) -mass fraction
f_{useful}	maximum useful-load fraction (*i.e.* maximum payload- and fuel- or battery-mass fraction)
g	gravitational constant (= 9.81 m/s^2)
h	aircraft height (m)
H_{ceil}	ceiling (m)
$H_{\max}$	maximum operating altitude (m)
$H_{\min}$	minimum operating altitude (m)
$H_{V\max}$	maximum-speed altitude (m)
$H_{V\max\text{-}\mathcal{R}}$	altitude at best-range condition (m)
l_{fuse}	fuselage length (m)
l_{total}	total aircraft or body length (m)
$(L/D)_{\max}$	maximum lift-to-drag ratio
m	mean UAV mass (kg)
m_{batt}	battery mass (kg)
m_{empty}	empty mass (kg)
m_{frame}	airframe mass (kg)
m_{fuel}	maximum fuel mass (kg)
$m_{\text{max-T/O}}$	maximum take-off mass, MTOM (kg)
m_{pay}	maximum payload mass (kg)
m_{propul}	propulsion-system (*e.g.* battery, fuel-cell, engine, or motor) mass (kg)
m_{useful}	maximum useful load (*i.e.* maximum payload and fuel or battery mass) (kg)
$P_{\text{av,max}}$	maximum available propulsive power (W)
$P_{\max\text{-}\mathcal{R}}$	best-range or cruise power (W)
$P_{\max\text{-}\mathcal{R},\text{stat}}$	stated best-range or cruise power (W)
P_{req}	power required to overcome drag (W)
$P_{\text{req},(R/C)_{\max}}$	power required to overcome drag at the maximum-climb condition (W)
P_{supp}	maximum supplied electrical or mechanical power (W)
$(R/C)_{\max}$	maximum rate of climb (m/s)
$Re_{\max-\mathcal{R}}$	Reynolds number based on best-range airspeed, mean wing chord, and air viscosity at sea level
Re_{op}	Reynolds number based on operating speed, mean wing chord, and air viscosity at sea level (evaluated for turbojet- and turbofan-powered UAVs and targets only)
$\mathcal{R}$	range (km)
$\mathcal{R}_{\text{ferry}}$	ferry range (km)
$\mathcal{R}_{\text{radius}}$	mission radius (km)

S_{fore}	fore-plane wing area (m^2)
S_{tail}	tail-unit wing area (m^2)
S_{total}	total lifting surface area (m^2)
S_{wet}	wetted area (m^2)
S_{wing}	main wing area (m^2)
$\mathcal{T}$	endurance (h)
$T_{\text{av,max}}$	maximum available propulsive thrust (N)
$T_{\text{max-}\mathcal{R}\text{,stat}}$	stated thrust at best-range or cruise condition (N)
T_{supp}	maximum supplied thrust (N)
V_{max}	maximum speed (m/s)
$V_{\text{max-}\mathcal{R}}$	best-range or cruise airspeed (m/s)
$V_{\text{min-}P}$	loiter or minimum-power speed (m/s)
$V_{\text{never-ex}}$	speed never to be exceeded (m/s)
$V_{(R/C)_{\text{max}}}$	speed of forward flight at the maximum-climb condition (m/s)
V_{stall}	stall speed (m/s)
$V_{\text{T/O}}$	launch or take-off speed (m/s)
W	mean UAV weight (N)
W_{empty}	empty UAV weight (N)
W_{max}	maximum weight for bird species (N)
$W_{\text{max-T/O}}$	maximum take-off weight for UAV (N)
$\eta_{\text{flight,max}}$	flight efficiency at best-range conditions
η_{propul}	propulsive efficiency
ν	air viscosity (1.46×10^{-5} m^2/s at sea level)
ρ	air density (1.22 kg/m^3 at sea level)

Units

h	hours
kg	kilograms
km	kilometres
m	metres
min	minutes
N	Newtons
s	seconds

List of Figures

1 Histogram showing the numbers of fixed-wing UAVs of various types in the *Database* (broken down by propulsion system and mission) as a function of mean mass 11

2 Wingspan *vs.* mean mass for all UAVs in the *Database*. Also shown are the scaling laws for manned aircraft derived by Liu [19] and for birds derived by use of the data provided by Tennekes [21] (via Liu), Alerstam *et al.* [22], and Chatterjee *et al.* [23]. 12

3 Total aircraft length *vs.* mean mass for all UAVs in the *Database*. Also shown are the scaling laws derived by Liu [19] for manned aircraft and by Templin [28] for birds. 14

4 Maximum fuselage width *vs.* mean mass for all UAVs in the *Database*. Also shown is the scaling law for manned aircraft derived by Liu [19]. 15

5 Wing area *vs.* mean mass for all UAVs in the *Database*. Also shown are the scaling laws for manned aircraft derived by Liu [19] and for birds derived by use of the data provided by Tennekes [21] (via Liu), Alerstam *et al.* [22], and Chatterjee *et al.* [23]. 16

6 Mean wing chord *vs.* mean mass for all UAVs in the *Database*. Also shown are the scaling laws for manned aircraft derived by Liu [19] and for birds obtained from the scaling laws for wingspan and wing area derived from the data provided by Tennekes [21] (via Liu), Alerstam *et al.* [22], and Chatterjee *et al.* [23]. 17

7 Wing aspect ratio *vs.* mean mass for all UAVs in the *Database*. Also shown are the values of aspect ratio obtained from the scaling laws for wingspan and wing area derived by Liu [19] for manned aircraft and by use of the data for birds provided by Tennekes [21] (via Liu), Alerstam *et al.* [22], and Chatterjee *et al.* [23].....18

8 Mean wing loading *vs.* mean mass for all UAVs in the *Database*. Also shown are the scaling laws for manned aircraft derived by Liu [19] and for birds derived by use of the data provided by Tennekes [21] (via Liu), Alerstam *et al.* [22], and Chatterjee *et al.* [23].....20

9 Best-range or operating airspeed *vs.* mean mass for all UAVs in the *Database*. Also shown are the scaling law for manned, propeller-driven aircraft derived by Liu [19], the mean value of operating airspeed for manned turbofan-powered aircraft, and a power law for birds derived by Alerstam *et al.* [22].....22

10 Ratio of best-range or operating airspeed to maximum airspeed *vs.* mean mass for all UAVs in the *Database*; and ratio of operating to maximum airspeed for turbojet- or turbofan-powered UAVs with $m_{max} > 10^3$ kg. 23

11 Best-range or operating airspeed *vs.* mean wing loading for all UAVs in the *Database*. Also shown are the scaling laws for manned aircraft derived by Liu [19] and for birds derived by Alerstam *et al.* [22]. 25

12 Reynolds number at sea level based on best-range or operating airspeed and mean wing chord *vs.* mean mass for all UAVs in the *Database*. Also shown are the scaling law for manned aircraft derived by Liu [19] and a scaling law developed from the power law for cruising airspeed given by Alerstam *et al.* [22] and the data for wingspan and wing area provided by Tennekes [21] (via Liu), Alerstam *et al.*, and Chatterjee *et al.* [23]. 26

13 Endurance *vs.* mean mass for all UAVs in the *Database*. Also shown are power laws with exponents of ⅓ and ½, which illustrate the approximate (purely empirical) dependence of $\mathcal{T}$ on m. 28

14 Range *vs.* mean mass for all UAVs in the *Database*. Also shown are power laws with exponents of ⅔ and ⅚, which illustrate the approximate (purely empirical) dependence of $\mathcal{R}$ on m. 30

15 Ceiling *vs.* mean mass for all UAVs in the *Database*. In the case of un-powered UAVs and targets, the values represented are operational ceiling values. 31

16 Supplied propulsive power *vs.* mean mass for all UAVs in the *Database*. Also shown are the empirically based power laws for manned aircraft and birds derived by Liu [19]. 32

17 Supplied propulsive power-to-mass ratio *vs.* mean mass for all UAVs in the *Database*. Also shown are the empirical power laws for manned aircraft and birds derived by Liu [19]. 34

18 Estimated and stated values of power required at cruise (*i.e.* best-range) conditions *vs.* mean mass for all UAVs in the *Database*. Also shown are the scaling laws for manned aircraft and birds derived by Liu [19]. 36

19 Estimated maximum flight efficiency or approximate maximum lift-to-drag ratio *vs.* mean mass for all UAVs in the *Database*. Also shown are the mean maximum flight efficiency for manned aircraft derived by Liu [19] and a power law for birds derived by use of the empirically based power law for cruising airspeed obtained by Alerstam *et al.* [22] and the scaling laws for maximum weight and cruise power derived by Liu. 37

20 Maximum available thrust *vs.* mean mass for all UAVs in the *Database*. Also shown are best-fit power laws for the installed thrust of the engines on manned, turbofan-powered and propeller-driven aircraft. 39

21 Maximum available thrust-to-weight ratio *vs.* mean mass for all UAVs in the *Database*. Also shown are empirically based best-fit power laws for the maximum available thrust-to-weight ratios for manned propeller- and turbofan-driven aircraft. 41

22 Ratio of maximum take-off to mean mass *vs.* mean mass for all UAVs in the *Database*. Also shown are the average maximum take-off–to–mean mass ratios for UAVs and for manned aircraft and birds (derived by Liu [19]). 42

23 Payload-mass fraction *vs.* mean mass for all UAVs in the *Database*. The solid black line shows the mean of the data for all UAVs for which payload mass was available (638 UAVs); and the dashed black line shows an estimate of the upper limit of useful-load fraction for aircraft, including UAVs. Also highlighted are the data for HALE ISTAR UAVs with different propulsion systems. 44

24 Fuel- or battery-mass fraction *vs.* mean mass for all UAVs in the *Database*. Also shown are averages for all types of UAVs and for ISTAR UAVs powered by ICEs and turbojet or turbofan engines. The solid lines show the averages for different classes of UAVs; and the dashed line shows an estimate of the upper limit of useful-load fraction for aircraft, including UAVs. 46

25 Maximum useful-load–mass fraction (*i.e.* maximum payload plus fuel- or battery-mass fraction) *vs.* mean mass for all UAVs in the *Database*. The solid lines show the means for all types of UAVs, ICE-powered UAVs, and turbojet- or turbofan-powered UAVs; and the dashed black line shows an estimate of the upper limit of useful-load fraction for aircraft. 47

26 Payload–range product *vs.* mean mass for all UAVs in the *Database*. Also shown are power laws with exponents of $\frac{5}{3}$ and $\frac{11}{6}$, which illustrate the approximate (purely empirical) dependence of $m_{\text{pay}} \times \mathcal{R}$ on m. 50

27 Number of UAVs in the *Database* with each payload type 51

28 Payload type *vs.* mean mass for all UAVs in the *Database*. The primary method is the first or only one listed in descriptions of each UAS. If any other method was mentioned, it is denoted as the secondary, tertiary, or quaternary method, depending on its order of appearance. 52

29 (a) Number of UAVs in the *Database* with each launch or launcher type; and (b) number of UAVs in the *Database* with each recovery method 54

30 Launch method or launcher type *vs.* mean mass for all UAVs in the *Database*. The primary method is the first or only one listed in descriptions of each UAS. If any other method was mentioned, it is denoted as the secondary or tertiary method, depending on its order of appearance. 55

31 Recovery method *vs.* mean mass for all UAVs in the *Database*. The primary method is the first or only one listed in descriptions of each UAS. If any other method was mentioned, it is denoted as the secondary or tertiary method, depending on its order of appearance 56

List of Tables

1 Descriptive data entered for each listing in the *DSTO UAS Database* 4

2 Mass and weight data entered (black) or computed (blue) for each listing in the *DSTO UAS Database* 5

3 Geometric and aerodynamic data entered (black) or computed (blue) for each listing in the *DSTO UAS Database* 5

4 Performance data entered (black) or computed (blue) for each listing in the *DSTO UAS Database* 6

5 Propulsion-system and power-requirement data entered (black) or computed (blue) for each listing in the *DSTO UAS Database* 7

6 Numbers of UAVs in each mean-mass range, categorised by propulsion-system and mission type 10

7 Average maximum payload-mass fraction for UAVs with various propulsion systems. ISTAR UAVs, UCAVs, targets, and scaled targets are included in the average labelled 'all types'; whereas targets are excluded from the other averages. 'Electric' UAVs include battery-, fuel-cell–, and solar-powered ISTAR UAVs. 45

8 Average maximum fuel- or battery-mass fraction for UAVs with various propulsion systems. ISTAR UAVs, UCAVs, targets, and scaled targets are included in the average labelled 'all types'; whereas targets are excluded from the other averages. 'Electric' UAVs include battery- and fuel-cell–powered ISTAR UAVs. 45

9 Average useful-load–mass fraction for UAVs with various power sources. ISTAR UAVs, UCAVs, targets, and scaled targets are included in the average labelled 'all types'; whereas targets were excluded from the other averages. 'Electric' UAVs include battery- and fuel-cell–powered ISTAR UAVs, but not solar-powered UAVs. 45

C.1 Scaling laws and empirical best-fit power laws for manned aircraft and birds that permit estimation of the aerodynamic and geometric characteristics of a flyer given its mean mass, m. The scaling laws for aircraft were derived by Liu [19] or obtained through least-squares fitting or averaging of the data provided by Liu. The scaling laws for birds were obtained by use of data provided by Liu, Alerstam *et al.* [22], and Chatterjee *et al.* [23]. Listed in parentheses with each entry is the relative uncertainty at 90% CFL. 77

C.2 Scaling laws and empirical best-fit power laws for manned aircraft and birds that permit the characteristics of a flyer to be estimated given its maximum mass

($m_{max\text{-}T/O}$ or m_{max} (kg) for aircraft or birds, respectively). The scaling laws for aircraft were obtained by fitting the data provided by Liu [19] or (when insufficient data were available) by re-casting Liu's scaling laws from dependence on m to dependence on $m_{max\text{-}T/O}$. The scaling laws for birds were obtained by re-casting those given in Table C.1 in terms of m_{max}. Listed in parentheses with each entry is the relative uncertainty at 90% CFL. 79

This page is intentionally blank

1 Introduction

The value of unmanned aircraft systems (UAS*) for intelligence, surveillance, target acquisition, and reconnaissance (ISTAR) missions has been demonstrated through their extensive recent and publicly acknowledged use in military and civilian operations [1]. Governments around the globe anticipate that UAS will fulfil the majority of their future ISTAR requirements and that unmanned combat air vehicles (UCAVs) will eventually replace manned air-combat and strike aircraft [2, 3]. Recent estimates indicate that UAS are commercially manufactured in at least forty countries [4] and that more than seventy countries operate them [5]. For these reasons, UAS have become an important topic of study for governmental, university, and industrial research organisations. Within DSTO, this has motivated the creation of a database of the aerodynamic and performance characteristics of systems relying on fixed-wing unmanned aerial vehicles (UAVs) that can serve as a repository of information about the various UAS in development or use worldwide and as a source of data for analyses of individual systems and groups.

The *DSTO UAS Database* (herein referred to as the *Database*) may be searched to provide information about a particular system or manufacturer or to create a list of UAS capable of conducting a mission with, for example, specified minimum payload capacity and range. Analysis of the data for UAVs utilising a given power source (*e.g.* solar or fuel cells) may yield a greater understanding of their current capabilities and promise for future technological advance. The cumulative data also permits projections of the capabilities and performance of a UAS about which one has limited knowledge. Conversely, the characterisation of UAVs of a given class or with a given power source, *etc.*, may permit partial verification of proposed designs. For example, if the claimed range and endurance of a proposed UAS is significantly greater than that of existing UAS of the same size and with the same type of propulsion system, explanation may be sought from the manufacturer. The advantages of new technologies incorporated in UAS may be explored by comparison with existing systems that would otherwise be expected to have similar performance characteristics (*e.g.* range, endurance, best-range or maximum airspeed, and ceiling).

The *Database* has to-date been utilised in several studies of UAS technology, including investigations of novel power sources for UAV propulsion and autonomous energy harvesting [6-8], as well as comparisons of small UAS with manned aircraft [9] and long-endurance UAVs with other efficient flyers [10]. Historical studies conducted by use of the *Database* include examinations of the development of the Predator family of tactical UAS [11] and of BAE Systems' Taranis program [12], which highlighted the challenges associated with the development of UCAVs. Information from the *Database* has also been used in proposing a risk-based airworthiness-certification approach for UAS [13, 14].

Under The Technical Cooperation Program (TTCP), members of the Aerospace Group Technical Panel 6 (AER TP-6), Unmanned Aerial Systems, have recently converted the

* Usage here is in accordance with the RTCA UAS Guidance Material DO-304, which states that 'the plural acronym is the same as the singular, UAS.' See http://www.rtca.org/onlinecart/product.cfm?id=408.

Database from its original Microsoft Excel® spreadsheet format to a relational *Database* format (Microsoft Access®). This development has made it more widely available to and searchable by potential users and will facilitate periodic updates and user additions. The panel has already overseen significant enhancements of the payload and datalink descriptions in the new version of the *Database*, with additional data categories being included in the Access® version. The aim of this report is to describe the construction of the original *DSTO UAS Database* and to enable readers' understanding of its aggregated contents. The enhancements made by TTCP AER TP-6 are outside the scope of this report.

Section 2 briefly describes the contents of the *Database* and the sources from which the information was obtained; while the reader is referred to Appendices A and B for detailed explanations of the data categories and of the methods used to estimate quantities not directly available from the published literature. The aggregated contents of the *Database* are discussed in some detail in Section 3, where histograms of the dataset are provided, along with plots of the geometric, aerodynamic, and performance parameters as functions of the mass of the UAV. Also shown in Section 3, for comparison, are geometric and aerodynamic scaling laws and best-fit power laws relating the characteristics of manned aircraft and birds to their mean masses, the derivations of which are described in Appendix C. Readers primarily interested in analyses of specific groups of UAS based on the information contained in the *Database* are advised to refer to Section 4, where two examples of such analyses are outlined. In Section 5, several conclusions on the utility of the *UAS Database* are presented, along with recommendations on its future development and usage.

2 *Database* Population

The data were extracted from a variety of unclassified sources, such as *Jane's All the World's Aircraft: Unmanned* [15], *Aviation Week & Space Technology* [16], Shephard's UVOnline [17], and the Online Guide to Unmanned Systems from the Association for Unmanned Vehicle Systems International (AUVSI) [18]. Included were UAS designed for close-range, tactical, medium-altitude, long-endurance (MALE), and high-altitude, long-endurance (HALE) intelligence, surveillance, and reconnaissance (ISR) missions; scaled targets used for training in aircraft identification; high-speed targets used for gunnery training; and unique designs, such as UAVs capable of vertical take-off and landing (VTOL) that transition to fixed-wing flight (*e.g.* stop- and tilt-rotor vehicles). The UAVs range in size from 'micro' air vehicles (MAVs), usually defined as having a maximum dimension of 150 mm or less, to ones with wingspans of up to 80 m and characteristics similar to those of large manned aircraft. Indeed, several of the vehicles proposed for HALE ISR missions may be produced in unmanned and manned or in optionally piloted versions.

The categories of data sought for each entry in the *Database* are listed in Tables 1–5. When conflicting information about a UAS was found, preference was given to data supplied by manufacturers directly (*e.g.* on their websites or in brochures) or, in its absence, by *Jane's All the World's Aircraft: Unmanned* [15], as the data it provides is from manufacturers and thus deemed accurate and current. All sources are listed as numbered references in the *Database*; and the date of the *Jane's* reference is provided (if appropriate).

Often, the available information about a particular UAS is incomplete; however, a description was entered into the *Database* if (at a minimum) the maximum take-off mass (MTOM) of the UAV and its wingspan were obtainable. All other information was considered non-essential and entered if found in published documents or computed if the values required to do so were available. Extensive information on nearly nine hundred UAS is contained in the *Database*, with about 100 more for which inadequate data were obtainable on a 'watch-list' to be re-considered if more information is obtained in the future. Detailed descriptions of the data categories and methods used to estimate quantities for which values were not directly available are provided in Appendix A.

Table 1 Descriptive data entered for each listing in the DSTO UAS Database

Name(s)		
Reference(s) and Jane's reference date		
Country(ies) of origin		
Manufacturer(s)		
Period of development and manufacture		
Estimated date of design fix		
Military or civilian customer(s)		
Region and time of deployment		
Mission description and category		
1 = ISTAR	2 = UCAV	3 = target
4 = scaled target	5 = lethal	
Payload description and type		
–1 = unspecified	0 = none	1 = EO*
2 = IR†	3 = radar	4 = environmental
5 = CBRN‡ detection	6 = acoustic	7 = ELINT§
8 = geophysical	9 = communication relay	10 = targeting system
11 = EW**	12 = munitions	13 = smoke, chaff, *etc.*
14 = cargo		
Launch system description and category		
0 = by hand	1 = bungee	2 = pneumatic
3 = ballistic	4 = air drop	5 = vehicle roof
6 = rocket boost	7 = vertical take-off	8 = hydraulic
9 = from ground	10 = wheeled trolley	11 = runway, wheeled
12 = submarine		
Landing/recovery system description and category		
0 = non-recoverable	1 = skid	2 = parachute/parafoil
3 = deep stall	4 = vertical	5 = water landing
6 = net or hook	7 = wheeled	8 = wheeled with hook
9 = air capture		
Navigational and control systems		
Datalink		
Materials		
Transportation and storage		
Ground crew		
Cost		
System composition		
Operational limits		
Name of person entering data		

* Electro-optical
† Infrared
‡ Chemical, biological, radiological, and nuclear
§ Electronic intelligence
** Electronic warfare

Table 2 *Mass and weight data entered (black) or computed (blue) for each listing in the* DSTO UAS Database

Mass-input method 0 = maximum take-off and empty masses known 1 = maximum take-off mass known, empty mass estimated 2 = empty mass known, maximum take-off mass estimated 3 = maximum take-off and empty masses estimated
Maximum take-off mass, $m_{\text{max-T/O}}$ (kg)
Empty mass, m_{empty} (kg)
Mean aircraft mass, $m = (m_{\text{empty}} + m_{\text{max-T/O}})/2$ (kg)
Maximum take-off weight, $W_{\text{max-T/O}} = g\, m_{\text{max-T/O}}$ (N)
Empty aircraft weight, $W_{\text{empty}} = g\, m_{\text{empty}}$ (N)
Mean aircraft weight, $W = g\, m$ (N)
Maximum payload mass, m_{pay} (kg)
Maximum payload-mass fraction, $f_{\text{pay}} = m_{\text{pay}}/m_{\text{max-T/O}}$
Maximum fuel mass, m_{fuel} (kg)
Maximum fuel-mass fraction, $f_{\text{fuel}} = m_{\text{fuel}}/m_{\text{max-T/O}}$
Battery mass, m_{batt} (kg)
Battery-mass fraction, $f_{\text{batt}} = m_{\text{batt}}/m_{\text{max-T/O}}$
Maximum useful mass, m_{useful} (kg)
Maximum useful-mass fraction, $f_{\text{useful}} = m_{\text{useful}}/m_{\text{max-T/O}}$
Airframe mass, m_{frame} (kg)
Airframe-mass fraction, $f_{\text{frame}} = m_{\text{frame}}/m_{\text{max-T/O}}$

Table 3 *Geometric and aerodynamic data entered (black) or computed (blue) for each listing in the* DSTO UAS Database

Total aircraft length, l_{total} (m)
Total aircraft height, h (m)
Fuselage length, l_{fuse} (m)
Maximum fuselage width, d_{fuse} (m)
Wingspan, b (m)
Wing area, S_{wing} (m^2)
Aerofoil type
Mean wing chord, $\bar{c} = S_{\text{wing}}/b$ (m)
Wing aspect ratio, $AR = b^2/S_{\text{wing}}$ or $b/\bar{c}$
Mean wing loading, W/S_{wing} (N/m^2)
Fore-plane span, b_{fore} (m)
Fore-plane area, S_{fore} (m^2)
Tail-unit span, b_{tail} (m)
Tail-unit area, S_{tail} (m^2)

Table 4 *Performance data entered (black) or computed (blue) for each listing in the* DSTO UAS Database

Stall airspeed, V_{stall} (m/s)
Loiter or minimum-power airspeed, $V_{min\text{-}P}$ (m/s)
Best-range (or operating) airspeed input method
0 = direct input
1 = based on Mach number at $H_{V\,max\text{-}\mathcal{R}}$
2 = estimated to be 1.32 $V_{min\text{-}P}$
Best-range or cruise airspeed, $V_{max\text{-}\mathcal{R}}$ (m/s)
Altitude at best-range condition, $H_{V\,max\text{-}\mathcal{R}}$ (m)
Operating airspeed, V_{op} (m/s)
Operating-airspeed altitude, $H_{V_{op}}$ (m)
Reynolds number at best-range airspeed, $Re_{max\text{-}\mathcal{R}} = V_{max\text{-}\mathcal{R}}\,\bar{c} / \nu$
Reynolds number at operating speed, $Re_{op} = V_{op}\,\bar{c} / \nu$
Maximum-airspeed input method
0 = direct input
1 = based on Mach number at $H_{V_{max}}$
Maximum airspeed, V_{max} (m/s)
Maximum-airspeed altitude, $H_{V_{max}}$ (m)
Never-exceed airspeed, $V_{never\text{-}ex}$ (m/s)
Launch or take-off airspeed, $V_{T/O}$ (m/s)
Maximum climb rate, $(R/C)_{max}$ (m/s)
Minimum operating altitude, H_{min} (m)
Maximum operating altitude, H_{max} (m)
Ceiling, H_{ceil} (m)
Ferry range, $\mathcal{R}_{ferry}$ (km)
Mission radius, $\mathcal{R}_{radius}$ (km)
Range, $\mathcal{R} = \mathcal{R}_{ferry}$ or 2 $\mathcal{R}_{radius}$ (km)
Mission limiter
1 = datalink
2 = fuel/battery capacity
Endurance, $\mathcal{T}$ (h)

Table 5 *Propulsion-system and power-requirement data entered (black) or computed (blue) for each listing in the* DSTO UAS Database

Power-plant description and propulsive category
0 = un-powered or ballistic
1 = electrical motor(s) with propeller(s)
2 = HC*- or H_2†-fuelled ICE(s)‡ with propeller(s)
3 = turboprop engine(s) with propeller(s)
4 = turbojet or turbofan engine(s)
5 = rocket motor
Electrical power source(s)
1 = battery
2 = fuel cell or fuel-cell/battery hybrid
3 = solar
4 = solar-augmented battery or H_2 fuel-cell
5 = battery augmented by harvesting from powerlines
Propulsion-system mass, m_{propul} (kg)
Propulsion-system–mass fraction, $f_{propul} = m_{propul}/m_{max\text{-}T/O}$
Supplied thrust, T_{supp} (N)
Supplied power, P_{supp} (W)
= stated value for propeller-driven aircraft
= $T_{supp}\ V_{max}$ or $T_{supp}\ V_{op}$ for turbojet-, turbofan-, or rocket-propelled aircraft
Supplied power-to-mass ratio, P_{supp}/m (W/kg)
Propulsive efficiency, η_{propul}, and input method
1 = stated
2 = assumed
Maximum available propulsive power, $P_{av,max}$ (W)
= $\eta_{propul}\ P_{supp}$ or $T_{supp}\ V_{max}$ for prop-driven aircraft
= P_{supp} for turbojet-, turbofan-, or rocket-propelled aircraft
Maximum available thrust, $T_{av,max} = P_{av,max}/V_{max}$ (N)
Maximum thrust-to-weight ratio, $T_{av,max}/W$
Stated power at best-range or cruise condition, $P_{max\text{-}\mathcal{R},stat}$ (W)
Stated thrust at best-range conditions, $T_{max\text{-}\mathcal{R},stat}$ (N) or $P_{max\text{-}\mathcal{R},stat}/V_{max\text{-}\mathcal{R}}$
Power required at best-range conditions, $P_{max\text{-}\mathcal{R}}$ (W)
= $3^{3/4}\ [P_{av,max} - W\ (R/C)_{max}]/2$ for propeller-driven aircraft
= $T_{supp}\ V_{max\text{-}\mathcal{R}}$ for turbojet- or turbofan-driven aircraft
Maximum flight efficiency, $\eta_{flight,max} = W_{max\text{-}T/O}\ V_{max\text{-}\mathcal{R}}/P_{max\text{-}\mathcal{R}}$
Maximum lift-to-drag ratio, $(L/D)_{max}$

* Hydrocarbon
† Hydrogen
‡ Internal-combustion engine(s)

3 Aggregated UAS Data

As described in this section, many of the parameters listed in Tables 1–5 have been plotted to indicate the scope of the *Database* and the characteristics of various types of UAS. The mean of the empty mass and MTOM of each UAV, m, as defined in Table 2, has been chosen as the representative quantity against which the characteristics of the UAS are plotted. Although the MTOM of a UAV is frequently more reliably known than its empty mass (and thus more reliably known than its mean mass), for the purposes of comparing UAS across the full size/weight range and of comparing them with birds and manned aircraft (the goal of other work [9, 10]), the mean mass is often more useful than MTOM.

Varying numbers of points appear on each plot, as a different (usually incomplete) combination of data is available for each UAS in the *Database*. The characteristics and performance of individual classes of UAS (*e.g.* close-range surveillance systems utilising MAVs or long-endurance ISTAR UAS, as described in Sections 4.1 and 4.2, respectively) may be examined in greater detail; however, the selection of plots presented in this section illustrates the contents of the *Database*, indicates some of the trends observable in the dataset, and suggests the sorts of analyses that may be performed using it.

Scaling laws for the characteristics of birds and manned aircraft as functions of mean mass are also plotted. The scaling laws for manned aircraft and a relation giving MTOM as a function of mean mass were derived by Liu [19] by use of data for general aviation and transport aircraft with piston, turboprop, and turbofan engines from *Jane's All the World's Aircraft* [20]. Liu derived a similar set of scaling laws for the characteristics of birds with data chiefly from Tennekes [21]. Other researchers [22, 23] have provided biometric data for birds that was used to refine Liu's results for presentation here. The basis of the scaling laws is the assumption of geometric (allometric) and aerodynamic similarity: length scaling as $m^{1/3}$, best-range airspeed as $m^{1/6}$, *etc.* [19]. For the reader's convenience, a summary of the scaling laws and empirically based power laws is provided in Appendix C.

The scaling laws are included on the plots of UAS characteristics provided in this section primarily to guide the reader's eye to the expected dependence of each quantity on mean mass (under the assumption of geometric and aerodynamic similarity) and to highlight departures from similarity. Mean relative errors for regression of the data for manned aircraft and birds as a function of mass were reported by Liu [19]; and the values were confirmed in the current work by use of raw data provided by Liu. The relative root-mean-squared (RMS) error, equivalent to the RMS error of the scaling-law coefficient, was also determined for each scaling law derived for manned aircraft, birds, or UAVs; and based on the size of the sample being considered, the relative uncertainty of each scaling-law coefficient at the 90% confidence level (CFL) [24] was computed. This value indicates a 90% probability that the scaling-law coefficient derived from another identically sized random sample of the same underlying population would lie within the confidence interval associated with the computed scaling-law coefficient [24]. The 90% CFLs associated with each scaling law are provided (in parentheses) on the plots that follow.

Table 6 and Figure 1 show the number of UAVs in each decade of mean aircraft mass represented in the *Database*.* As indicated in the first row of Table 6, the majority of UAVs (~65%) have a mean mass of less than 100 kg, which is under the lower limit for manned aircraft, dictated by the weight of a human pilot. Values of mean mass for fewer than 20% of the UAVs fall outside the range of 1–10^3 kg; and the heaviest (*e.g.* Global Hawk with $m = 8 \times 10^3$ kg and the RQ-37A, a proposed unmanned version of the C-37, at 3×10^4 kg) weigh at least an order of magnitude less than large transport aircraft (*e.g.* the Boeing Boeing 747-400 and the Antonov An-124, both at slightly less than 3×10^5 kg [19], and the Airbus A380-800 at 4×10^5 kg [19]).

The UAS data displayed in Table 6 and Figure 1 are categorised according to the type of propulsion system used and the mission to indicate the applicability of the various methods of propulsion. The numbers of propeller-driven ISTAR UAVs with HC- or H_2-fuelled ICEs, with turboprop engines, with (in a single case) a hydrazine (rocket-motor)-powered engine, and with electric motors powered by batteries, solar cells, and H_2 fuel cells are displayed, as are the numbers of turbojet- and turbofan-powered ISTAR UAVs and UCAVs and un-powered ISTAR UAVs (*i.e.* gliders). Also shown are data for: propeller-driven, ICE-powered high-speed and scaled targets; targets powered by rocket motors; turbojet- and turbofan-powered targets; and ballistic (un-powered) targets.

The usage (and current limitations) of electric propulsion systems powered by batteries, solar cells, and H_2 fuel cells is illustrated by the data displayed in Table 6 and Figure 1. Batteries are rarely used to power UAVs with masses of more than 10 kg; and no UAV weighing more than 100 kg uses battery power alone; however, there are at present several projects worldwide on the use of hybridised battery and fuel-cell power systems for manned aviation and long-endurance ISTAR UAVs [6, 8, 25, 26]. The latter often aim to use energy-storage devices in combination with solar collection [27].

A wide mass range ($0.1 \text{ kg} < m < 10^5$ kg) is accommodated by propulsion systems with propellers and ICEs or turboprop engines; although only 6% of the ISTAR UAVs powered by ICEs have masses less than 10 kg, because of the inherent inefficiencies of combustion at small scales. About a third of the turboprop-powered ISTAR UAVs have masses less than 10^3 kg. Turbojets and turbofans are used for targets, ISTAR UAVs, and UCAVs (or subscale UCAV demonstrators) with masses of at least 10 kg.

3.1 Geometric and Aerodynamic Characteristics

3.1.1 Wingspan

Figure 2 shows the data for wingspan as a function of mean mass for the nearly nine hundred individual UAVs associated with the UAS represented in the *Database*. Immediately

* The colour coding used in Table 6 and Figure 1 is used throughout the following plots and tables to identify UAS by propulsive method, *i.e.* red points and text always represent turbojet- and turbofan-powered aircraft, orange represents solar-powered aircraft, *etc.*

Table 6 Numbers of UAVs in each mean-mass range in the Database*, categorised by propulsion-system and mission type*

vehicle type		range of UAV mean mass, m (kg)								
		10^{-3} – 10^{-2}	10^{-2} – 10^{-1}	10^{-1} – 10^{0}	10^{0} – 10^{1}	10^{1} – 10^{2}	10^{2} – 10^{3}	10^{3} – 10^{4}	10^{4} – 10^{5}	All
All		2	9	50	217	291	214	78	14	875
propeller-driven	battery-powered UAVs	–	7	37	136	14	–	–	–	194
	H_2-fuel-cell–powered UAVs	–	1	1	10	5	4	–	–	21
	solar-powered UAVs	–	1	8	11	8	8	1	–	37
	ICE-powered UAVs	–	–	3	21	147	139	25	1	336
	ICE-powered targets	–	–	–	19	49	6	–	–	74
	ICE-powered scaled targets	–	–	–	16	23	–	–	–	39
	turboprop ISTAR UAVs and UCAVs	–	–	–	–	–	5	10	–	15
	turboprop-powered target	–	–	–	–	1	–	–	–	1
	hydrazine (rocket-motor)-powered UAV	–	–	–	–	1	–	–	–	1
turbojet- or turbofan- and rocket-driven	turbojet- and turbofan-powered ISTAR UAVs	–	–	–	1	12	15	21	8	57
	turbojet- and turbofan-powered UCAVs	–	–	–	–	9	3	11	3	26
	turbojet- and turbofan-powered targets	–	–	–	–	22	25	7	2	56
	rocket-powered UAVs	–	–	–	–	–	4	–	–	4
un-driven	un-powered UAVs	2	–	1	3	–	2	–	–	8
	ballistic targets	–	–	–	–	–	3	–	–	3

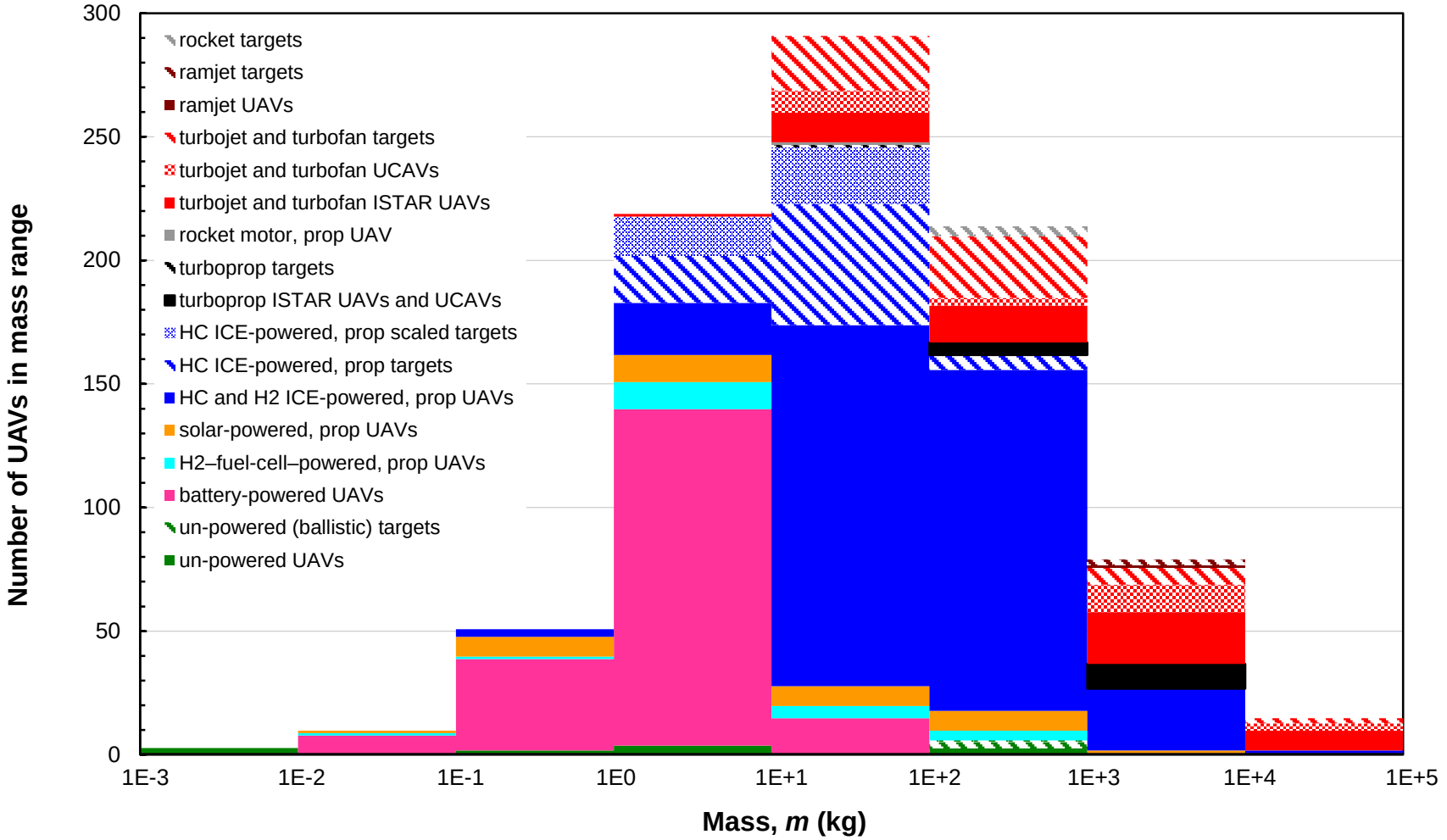

Figure 1 Histogram showing the numbers of fixed-wing UAVs of various types in the Database *(broken down by propulsion system and mission) as a function of mean mass*

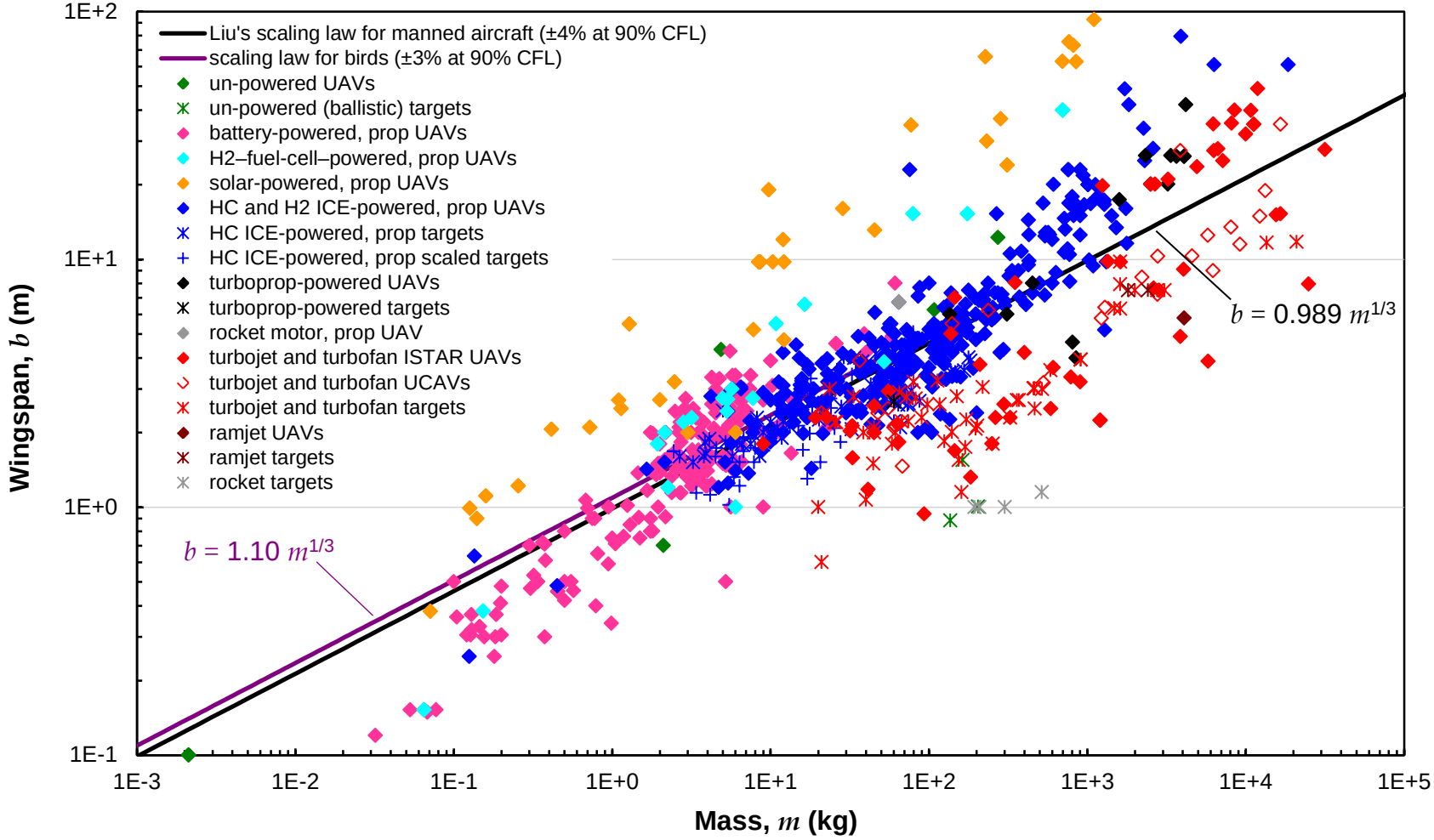

Figure 2 *Wingspan* vs. *mean mass for all UAVs in the* Database. *Also shown are the scaling laws for manned aircraft derived by Liu [19] and for birds derived by use of the data provided by Tennekes [21] (via Liu), Alerstam* et al. *[22], and Chatterjee* et al. *[23].*

noticeable are the systematic departures of some classes of UAVs from the mean value of wingspan at a given mass, which is approximately described by the scaling law for manned aircraft. For example, the wingspans of battery-powered UAVs are seen to decrease with decreasing mass significantly faster than expected for geometrically similar aircraft, a finding attributable to the fact that their designers usually aim for compact size and as large a chord-based Reynolds number as possible [9]. In contrast, the wingspans of turbojet- and turbofan-powered UAVs generally follow the expected relationship (*i.e.* scaling with $m^{1/3}$), but are on average roughly half the size expected from the scaling law, with the exception of the HALE ISTAR UAVs (grouped above the scaling law at $10^3 \text{ kg} < m < 3 \times 10^4 \text{ kg}$), for which long-span, high–aspect-ratio wings are the norm [10]. Another exceptional group apparent in Figure 2 is solar-powered UAVs, which are discussed further in this section, in Section 4.2, and in [10].

3.1.2 Length and Fuselage Dimensions

Along with wingspan, other significant geometric parameters for an aircraft include its total length and the length and maximum width of its fuselage. For UAVs with conventional planforms, the fuselage length is usually identical to the total aircraft length; whereas many novel UAV designs (*e.g.* tailless flying-wing UCAVs and other blended-body designs that comprise ~6% of the *Database*) do not include a separately identifiable fuselage. Figure 3 shows the total aircraft length as a function of mean aircraft mass. This parameter is available for ~72% of the UAVs with distinct fuselages. Also shown in Figure 3 are scaling laws for manned aircraft [19] and birds [28].

In the majority of cases, UAVs are seen to be somewhat shorter than equivalently scaled manned aircraft, but not as short as the 'mean' bird of the same mass. For example, the total lengths of ICE-powered UAVs, which correspond closely to their fuselage lengths, are better described by a newly derived scaling law, $0.71\, m^{1/3}$, than by the scaling law for manned aircraft [11] provided in Appendix C ($0.88\, m^{1/3}$), which implies that UAVs are roughly 80% as long as manned aircraft scaled to the same mass. Frequent exceptions to this are seen at the smallest scales, where MAVs appear on the plot. Most MAVs have non-traditional planforms, often being flying wings or disk-shaped, and are relatively shorter than their larger, heavier counterparts. Indeed, Figure 3 illustrates that their values of total length are better represented by the scaling law for birds ($0.31\, m^{1/3}$, Appendix C).

Values for fuselage width were available for only ~30% of the UAVs in the *Database* that are known to have fuselages; and the available data are displayed in Figure 4 as a function of mean mass. The sparsity of data for UAVs with $m < 1$ kg results from the fact that up to 75% of the UAVs for which basic geometries are known have no fuselages. At the other end of the mass range, for UAVs with $m > 10^3$ kg, 11% of the entries in the *Database* for which the basic layouts of the UAVs are known have no separate fuselages.

3.1.3 Wing Area, Chord, and Aspect Ratio

The data for wing area contained in the *Database* are displayed in Figure 5; while Figures 6 and 7 show the values of mean wing chord and aspect ratio, respectively, computed from

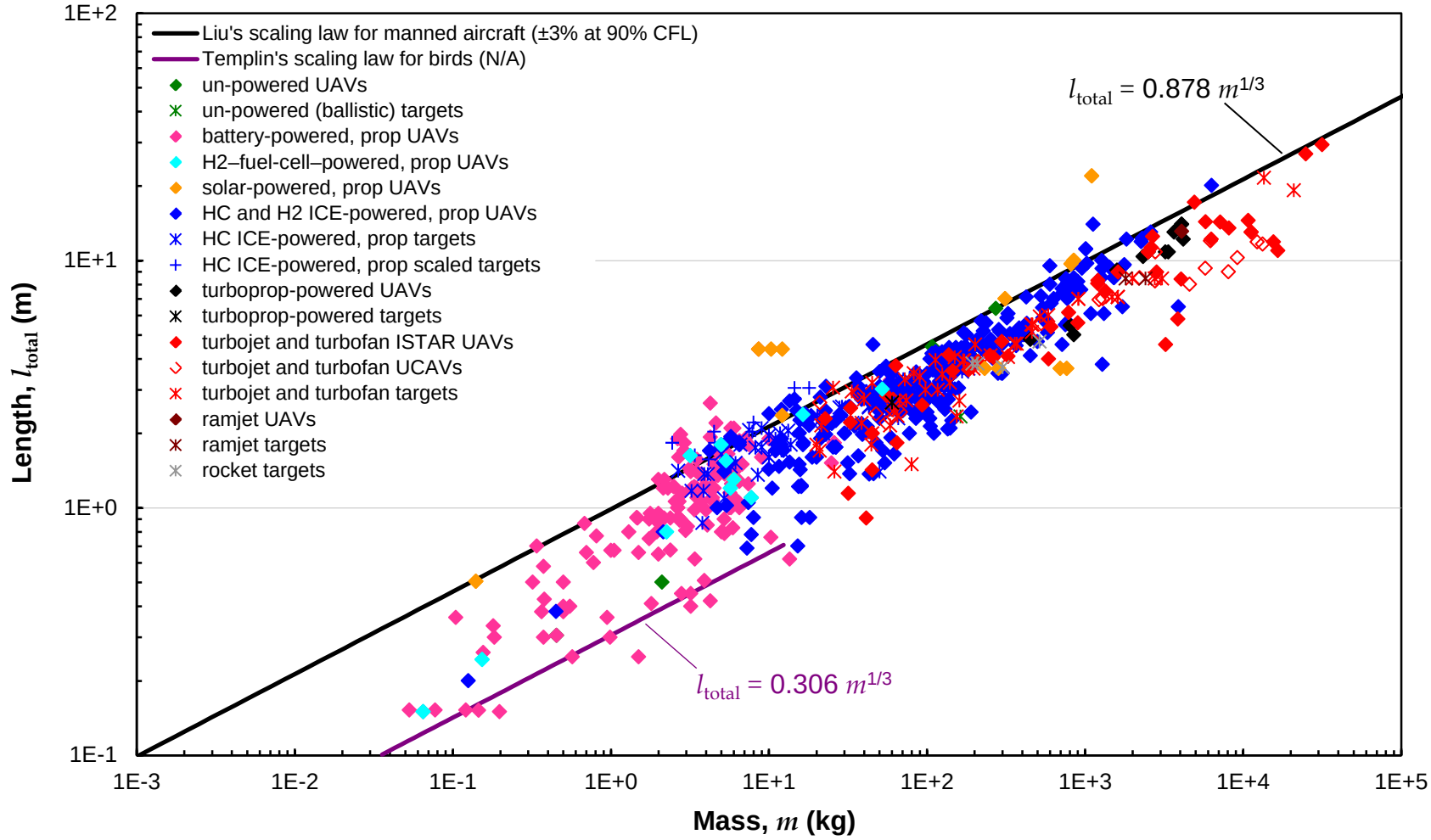

Figure 3 Total aircraft length vs. *mean mass for all UAVs in the* Database. *Also shown are the scaling laws derived by Liu [19] for manned aircraft and by Templin [28] for birds.*

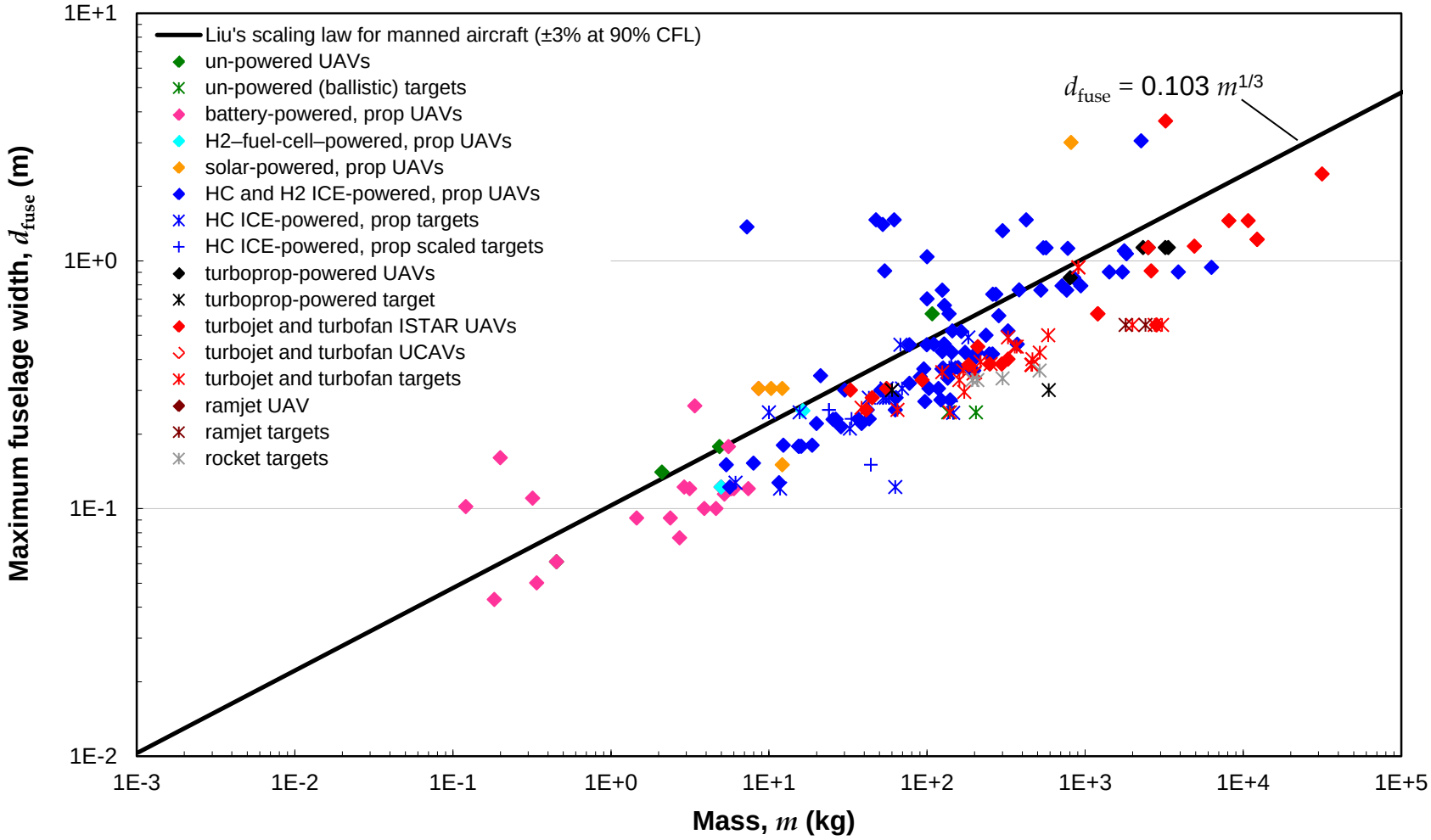

Figure 4 *Maximum fuselage width* vs. *mean mass for all UAVs in the* Database. *Also shown is the scaling law for manned aircraft derived by Liu [19].*

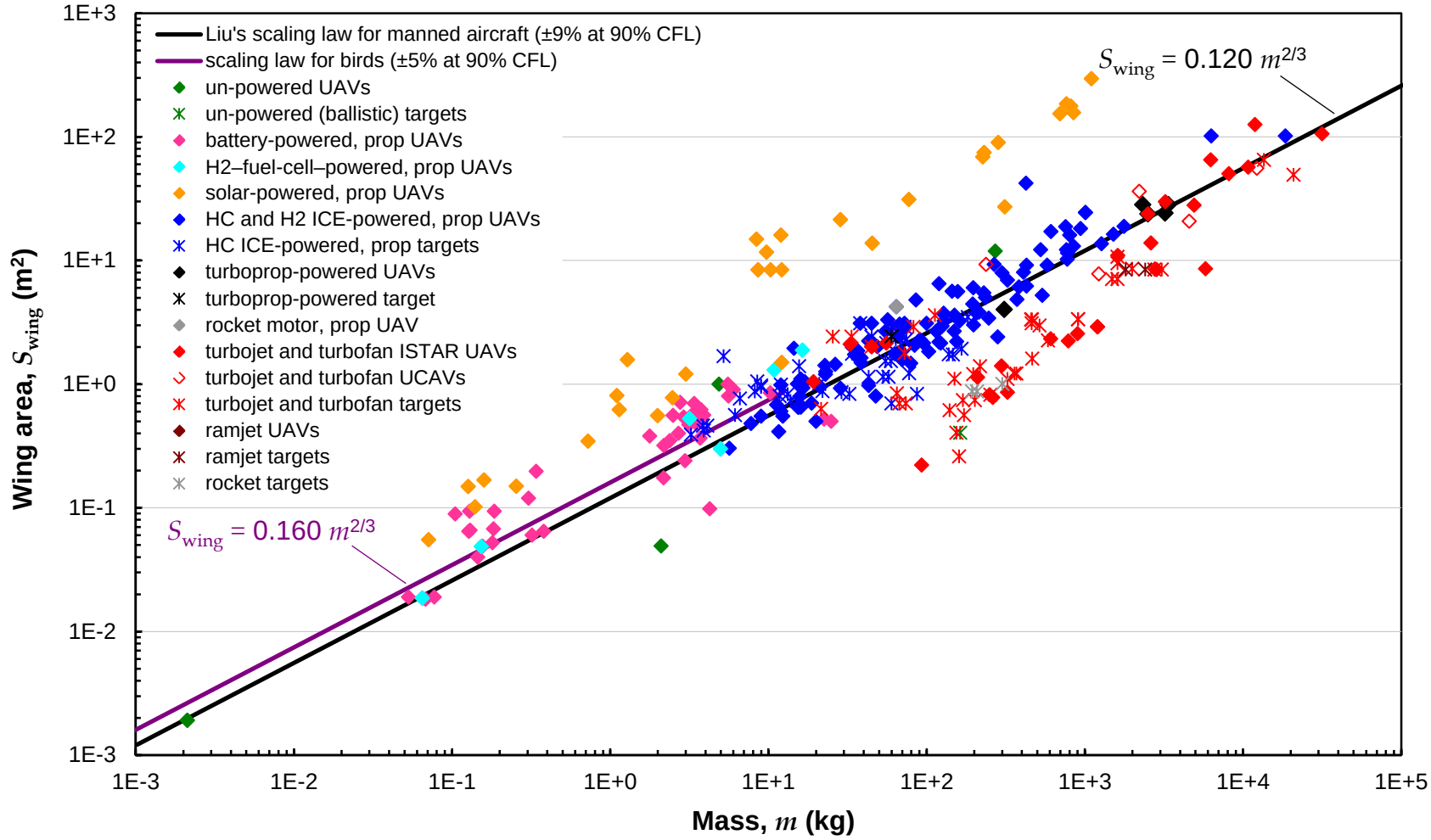

Figure 5 *Wing area* vs. *mean mass for all UAVs in the* Database. *Also shown are the scaling laws for manned aircraft derived by Liu [19] and for birds derived by use of the data provided by Tennekes [21] (via Liu), Alerstam* et al. *[22], and Chatterjee* et al. *[23].*

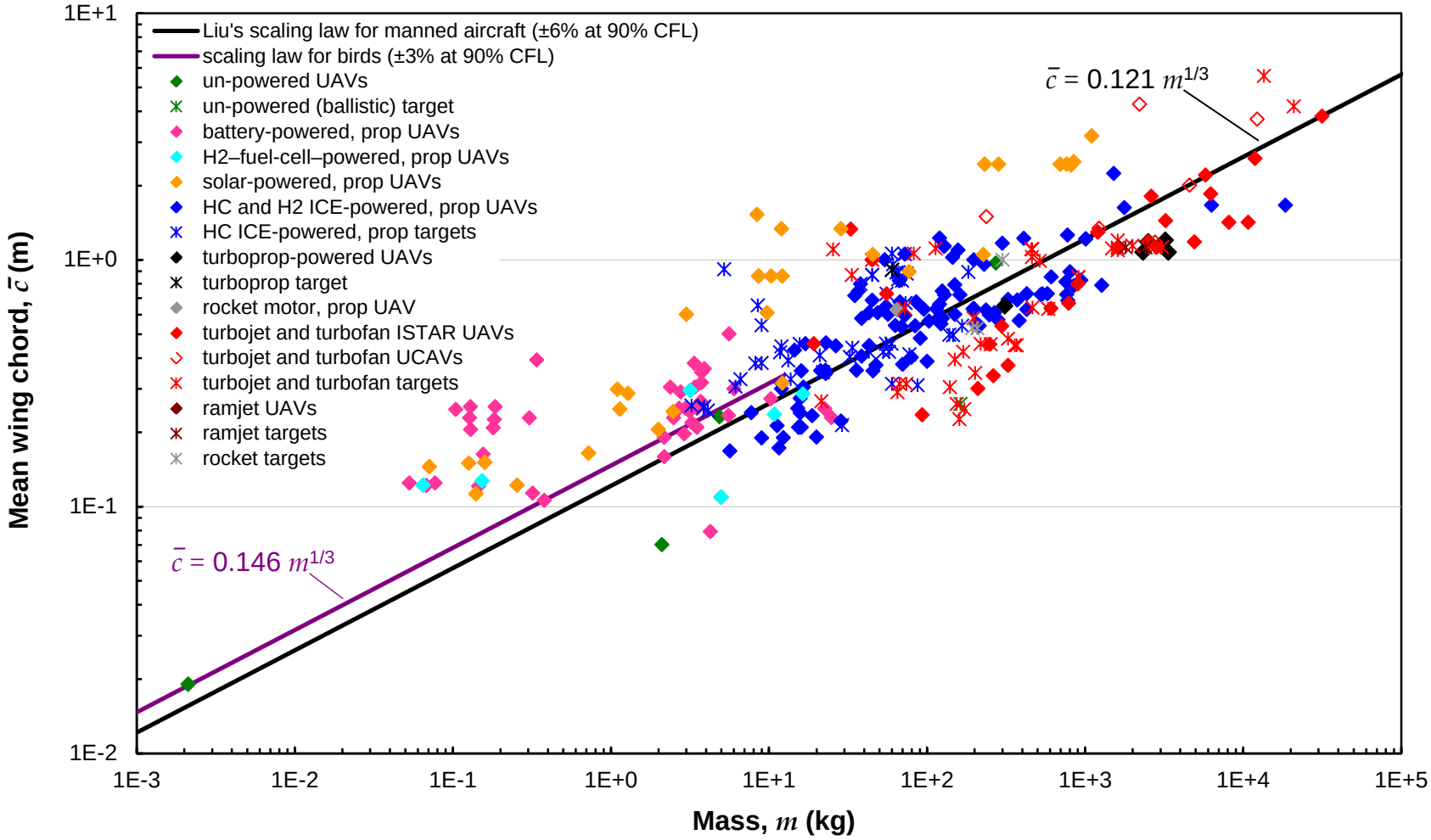

Figure 6 *Mean wing chord* vs. *mean mass for all UAVs in the* Database. *Also shown are the scaling laws for manned aircraft derived by Liu [19] and for birds obtained from the scaling laws for wingspan and wing area derived from the data provided by Tennekes [21] (via Liu), Alerstam* et al. *[22], and Chatterjee* et al. *[23].*

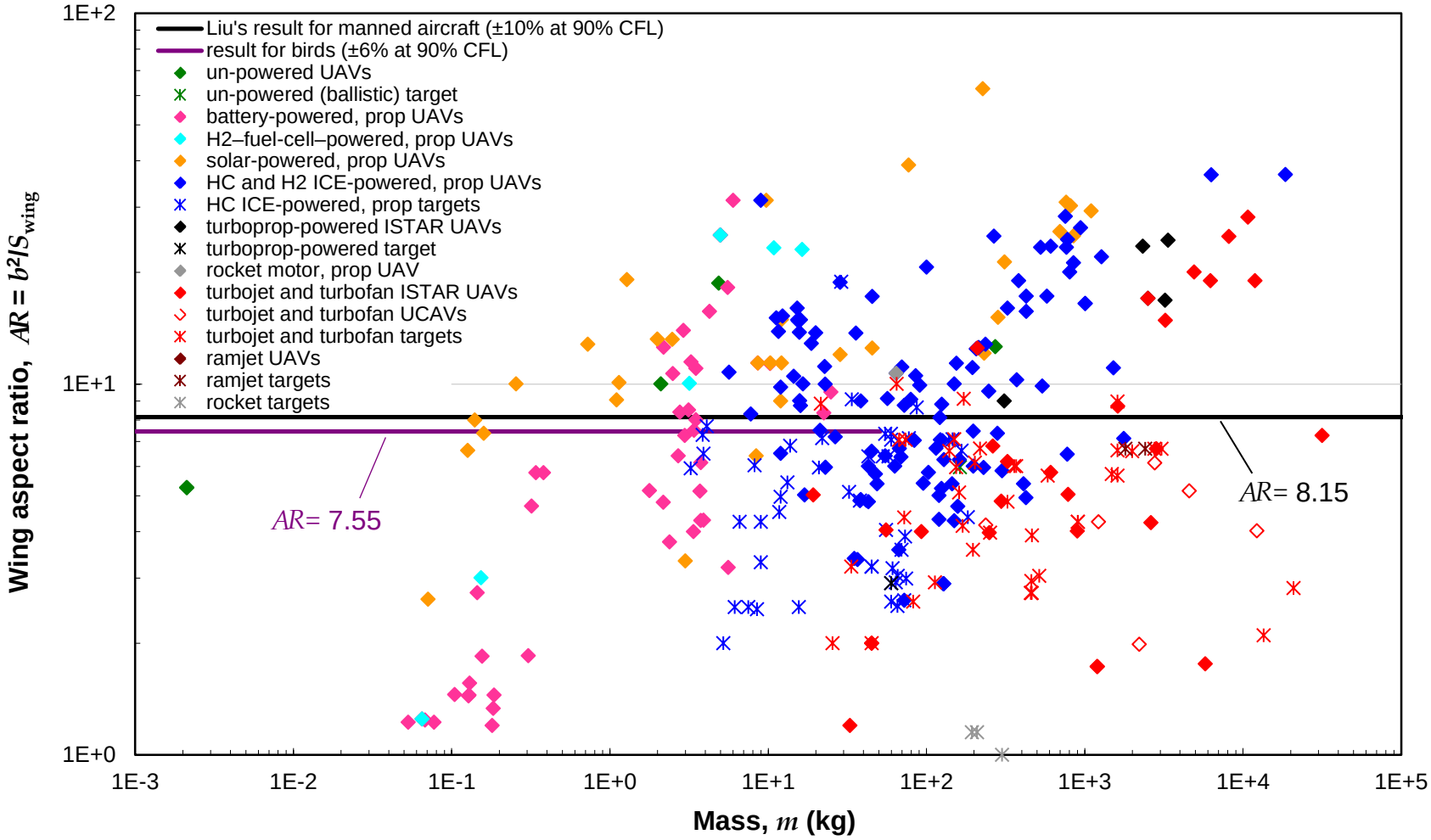

Figure 7 *Wing aspect ratio* vs. *mean mass for all UAVs in the* Database. *Also shown are the values of aspect ratio obtained from the scaling laws for wingspan and wing area derived by Liu [19] for manned aircraft and by use of the data for birds provided by Tennekes [21] (via Liu), Alerstam* et al. *[22], and Chatterjee* et al. *[23].*

the wingspan and wing area for each UAV (using the definitions given in Table 3). As is the case for the data for wingspan plotted in Figure 2, the wing areas of solar- and turbojet- or turbofan-powered UAVs are seen to differ in significant ways from the mean, as approximately represented by the scaling laws for manned aircraft. For example, solar-powered UAVs are found to have much larger values of wing area than manned aircraft scaled to the same masses would, while many turbojet- or turbofan-powered UAVs have smaller values.

In Figure 5, the point representing the RQ-37A, with a mean mass of 3×10^4 kg, falls almost directly on the scaling law representing wing area for manned propeller- and turbofan-driven aircraft, as is also the case for its values of wingspan and total length and their associated scaling laws, as shown in Figures 2 and 3; although its fuselage width is relatively smaller than that predicted by the scaling law for manned aircraft (Fig. 4). These observations highlight the fact that the RQ-37A is an unmanned variant of a transport aircraft. In contrast, UAVs designed for HALE roles have wings with areas similar to those of manned aircraft of the same mass, but significantly larger wingspans and, consequently, much larger values of aspect ratio.

Battery-powered UAVs are seen to have average or slightly above-average values of wing area, which, given the data for wingspan, lead to higher than average values of mean chord length and lower than average values of aspect ratio for their wings. This finding, particularly true for MAVs, has been noted by other researchers and is explained by MAV designers' desire to maximise wing efficiency in order to maximise the flight efficiency of the aircraft (*i.e.* to maximise the lift-to-drag ratio) [29]. For very small air vehicles, such as the Black Widow MAV [30], the mean chord length of the wing is made as large as possible within the imposed size constraint. This has the effect of minimising aspect ratio and maximising the chord-based Reynolds number associated with cruising, fixed-wing flight, as defined in Table 4. It also creates the largest possible value of wing area, thus reducing the wing loading (the ratio of aircraft weight to wing area) and the best-range airspeed (discussed in Section 3.2.1).

3.1.4 Wing Loading

Plotted in Figure 8 is the mean wing loading (W/S_{wing}) for each UAV for which wing area is available in the *Database*, along with scaling laws for the wing loadings of birds and manned aircraft. These data again emphasise the differences amongst classes of UAVs. Low-powered UAVs (*e.g.* battery- and solar-powered UAVs) have significantly (often as much as a factor of 30 times) lower wing loadings than the 'mean' UAV at a given mass, as approximately represented by the scaling law for manned aircraft. These differences are discussed further in §4.2. In contrast, the mean wing loading for ICE-powered UAVs is reasonably well predicted by the scaling law. For a large proportion of turbojet- and turbofan-powered UAVs, the wing loading is well above the mean value at a given mass and is nearly independent of mass, a finding also observable from the data in Figure 5, where wing area is seen to decrease significantly more rapidly with decreasing mass than anticipated from scaling arguments (*i.e.* wing area is approximately proportional to mean mass, therefore, wing loading is approximately constant).

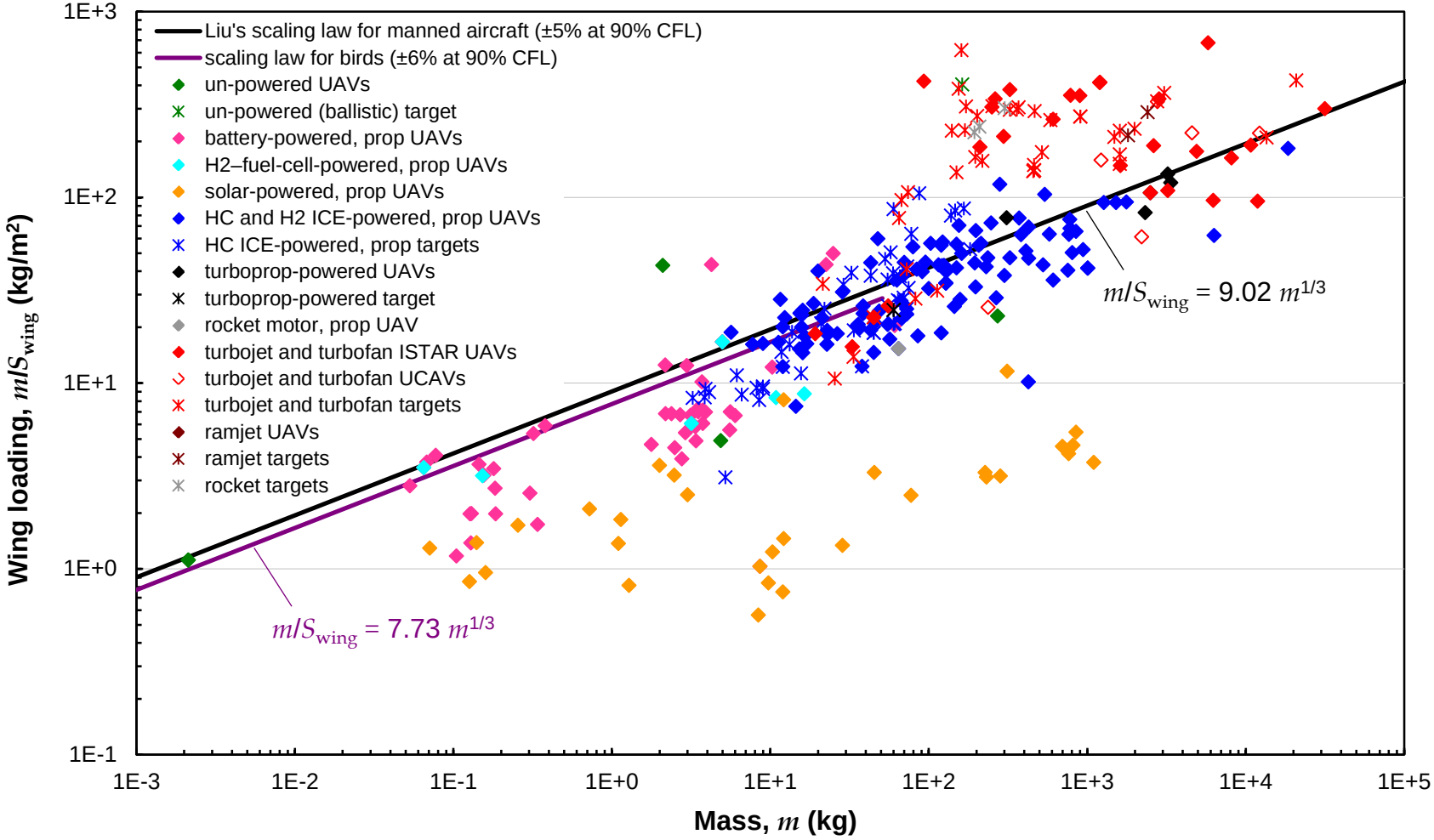

Figure 8 *Mean wing loading* vs. *mean mass for all UAVs in the* Database. *Also shown are the scaling laws for manned aircraft derived by Liu [19] and for birds derived by use of the data provided by Tennekes [21] (via Liu), Alerstam* et al. *[22], and Chatterjee* et al. *[23].*

3.2 Performance Characteristics

3.2.1 Best-Range and Operating Airspeeds and Reynolds Numbers

Figure 9 shows the data for best-range airspeed available in the *Database* as a function of mean UAV mass. As noted in Appendix A, for turbojet-, turbofan-, and rocket-powered UAVs, often the only available data are for the operating airspeed, which is not usually the same as the best-range airspeed. For comparison, data for operating airspeed have been plotted in Figure 9. Also shown are a best-fit power law for birds, a scaling law for manned propeller-driven aircraft, and the mean value for the operating airspeeds of manned, turbofan-powered aircraft, which corresponds to a Mach number of 0.7 at sea level.

The data for propeller-driven UAVs are seen generally to follow the scaling behaviour expected for geometrically and aerodynamically similar aircraft [19]; however, the scatter is substantial because of the great morphological, propulsive, and mission diversity of the UAVs represented. The mean value of the best-range airspeed for propeller-driven UAVs at any given mass is somewhat lower than that for an equivalently scaled manned transport aircraft. For turbojet- and turbofan-powered ISTAR UAVs and UCAVs, the data points for best-range airspeed, though limited in number and scattered, appear to largely follow the expected dependence. While the plotted values of operating airspeed are usually greater than the range of values of best-range airspeed, in some cases published data entered into the *Database* as operating airspeed may actually represent values of best-range airspeed (*e.g.* the points at 10^3 kg < m < 10^5 kg and operating airspeeds of 80–100 m/s). An effort was made to determine the correct notation of all airspeeds before their entry into the *Database*, but this was not always definitive; and validation of these entries is warranted prior to their use in further analysis.

As discussed in Appendix A, the maximum airspeed for large, turbojet- and turbofan-powered UAVs (*i.e.* ISTAR UAVs, UCAVs, and targets) was estimated, when it was unavailable from the source literature, by dividing the value of operating airspeed by 0.92; and, conversely, the operating airspeed was estimated by multiplying a given value of maximum airspeed by the same factor, if only the latter was available. This factor was derived from the data for turbojet- and turbofan-powered UAVs displayed in Figure 10, where the ratios of best-range–to–maximum airspeed for all UAVs in the *Database* are plotted, along with the ratios of operating-to-maximum airspeed for all turbojet- and turbofan-powered platforms. Values of the ratio of operating-to-maximum airspeed have only been plotted for turbojet- and turbofan-powered UAVs and targets for which both values were supplied in the literature. Instances in which either value was estimated are excluded.

Figure 10 illustrates why there is a lower limit of m to which this method of estimating operating or maximum airspeed was applied. For MTOM > 5×10^3 kg, in no case is the ratio of operating-to-maximum airspeed less than 0.88 or greater than 0.96; and the limited data clusters strongly about a mean value of 0.92 (with a ±2% relative RMS error). Whereas for MTOM < 5×10^3 kg, a few reports of much lower values of operating–to–maximum-

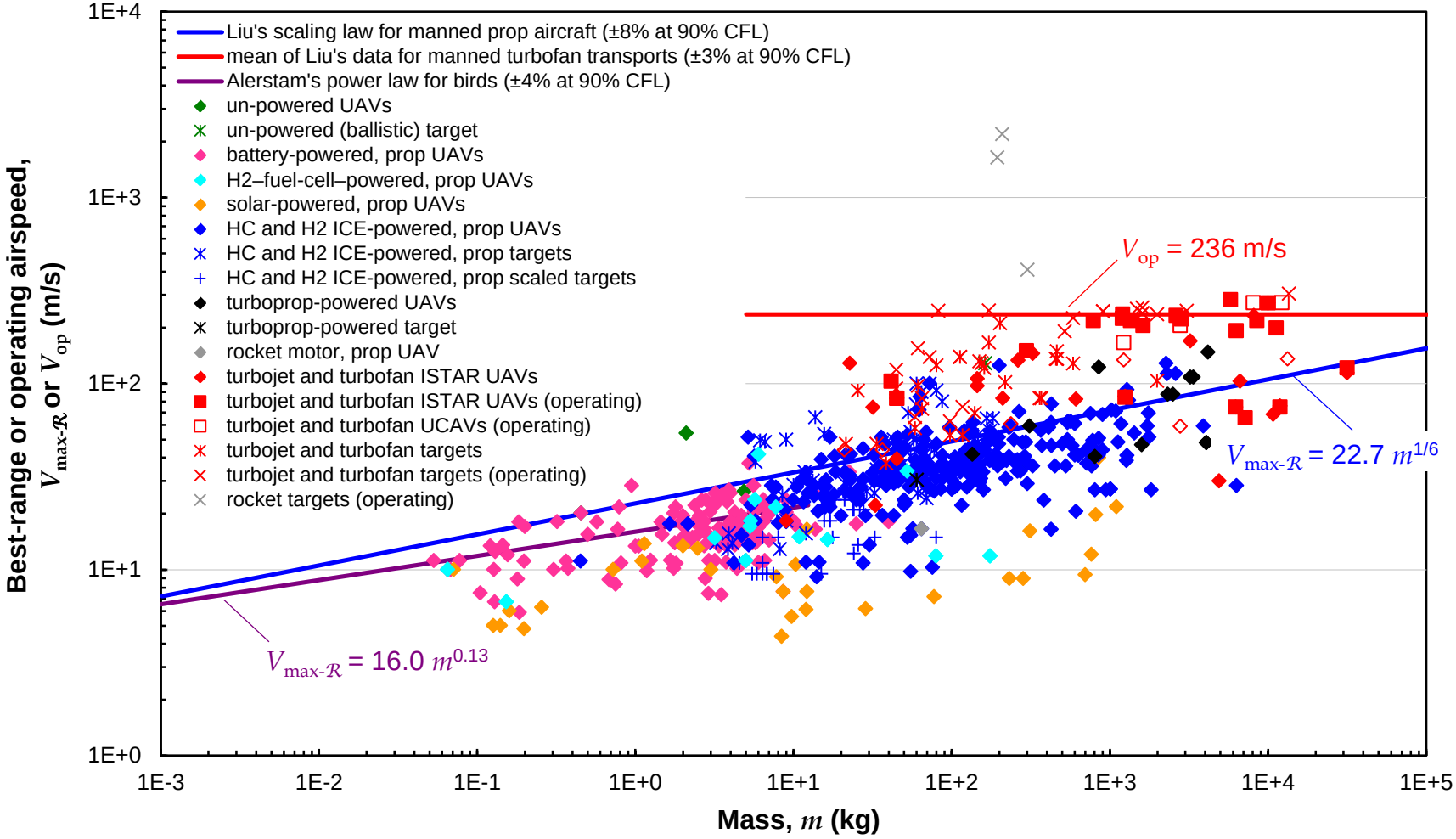

Figure 9 *Best-range or operating airspeed* vs. *mean mass for all UAVs in the* Database. *Also shown are the scaling law for manned, propeller-driven aircraft derived by Liu [19], the mean value of operating airspeed for manned turbofan-powered aircraft, and a power law for birds derived by Alerstam* et al. *[22].*

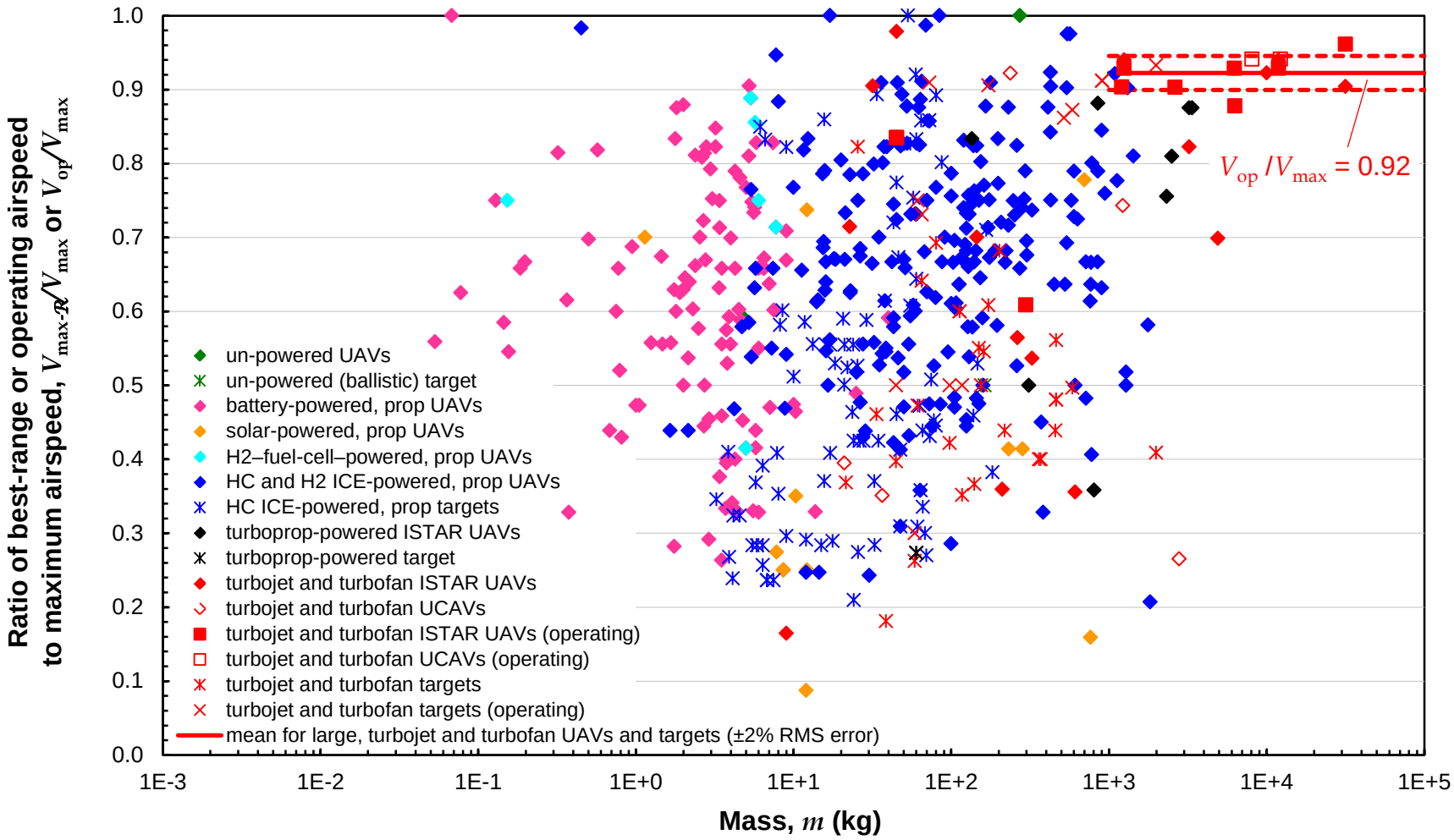

Figure 10 Ratio of best-range or operating airspeed to maximum airspeed vs. *mean mass for all UAVs in the* Database*; and ratio of operating to maximum airspeed for turbojet- or turbofan-powered UAVs with* $m_{max} > 10^3$ *kg.*

airspeed ratio exist. Figure 10 also highlights the fact that, in some cases, values of best-range airspeed reported in the literature may actually correspond to the operating airspeed and *vice versa*.

The data shown in Figure 10 for the other types of UAS reveal that the best-range and maximum airspeeds are un-correlated for most UAVs. This is explained by the diversity of mission, propulsion type, and design influences of the individual UAVs. In some cases, a UAV with a relatively low best-range (and, hence, loiter) airspeed, coupled with an ability to dash at relatively high speed may be required; while, in others, the number of propulsion systems (*e.g.* ICE, turbojet, or turbofan engines) open for selection may have been limited, resulting in platforms with far more available power and resultant maximum airspeed than is necessary (or even safe) for their normal operation. In a few cases, the value of the ratio of best-range–to–maximum airspeed shown in Figure 10 is unity. This most often indicates a case in which the literature reports the same values for best-range and maximum airspeed, which may not reflect the true characteristics of the UAV, but are the best available values and were, therefore, entered into the *Database*.

Another method of examining the aggregated UAS performance data is illustrated in Figure 11, which shows the best-range airspeed across the dataset as a function of wing loading. Also shown are: the average value of operating airspeed for manned, turbofan-powered aircraft, which agrees with a significant portion of the data for turbojet- and turbofan-powered UAVs and targets; the scaling law derived by Liu for manned, propeller-driven general aviation and manned turbofan aircraft; and a best-fit power law for the data for the best-range speed of birds derived from biometric data provided by Alerstam *et al.* [22] (see Appendix C). It is apparent that the geometric characteristics of birds are well described by scaling laws with exponents that are governed by geometric similarity; while, in contrast, the best-range airspeed of birds, an aerodynamic characteristic, does not follow aerodynamic-similarity behaviour as a function of m or wing loading (W / S_{wing}).

As shown in Figure 11, the scaling law for best-range airspeed as a function of wing loading for manned aircraft over-predicts its value for many UAVs. This situation is similar to that seen in Figure 9; however, some of the outlying points in Figure 9 fall within the band of the aggregated data in Figure 11. For example, the wingspans, wing areas, mean wing chords, wing loadings, and best-range airspeeds (Figures 2, 5, 7, 8, and 9, respectively) of solar-powered UAVs show systematic departures from the aggregated data and from the scaling laws for manned aircraft. This results from their relative lack of geometric similarity to the other classes of UAVs. However, they are comparatively more aerodynamically similar to other UAVs, as evidenced by the points shown in Figure 11, which implies that the lift coefficient at best-range conditions is relatively constant across the UAS dataset, because of its relationship to wing loading and best-range airspeed [31].

The chord-based Reynolds number associated with cruising, fixed-wing flight is plotted in Figure 12 as a function of m for UAVs for which values of best-range airspeed and mean chord length are available, along with a scaling law for manned aircraft and a power law for birds. If a value of operating airspeed is available, as it is in the case of some turbojet- and turbofan-powered UAVs, the Reynolds number based on operating airspeed is plotted

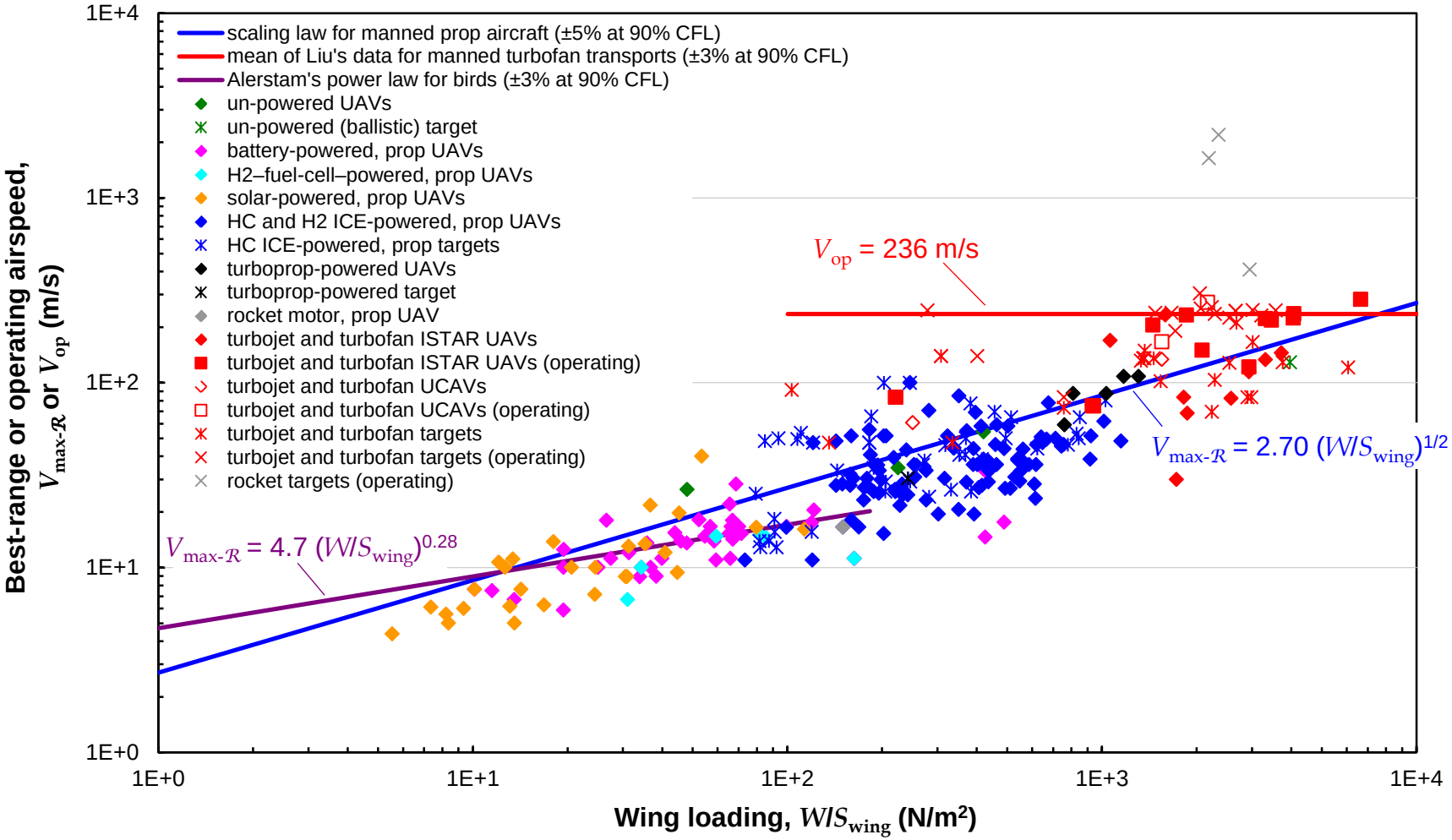

Figure 11 Best-range or operating airspeed vs. *mean wing loading for all UAVs in the* Database. *Also shown are the scaling laws for manned aircraft derived by Liu [19] and for birds derived by Alerstam* et al. *[22].*

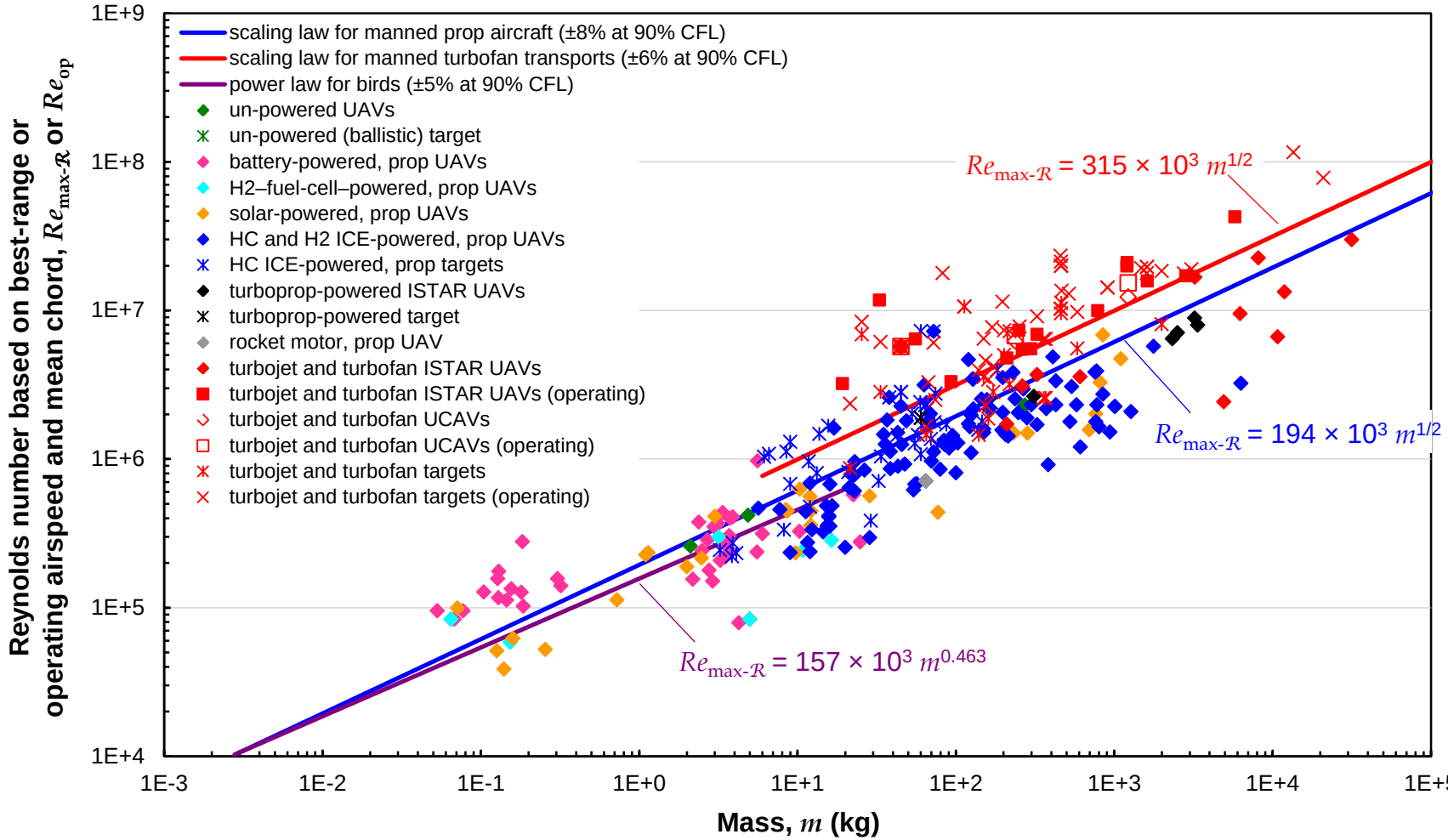

Figure 12 Reynolds number at sea level based on best-range or operating airspeed and mean wing chord vs. *mean mass for all UAVs in the* Database. *Also shown are the scaling law for manned aircraft derived by Liu [19] and a scaling law developed from the power law for cruising airspeed given by Alerstam* et al. *[22] and the data for wingspan and wing area provided by Tennekes [21] (via Liu), Alerstam* et al.*, and Chatterjee* et al. *[23].*

as well. Figure 12 reveals that the dependence of Reynolds number on m is essentially consistent with that anticipated from geometric and aerodynamic similarity arguments (see Appendix C and Liu [19]), including the data for solar-powered UAVs, which might be expected to show a systematic discrepancy, based on the results discussed above. However, it would appear that the relative decrease in best-range airspeed values for solar-powered UAVs with respect to the scaling law for manned aircraft is balanced by their relatively higher values of mean chord length, such that the Reynolds number based on best-range airspeed agrees reasonably well with the scaling law derived for manned aircraft.

The attempts of designers of small-scale fixed-wing UAVs to maintain high values of Reynolds number for the sake of aerodynamic efficiency are well documented [9]. Their success in doing so is illustrated in Figure 12 by the fact that Reynolds number values for battery-, ICE-, and turboprop-powered UAVs with $m > 1$ kg are mostly over-predicted by the scaling law derived for manned aircraft, whereas for the smallest UAVs (*i.e.* those with $m < 1$ kg) the scaling law under-predicts most of the values of Reynolds number, the exceptions being for solar- and fuel-cell–powered UAVs.

3.2.2 Endurance and Range

Several mission-performance characteristics of the UAS in the *Database* are available for examination. Figure 13 shows the data for UAV endurance as a function of m. The endurance of an air vehicle is governed by many factors, including its fuel or battery capacity and its specific energy, the propulsive power required to overcome drag at a given flight condition (here, assumed to be the best-range airspeed), and the efficiency with which the propulsion system converts stored energy into propulsive power.

In Figure 13, two purely empirically based best-fit power laws of endurance as a function of m are shown to illustrate the approximate dependence of flight endurance on m. The exponents, ⅓ and ½, were chosen because of their occurrence in the scaling analysis [19] and because they represent the data (or portions of it) in a reasonable manner. The scatter in the data precludes a conclusion on the choice of an exponent around or between these values; and little significance should be placed on the coefficients of the power laws (0.4 and 0.9), which is the reason that the uncertainty levels associated with them are not provided here. However, an exponent of ½ yields a scaling law that represents the dependence of endurance on W for ICE-powered UAVs fairly well; whereas, an exponent of ⅓ somewhat better describes the data for turbojet- and turbofan-powered UAVs.

The trends seen in the data in Figure 13 indicate that an ICE-powered UAV with the same weight as another that is turbojet or turbofan powered will tend to have a higher endurance (though, based on the data in Figure 9, a lower best-range or operating airspeed). In addition, the endurance data for targets, both ICE- and turbojet- or turbofan-powered, indicate that they have lower values of endurance than do most ISTAR UAVs, as one might anticipate from their respective missions; and the turbojet- and turbofan-powered UCAVs represented in Figure 13 display lower values of endurance than the average for other turbojet- and turbofan-powered platforms at a given value of m.

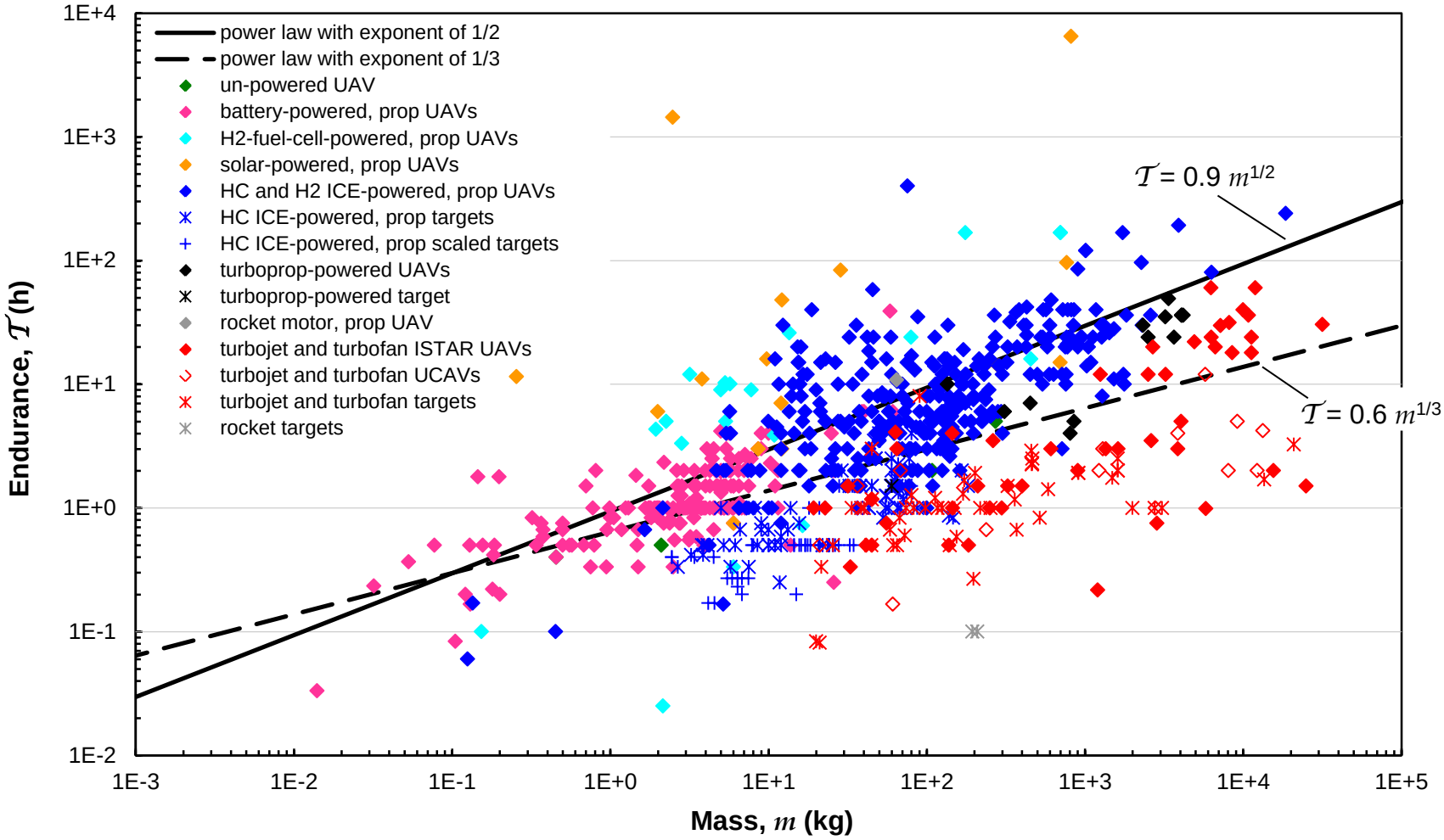

Figure 13 Endurance vs. *mean mass for all UAVs in the* Database. *Also shown are power laws with exponents of ⅓ and ½, which illustrate the approximate (purely empirical) dependence of $\mathcal{T}$ on m.*

Figure 14 displays the data for UAV range (as defined in Table 4), as a function of m and two best-fit power laws describing the data with exponents obtained by increasing those used to represent endurance in Figure 13 by ⅓. This reduction was used to represent the trend of endurance with m and is greater than the quantity of ⅙ that would be expected based on the argument that endurance is approximately equal to the range multiplied by the best-range airspeed, which itself is proportional to $m^{1/6}$. Again, little significance can be placed on the specific values of the exponents or on the coefficients. Nonetheless, power laws with exponents of ⅔ and ⅚ may be seen in Figure 14 to reasonably follow the trend of the aggregated UAS data, with the power law having an exponent of ⅚ seemingly providing somewhat better agreement than the one with an exponent of ⅔. The scatter seen in the data is comparable to that of the endurance values displayed in Figure 13 and makes a conclusion about the dependence of range on m impossible, other than to say that the range is roughly proportional to $m^{5/6}$.

3.2.3 Ceiling

Figure 15 shows the data for the ceilings of the UAVs in the *Database*. As described in Appendix A, the recorded ceiling values often represent service ceilings, but may also be absolute ceilings, or maximum operational altitudes. The latter is true of most of the data for aerial targets and for battery-powered UAVs. It is also the case for un-powered ISTAR UAVs, which have no propulsion systems and, therefore, no density-altitude limit imposed by a propulsion system [31]. They are sometimes air launched or released at high altitude from a balloon; and thus their 'ceilings' represent maximum operating altitudes.

The data in Figure 15 indicate that the average ceiling of UAVs increases with m, although there are examples of UAVs throughout the mass range with extremely high maximum altitudes (up to 76 km). The ceilings of ICE-, turboprop-, turbojet-, and turbofan-powered ISTAR UAVs and turbojet- and turbofan-powered UCAVs asymptotically approach an upper limit of ~20–25 km with increasing m, as one might expect as well for manned aircraft, with turboprop and turbojet or turbofan propulsion enabling higher ceilings for larger UAVs than most ICE-powered UAVs attain. One may also observe that solar-powered UAVs have almost uniformly high ceiling values (*i.e.* an average of ~25 km). This is a result of many of their designs being aimed at HALE operation, as it is for the single hydrazine-powered, propeller-driven ISTAR UAV represented.

3.3 Power Requirements

3.3.1 Supplied Power and Power-to-Weight Ratio

The power supplied by the propulsion system of a UAV at sea level is often provided in published reports, either directly, as is usual for propeller-driven aircraft, or indirectly. As explained in Appendix A, published values of maximum thrust and operating airspeed may be used to estimate supplied power in the latter case (typical for turbojet-, turbofan-, and rocket-propelled UAVs). Figure 16 shows the data for supplied power for the entire UAS dataset, along with best-fit power laws for data for manned propeller- and turbofan-driven aircraft [19]. The data for propeller- and turbojet- or turbofan-driven UAVs

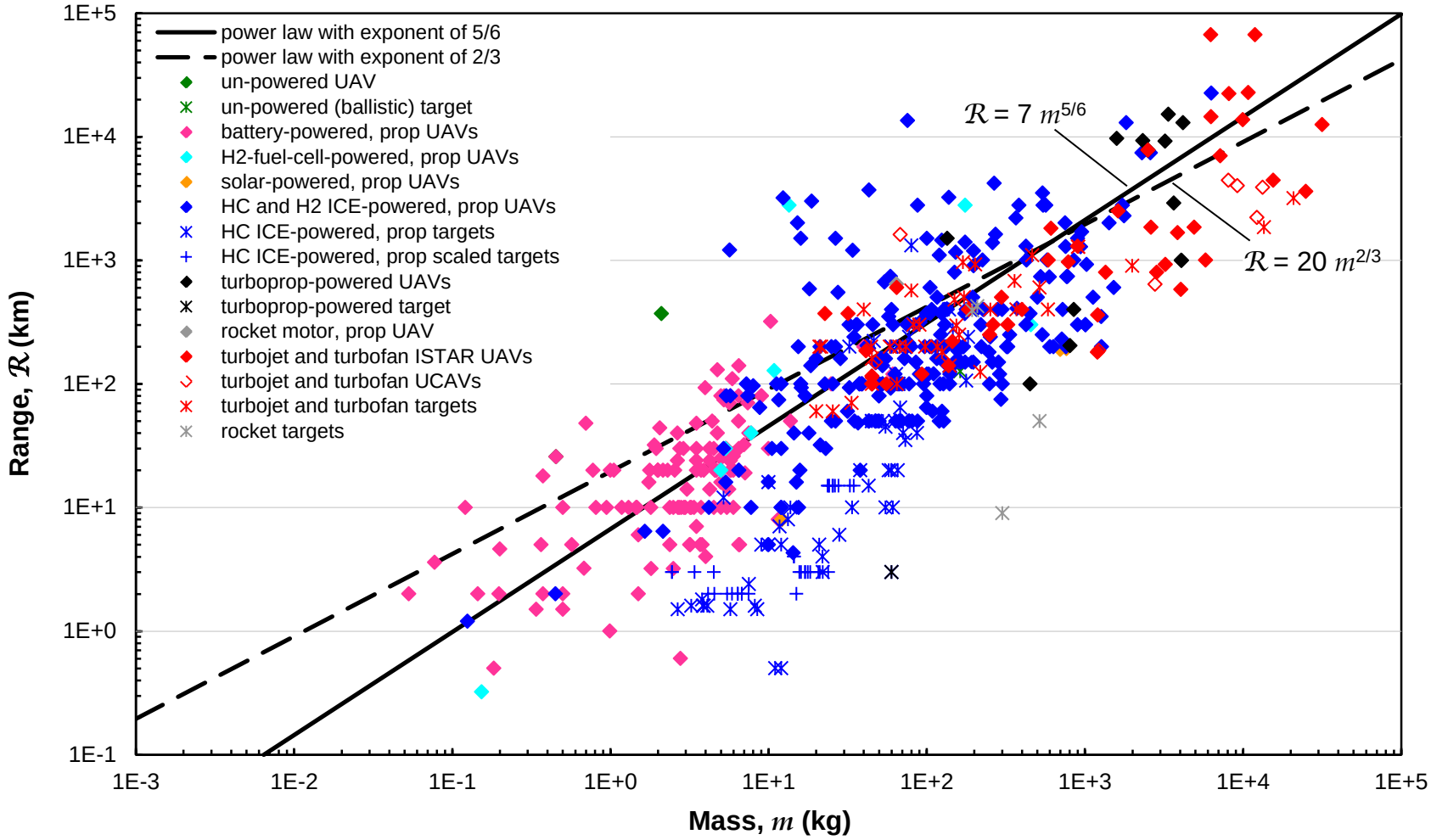

Figure 14 Range vs. *mean mass for all UAVs in the* Database. *Also shown are power laws with exponents of ⅔ and ⅚, which illustrate the approximate (purely empirical) dependence of $\mathcal{R}$ on m.*

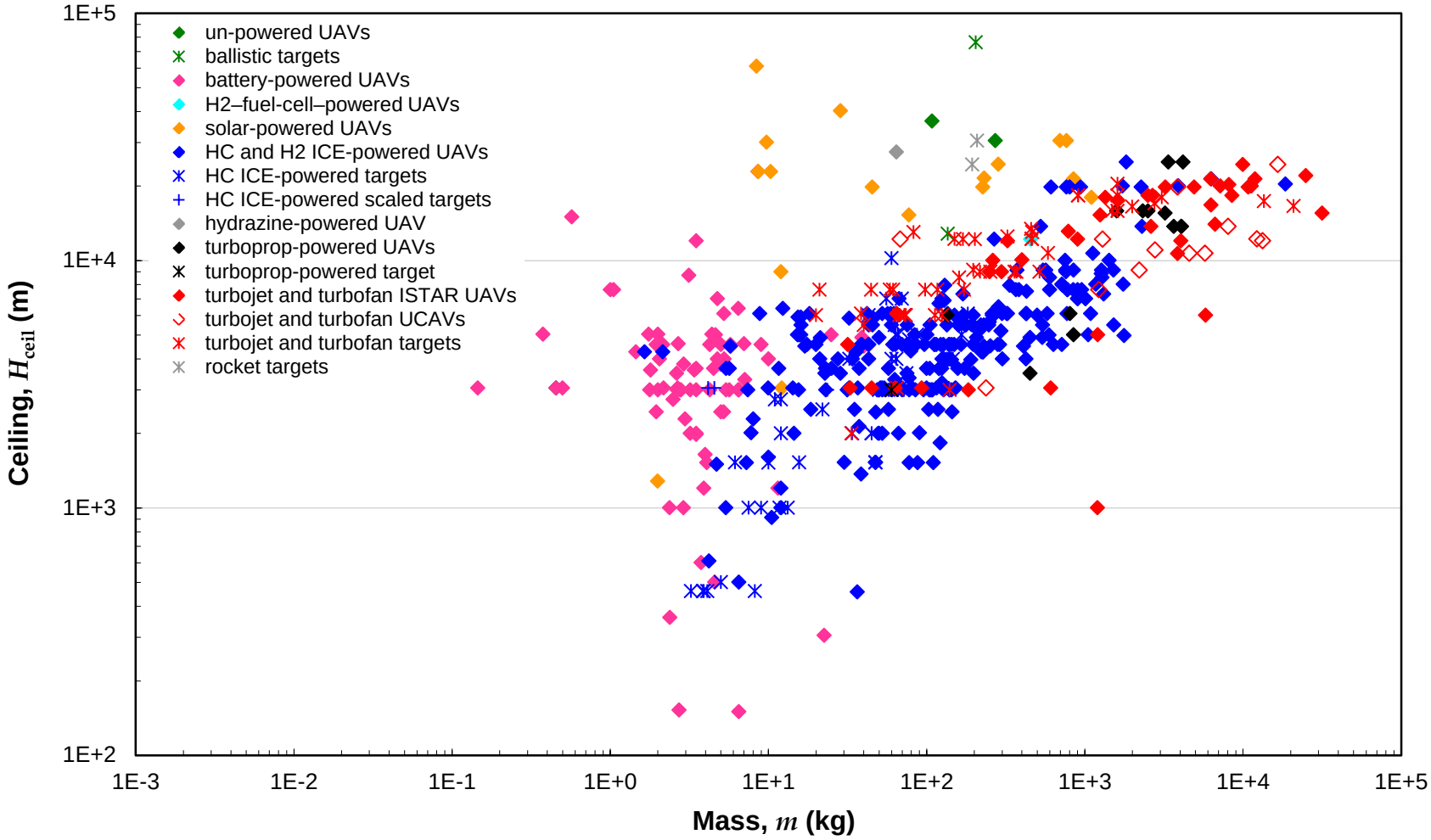

Figure 15 Ceiling vs. *mean mass for all UAVs in the* Database. *In the case of un-powered UAVs and targets, the values represented are operational ceiling values.*

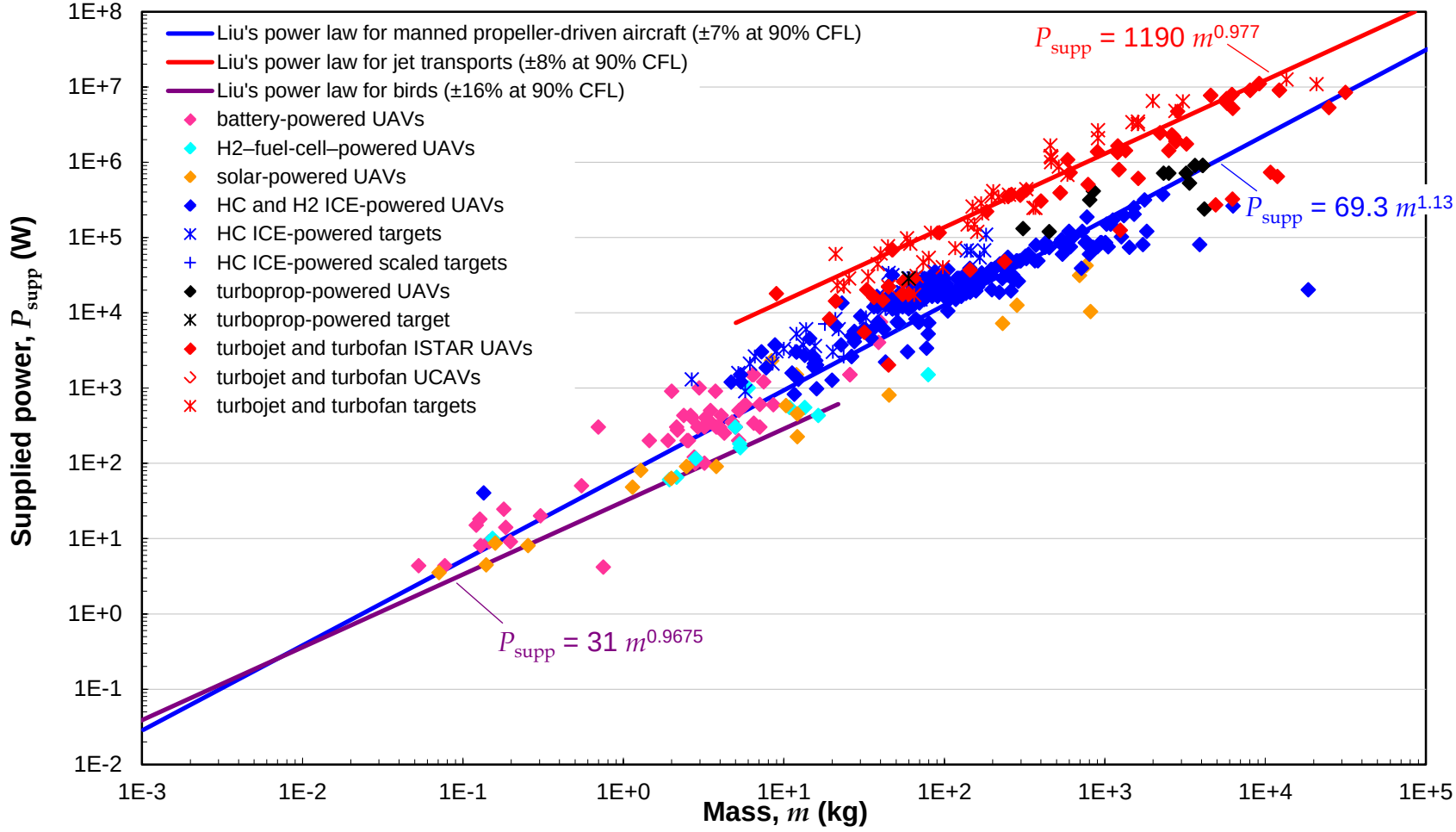

Figure 16 Supplied propulsive power vs. *mean mass for all UAVs in the* Database. *Also shown are the empirically based power laws for manned aircraft and birds derived by Liu [19].*

generally agree well with the respective best-fit power laws, with a few classes of UAS differing in significant ways, because of their particular roles.

Figure 16 indicates that turbojet- and turbofan-powered aircraft, both manned and unmanned, are often supplied with significantly more power than are propeller-driven aircraft (12 times more at $m = 10$ kg and 4 times more at 10^4 kg). Targets of all kinds are seen to have higher values of supplied power than do their ISTAR counterparts; and UCAVs, all of which are turbojet- or turbofan-propelled, are seen to have more supplied power than do most turbojet- and turbofan-propelled ISTAR UAVs of the same mass, as a consequence of the latter mostly being HALE designs without a requirement for high propulsive power for manoeuvring or high speed.

The ratio of supplied propulsive power to UAV mass is displayed as a function of m in Figure 17, which also shows versions of the best-fit power laws shown in Figure 16 converted to power laws for UAV power-to-mass ratio. In the cases of birds and manned, turbofan-powered aircraft, the power laws indicate expected slow decreases in power-to-mass ratio with increasing m; while, conversely, the power law derived for propeller-driven aircraft indicates that their power-to-mass ratio increases moderately with m. The scatter in the data is quite large, but, for each category of UAV shown in Figure 17, the trend in the power-to-mass ratio is toward smaller values as m increases. This confirms the negative exponents of the power laws derived for birds and for manned, turbofan-propelled aircraft. The contradictory, small, positive exponent of the power law for manned, propeller-driven aircraft is likely the result of the fact that both ICE- and turboprop-powered aircraft were included in the data used by Liu in its derivation [19].

Figure 17 also highlights the differences in the supplied power at a given m amongst the various classes of UAVs, which are also observable, though perhaps less clearly in Figure 16. At any value of m, UAVs powered by solar cells have lower values of power-to-mass ratio than do those powered by batteries or fuel cells (or birds), which in turn have lower values of power-to-mass ratio than do UAVs powered by ICEs and turboprops. UAVs (and manned aircraft) propelled by turbojet or turbofan engines have the highest values of power-to-mass ratio, roughly a factor of 40 times greater than a bird scaled to the same mass and a factor of 100 times more than an equivalently scaled solar-powered UAV.

3.3.2 Power Required at Best-Range Conditions

The methods described in Appendix B were used to estimate the power required to achieve the best-range airspeed of each UAV for which sufficient data were available to do so. The results are displayed in Figure 18, along with a few values of the power at the best-range airspeed stated in the literature and scaling laws for manned aircraft and birds derived under the assumptions of geometric and aerodynamic similarity [19]. As illustrated by Figure 18, the estimates of the power at the best-range airspeed for propeller-driven UAVs generally follow the scaling law for manned aircraft, although they exhibit significant scatter. In contrast, the mean of the estimates for turbojet- and turbofan-propelled UAVs (ISTAR UAVs, UCAVs, and targets) is significantly higher than the mean of those for propeller-driven UAVs and the scaling law at a given value of m. At the lower

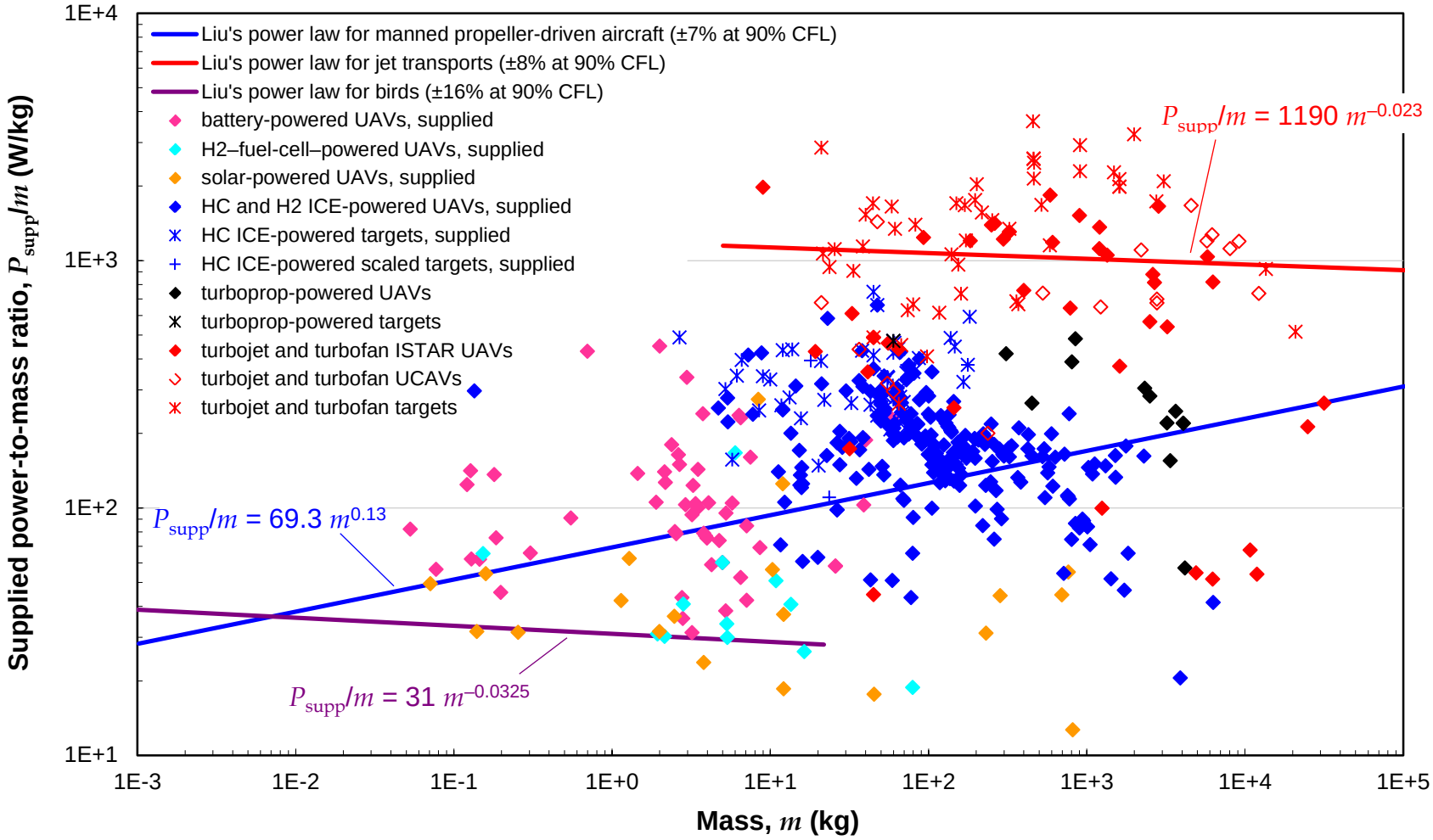

Figure 17 Supplied propulsive power-to-mass ratio vs. *mean mass for all UAVs in the* Database. *Also shown are the empirical power laws for manned aircraft and birds derived by Liu [19].*

end of the mass range, the estimated and stated values of the power required at the best-range airspeed for battery-powered UAVs, while scattered, also follow the scaling law reasonably well; whereas the values for solar-powered UAVs uniformly lie below the scaling law, as would be expected from their usual design requirement for minimum power consumption [32, 33].

For several battery- and solar-powered UAVs, estimated and stated values of the power required at the best-range airspeed are available for comparison; and the pairs of values seen in Figure 18 may be used to confirm (or invalidate) the method used to estimate the required power for propeller-driven aircraft, outlined in Appendix B. In each of the three cases (for two battery-powered UAVs and a solar-powered UAV) for which stated and estimated values of required power at the best-range airspeed are available, the stated value is 41–45% less than the estimate. The significance of this systematic difference is difficult to assess because of the limited number of data points and because of the large scatter in the estimates of required power at a given m.

Inaccuracies in the computations of required power for electrically powered UAVs may be attributable to error in the assumed value of propulsive efficiency used to convert the supplied power of the motor(s) to a value of propulsive power available to overcome drag. This source of uncertainty may be eliminated for the single solar-powered UAV under consideration here because a value of propulsive efficiency is provided in the literature. It may also be discarded as an explanation of the over-estimate of required power at the best-range airspeed for one of the battery-powered UAVs, because a reported value of supplied thrust was used to estimate the maximum available propulsive power (see Table 5), and no value of supplied power is available in the literature. The error involved in the method used here to approximate the power required at the best-range airspeed for propeller-driven UAVs was estimated to be less than ±10% [19], which would appear to be overly optimistic for small UAVs. It may be more realistic, however, for manned aircraft, the context in which the statement was made, because the data published in the open literature may be more reliable for manned aircraft than are the data for many small UAVs.

3.3.3 Flight Efficiency and Maximum Lift-to-Drag Ratio

The maximum flight efficiency computed for each UAV in the dataset (for which sufficient data is available to do so) is plotted as a function of m in Figure 19. The maximum flight efficiency was obtained from the product of best-range airspeed and MTOM of each UAV divided by its estimated value of power required at the best-range airspeed. Also shown are values of maximum flight efficiency obtained by use of stated values of required power for specific UAVs and any published values of maximum lift-to-drag ratio, which is approximately equivalent to the maximum flight efficiency [19]. The mean value of the maximum flight efficiency for manned aircraft [19] and a relation describing its variation with m for birds (see Appendix B) are displayed, as well.

The scatter in the data shown in Figure 19 about the mean for manned aircraft and the best-fit power law for birds is large, although certain classes of UAS show systematic departures explainable by their missions. For example, targets of all kinds are seen to have

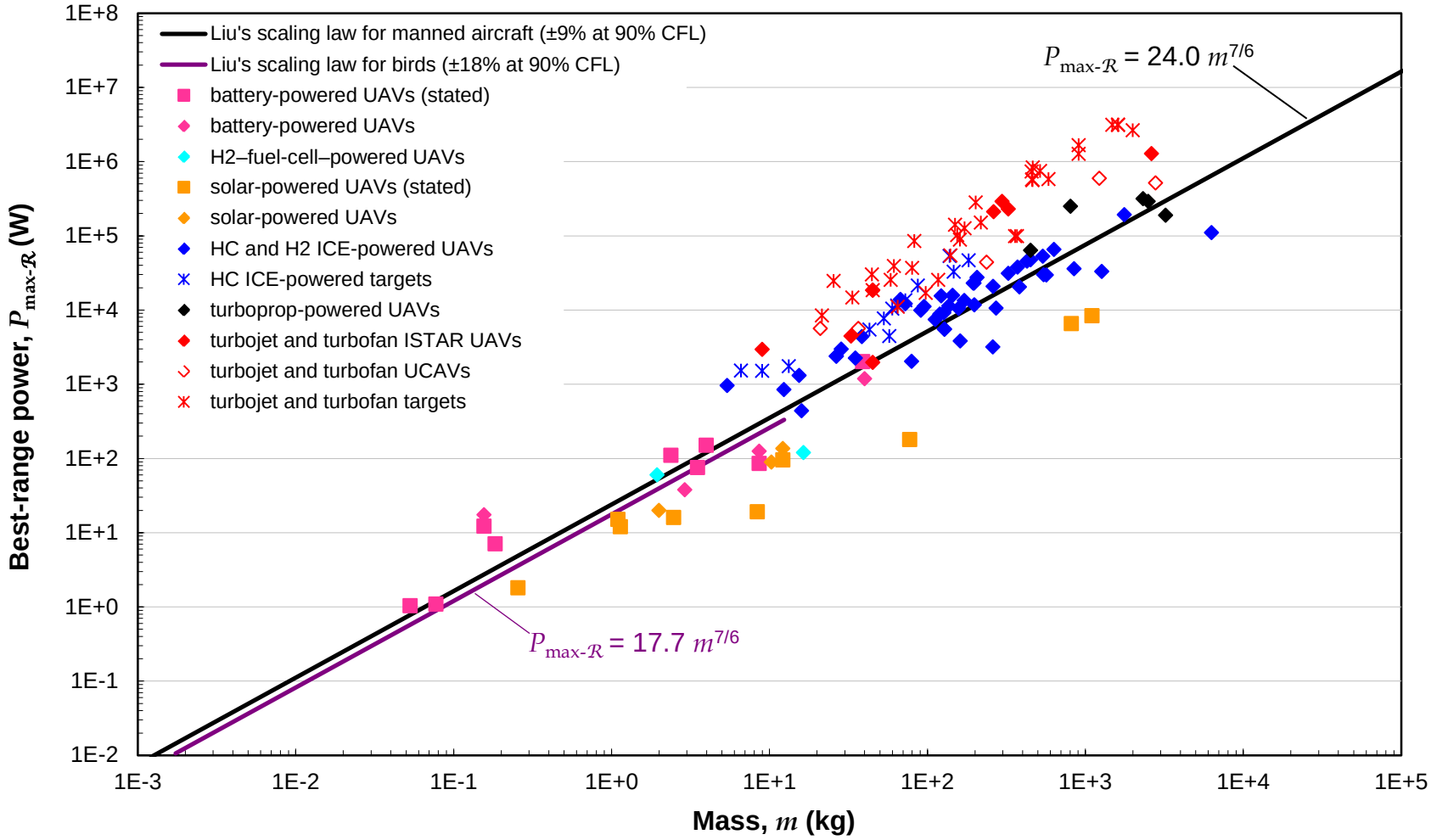

Figure 18 Estimated and stated values of power required at cruise (i.e. *best-range) conditions* vs. *mean mass for all UAVs in the* Database. *Also shown are the scaling laws for manned aircraft and birds derived by Liu [19].*

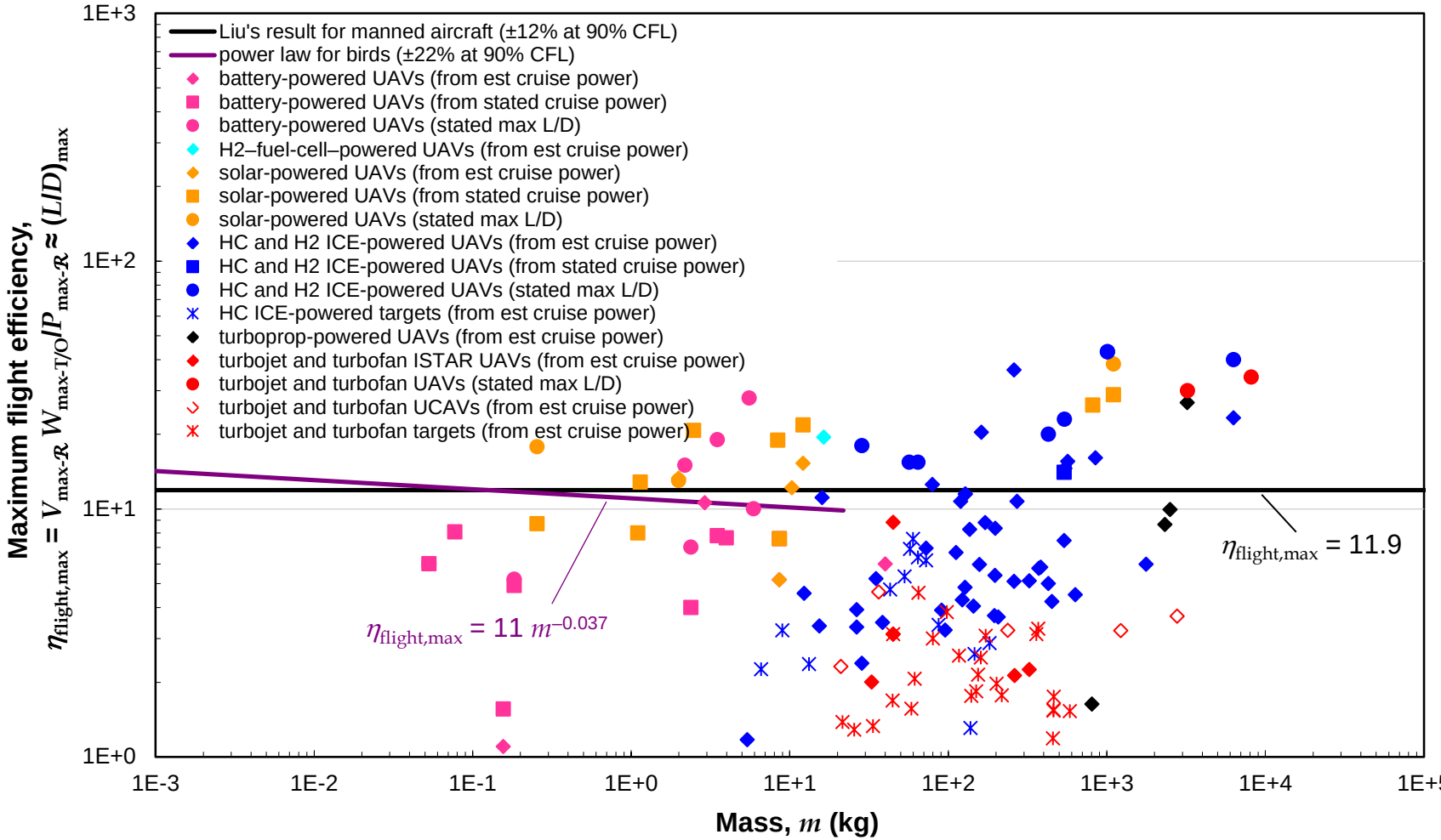

Figure 19 Estimated maximum flight efficiency or approximate maximum lift-to-drag ratio vs. *mean mass for all UAVs in the* Database. *Also shown are the mean maximum flight efficiency for manned aircraft derived by Liu [19] and a power law for birds derived by use of the empirically based power law for cruising airspeed obtained by Alerstam* et al. *[22] and the scaling laws for maximum weight and cruise power derived by Liu.*

below-average values of maximum flight efficiency, with turbojet- and turbofan-powered targets being less efficient than their ICE-powered counterparts; whereas solar- and fuel-cell–powered UAVs display values of maximum flight efficiency and maximum lift-to-drag ratio that are almost uniformly higher than those of other UAVs. Battery-powered UAVs, in contrast, often have low values of maximum flight efficiency and maximum lift-to-drag ratio, compared with other UAVs and with manned aircraft. The similarity of the values of maximum flight efficiency derived using stated values of power required at the best-range airspeed and some of the data for maximum lift-to-drag ratio for battery-powered UAVs lends credence to this conclusion, which might be expected based on the fact that their flight often occurs in a Reynolds number regime in which viscous effects are relatively more important than at higher Reynolds numbers [9], making their propulsion systems necessarily more powerful than would be required for a manned aircraft or for a larger UAV scaled to the same mass.

3.3.4 Available Thrust and Thrust-to-Weight Ratio

Displayed in Figure 20 are the data for maximum available thrust plotted against m, for all UAVs in the *Database*. Maximum available thrust is defined in Table 5 and, as discussed in Appendix A, is estimated from published values of supplied motor or engine power and maximum airspeed for propeller-driven UAVs or taken directly from the literature for turbojet-, turbofan-, and rocket-propelled UAVs and for a few (eight, mostly electrically powered) propeller-driven ones. The values of maximum available thrust for ICE- and turboprop-powered UAVs and for turbojet- and turbofan-powered UAVs may be seen to be in reasonable agreement with the power laws obtained for manned propeller- and turbofan-driven aircraft (see Appendix B), respectively; whereas the values of maximum available thrust for two rocket-propelled targets are observed to be three times higher than the value predicted by the power law for manned, turbofan aircraft, as might be expected from their required operation at high-subsonic to supersonic speeds (Fig. 9).

Conversely, the values of maximum available thrust estimated from data for battery-, solar-, and fuel-cell–powered UAVs are systematically over-predicted by (on average) a factor of 4–5 by the power law for propeller-driven aircraft. This finding implies either that electrically powered UAVs have significantly lower levels of available thrust than do equivalently scaled manned aircraft and other types of propeller-driven UAVs or that the method used to compute the maximum available thrust for electrically powered, propeller-driven UAVs significantly underestimates its value. The latter would appear more likely, because, for the five battery-powered UAVs for which published values of maximum available thrust (or supplied thrust, see Table 5) are available, four of the five lie on or above the best-fit power law for manned propeller-driven aircraft. The published values of maximum available thrust for the single solar- and fuel-cell–powered UAVs represented in Figure 20 are seen to agree with the estimates for similar UAVs at the same value of m. The implication that solar- and fuel-cell–powered UAVs have relatively low values of maximum available thrust compared with other UAVs of the same weight is not surprising, because of the limited power available from such systems, as shown in Figure 16. Investigation into the source of the discrepancy between the estimated and published values of maximum available thrust for battery-powered UAVs is recommended.

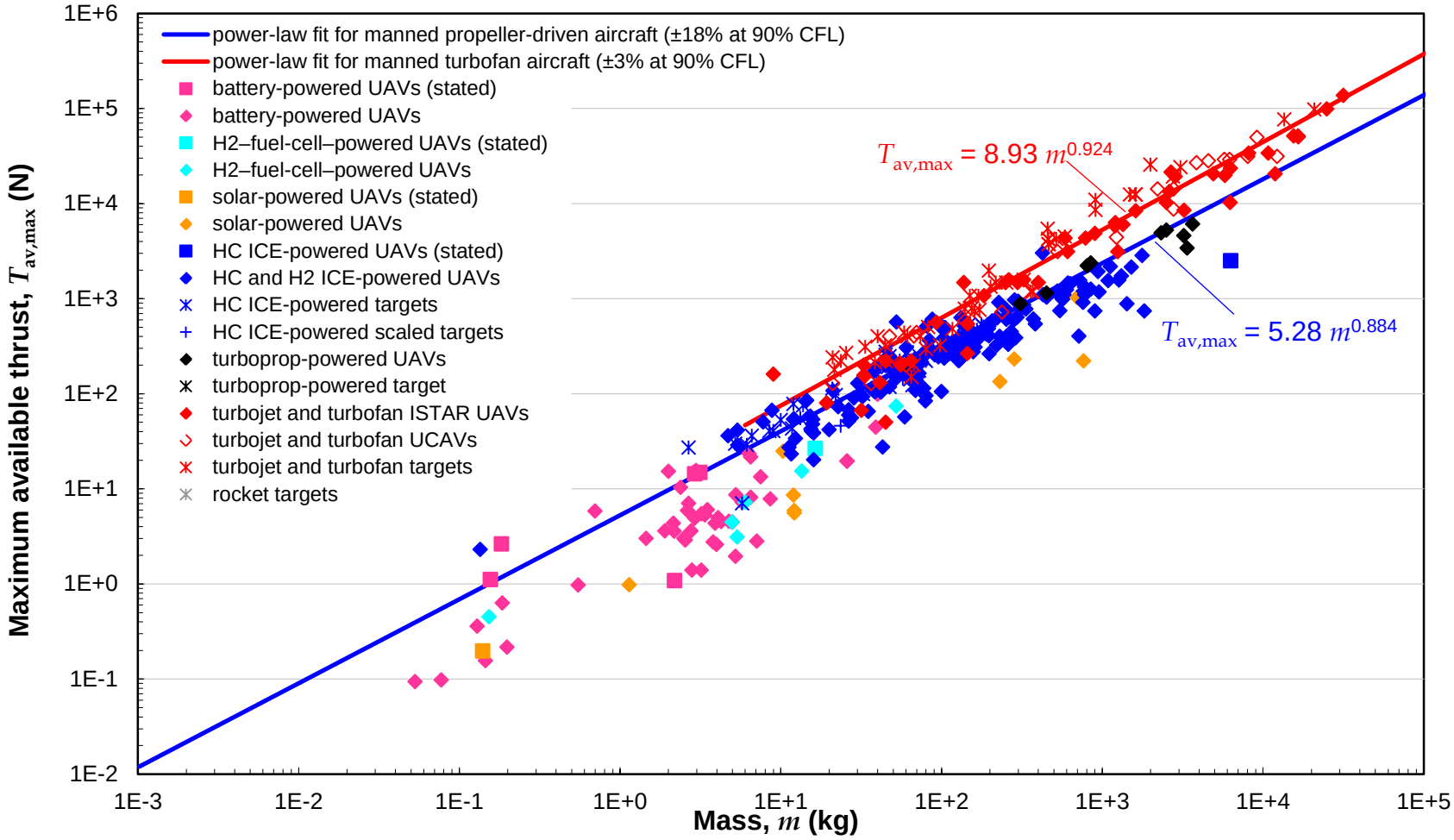

Figure 20 Maximum available thrust vs. *mean mass for all UAVs in the* Database. *Also shown are best-fit power laws for the installed thrust of the engines on manned, turbofan-powered and propeller-driven aircraft.*

A single published (stated) value of maximum available thrust for a UAV powered by ICEs, in this case, a UAV optimised for HALE flight [34], is also plotted in Figure 20. It is a factor of ~5 lower than the value one might expect based on the aggregated data for other ICE-powered UAVs and the power law for manned propeller-driven aircraft, likely because of its unique mission and design.

Figure 21 shows the data for the ratio of the maximum available thrust to UAV weight contained in the *Database*, as a function of m, along with best-fit power laws of data for manned, propeller- and turbofan-driven aircraft [19]. Disregarding the trends for the individual classes of UAS, the cumulative data yielded an average value of maximum-available-thrust–to–weight equal 0.35 for all UAVs; however, a slight negative dependence is observed in the data for each class of UAS. The decrease in available-thrust–to–weight with increasing m is also predicted by the power laws obtained for manned, propeller- and turbofan-driven aircraft by use of the methods described in Appendix B and data supplied by Liu [19]. This is reminiscent of the decreases in supplied-power–to–weight ratio with increasing m seen in Figure 17.

The data shown in Figure 21 also indicate that, at a given m, battery-, solar-, and fuel-cell–powered UAVs have lower maximum-available-thrust–to–weight ratios ($T_{\mathrm{av,max}}/W$) in a mean sense than do other propeller-driven UAVs (*i.e.* ICE- and turboprop-powered UAVs), which in turn have lower values of $T_{\mathrm{av,max}}/W$ (on average) than do turbojet- and turbofan-propelled UAVs. These findings are similar to those from Figure 21, described in Section 3.3.1, where the values of supplied power-to-mass ratio (P_{supp}/m) are seen to increase across the different types of UAVs in the same order that $T_{\mathrm{av,max}}/W$ does. However, the previously discussed discrepancies between published and estimated values of $T_{\mathrm{av,max}}$ for battery-powered UAVs make these findings less conclusive than those taken from Figure 21; and further investigation is warranted, particularly because the published values of $T_{\mathrm{av,max}}/W$ for several of battery-powered UAVs are reasonably represented by the best-fit power law for manned propeller-driven aircraft and thus in agreement with the bulk of the data for ICE-powered UAVs, when equivalently scaled.

3.4 Load Capacity and Usage

3.4.1 Load Capacity

The relationship between mean aircraft mass and MTOM is important because it indicates the capacity of an aircraft to carry payload and fuel or battery mass and thus the utility of the aircraft for various missions. The relationship between the mean mass and MTOM of an aircraft indicates the relative efficiency of its design compared with others of the same type. As illustrated in Figure 22, the ratio of the MTOM to mean mass for UAVs ranges from a value of unity up to ~1.75 for two large turbofan-powered UAVs. For UAVs with unknown values of payload and fuel or battery mass, a value of MTOM equal to mean mass was input to the *Database*; thus, the ratio of MTOM to mean mass for those aircraft is shown as unity. The mean value of the ratio of MTOM to mean mass for the 325 UAVs in the *Database* with known values of payload and fuel or battery mass is 1.25. A relative root-mean-squared (RMS) error of ±9.4% is associated with this mean. This equates to a

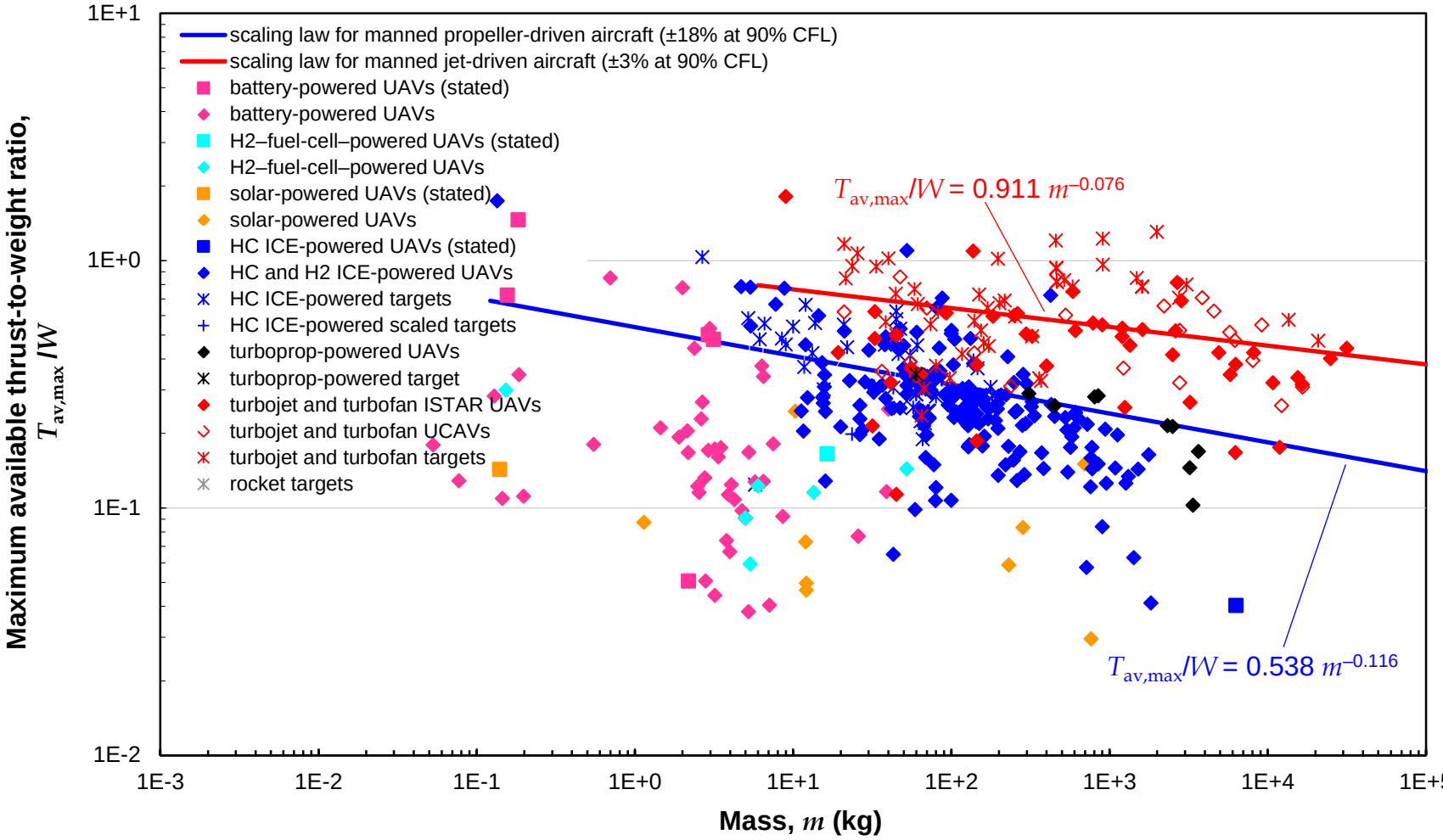

Figure 21 Maximum available thrust-to-weight ratio vs. *mean mass for all UAVs in the* Database. *Also shown are empirically based best-fit power laws for the maximum available thrust-to-weight ratios for manned propeller- and turbofan-driven aircraft.*

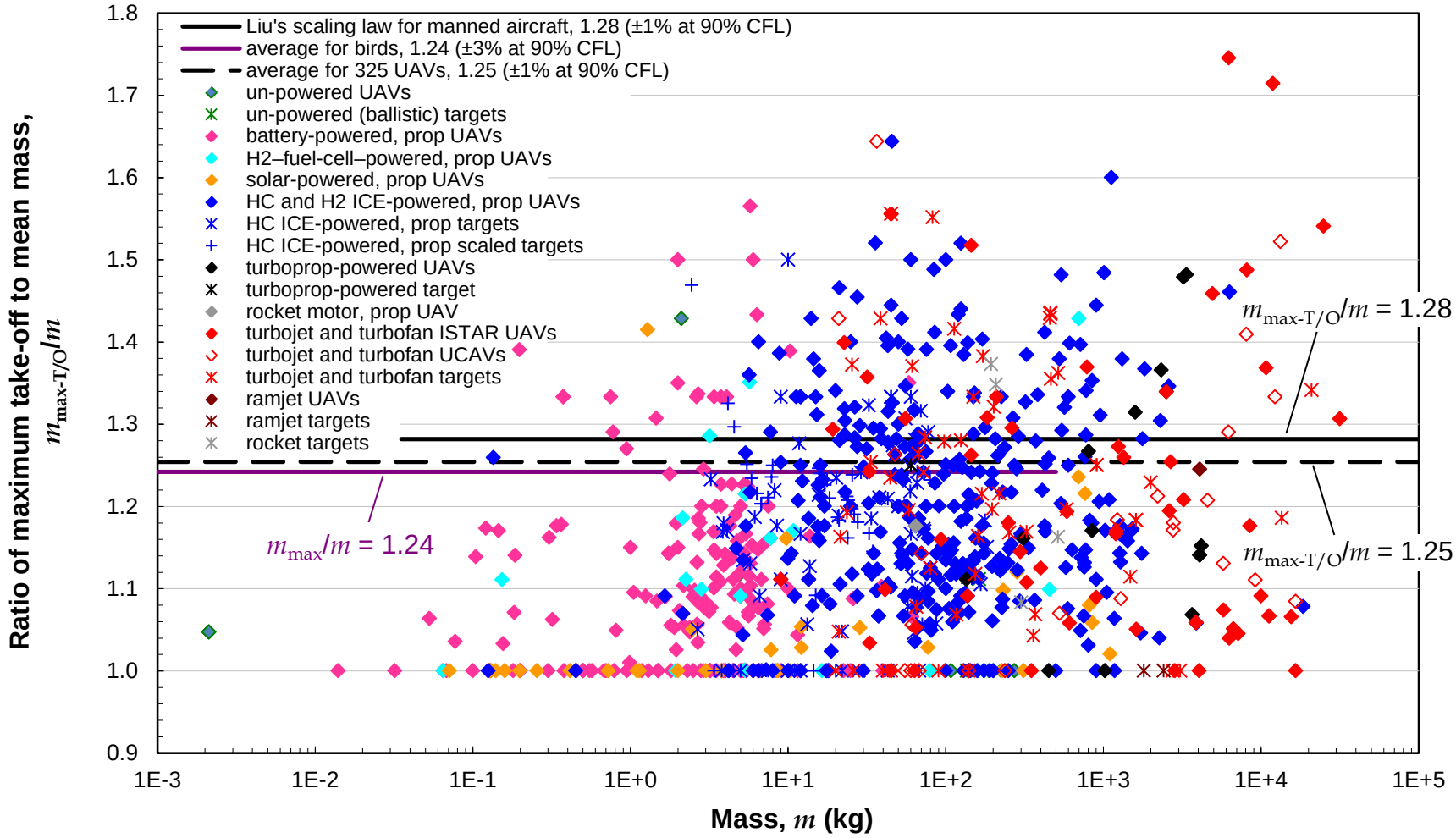

Figure 22 Ratio of maximum take-off to mean mass vs. *mean mass for all UAVs in the* Database. *Also shown are the average maximum take-off–to–mean mass ratios for UAVs and for manned aircraft and birds (derived by Liu [19]).*

relative uncertainty of ±1.4% at 90% confidence level (CFL), indicating a 90% probability that the mean of another identically sized random sample of the underlying population would lie within ±1.4% of the computed value [24]. It also agrees closely with the expressions provided by Liu [19]: MTOM equals 1.28 m (±1.2% at 90% CFL) for manned transport aircraft and maximum mass equals 1.24 m (±3.1 at 90% CFL) for birds.

An examination of the data for battery-powered UAVs in Figure 22 indicates that the majority have lower ratios of MTOM to mean mass than the average value for all UAVs, because of the way in which empty mass was defined for battery-powered UAVs (*i.e.* because it includes the battery, as described in Appendix A). Similarly, solar-powered UAVs demonstrate lower values of MTOM–to–mean-mass ratio than the average, at least partially because the solar collectors and any associated batteries or fuel cells were taken to be part of the aircraft and were thus included in their empty weights. Evaluating the average ratio of the MTOM to mean mass for the 663 UAVs for which MTOM and mean mass were non-identical, and thus including many of the battery-powered UAVs *i.a.* that were excluded from the previous conditional average, yields a slightly lower value: MTOM equals 1.21 m, with a relative uncertainty of ±0.9% at the 90% CFL.

3.4.2 Payload, Battery or Fuel, and Useful-Load Masses

Figure 23 shows the data for maximum payload-mass fraction as a function of mean weight for all UAVs in the *Database*, along with average values of payload-mass fraction for various classes of UAVs. The means are also tabulated in Table 7. Data for maximum battery- or fuel-mass fraction is provided in Figure 24 and in Table 8; and data for the maximum useful-load–mass fraction is shown in Figure 25 and in Table 9. In each plot, an estimate of the maximum useful load for manned and unmanned aircraft is displayed to indicate the upper limit expected for any of the mass fractions. This limit is based on data for manned HALE aircraft and corresponds to the maximum value of useful-load fraction for any of the aircraft, that for Scaled Composites' Global Flyer [35], which holds the long-distance aviation record for non-stop, non-refuelled flight [36].

The scatter in the data displayed in Figures 23–25 is significant, as evidenced by the relative uncertainties of the means at 90% CFL given in Tables 7–9; however, Student's t-tests of pairwise combinations of the datasets (all UAV types *vs.* electric, electric *vs.* ICE-powered, *etc.*), performed with Welch's correction for non-equal sample sizes [24], confirm that there is a vanishingly small probability that the underlying populations have identical means. This confirms that the differences amongst the computed mean values of payload, fuel, and useful-load fractions for the different classes of UAS are statistically significant.

Some trends in the payload, battery or fuel, and useful-load–mass fractions as functions of mean weight are also observable. Focussing for the moment on ISTAR UAVs (and ignoring targets, the data for which have been excluded from the means for the individual classes of UAVs), one may see from Figure 23 and Table 7 that ICE-powered UAVs generally have larger payload capacities than battery-, turboprop-, and turbojet- or turbofan-powered UAVs and (from Figure 23) that the typical payload-mass fraction decreases slightly with increasing mean weight. In contrast, turbojet- and turbofan-powered ISTAR UAVs

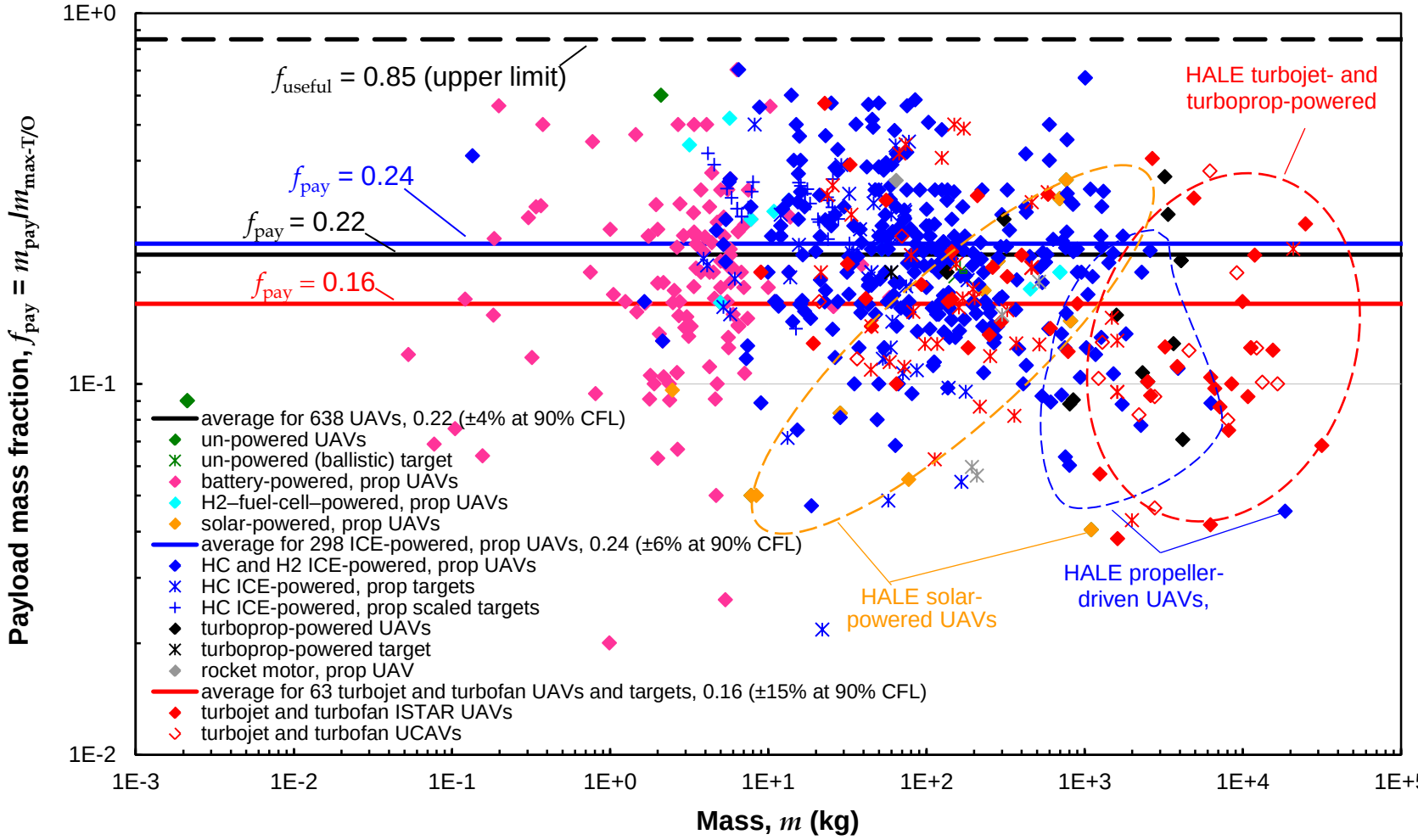

Figure 23 Payload-mass fraction vs. *mean mass for all UAVs in the* Database. *The solid black line shows the mean of the data for all UAVs for which payload mass was available (638 UAVs); and the dashed black line shows an estimate of the upper limit of useful-load fraction for aircraft, including UAVs. Also highlighted are the data for HALE ISTAR UAVs with different propulsion systems.*

Table 7 *Average maximum payload-mass fraction for UAVs with various propulsion systems. ISTAR UAVs, UCAVs, targets, and scaled targets are included in the average labelled 'all types'; whereas targets are excluded from the other averages. 'Electric' UAVs include battery-, fuel-cell–, and solar-powered ISTAR UAVs.*

power source	# of data points	$f_{pay} = m_{pay}/m_{max\text{-}T/O}$	relative uncertainty (90% CFL)
all types	638	0.22	±4%
electric	141	0.21	±9%
ICE	298	0.24	±6%
turbojet or turbofan	63	0.17	±15%

Table 8 *Average maximum fuel- or battery-mass fraction for UAVs with various propulsion systems. ISTAR UAVs, UCAVs, targets, and scaled targets are included in the average labelled 'all types'; whereas targets are excluded from the other averages. 'Electric' UAVs include battery- and fuel-cell–powered ISTAR UAVs.*

power source	# of data points	$f_{fuel} = m_{fuel}/m_{max\text{-}T/O}$ or $f_{batt} = m_{batt}/m_{max\text{-}T/O}$	relative uncertainty (90% CFL)
all types	325	0.23	±7%
electric	21	0.30	±25%
ICE	155	0.24	±7%
turbojet or turbofan	35	0.32	±17%

Table 9 *Average useful-load–mass fraction for UAVs with various power sources. ISTAR UAVs, UCAVs, targets, and scaled targets are included in the average labelled 'all types'; whereas targets were excluded from the other averages. 'Electric' UAVs include battery- and fuel-cell–powered ISTAR UAVs, but not solar-powered UAVs.*

power source	# of data points	$f_{useful} = m_{useful}/m_{max\text{-}T/O}$	relative uncertainty (90% CFL)
all types	325	0.40	±4%
electric	21	0.36	±22%
ICE	155	0.40	±5%
turbojet or turbofan	35	0.44	±13%

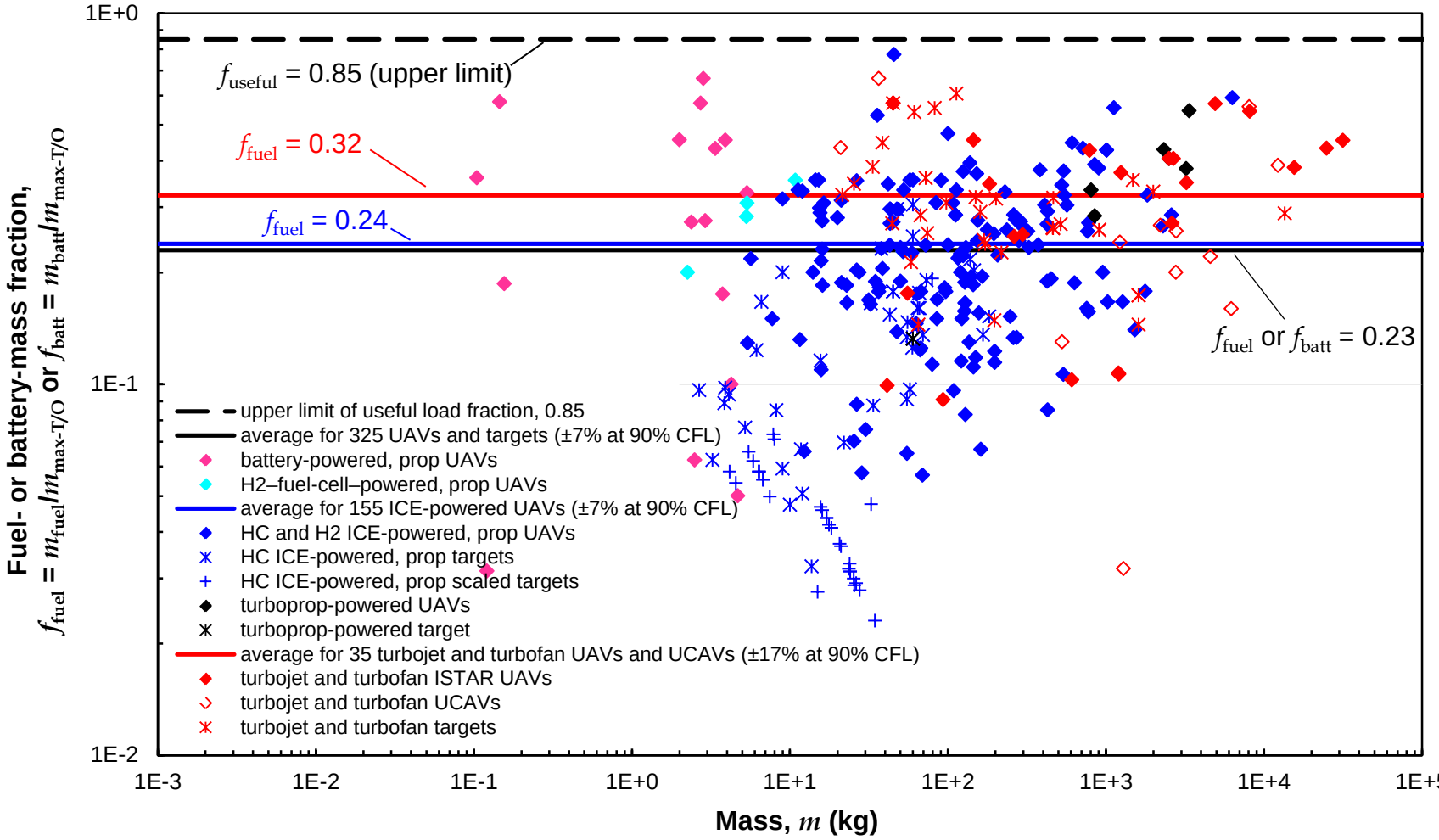

Figure 24 Fuel- or battery-mass fraction vs. *mean mass for all UAVs in the* Database. *Also shown are averages for all types of UAVs and for ISTAR UAVs powered by ICEs and turbojet or turbofan engines. The solid lines show the averages for different classes of UAVs; and the dashed line shows an estimate of the upper limit of useful-load fraction for aircraft, including UAVs.*

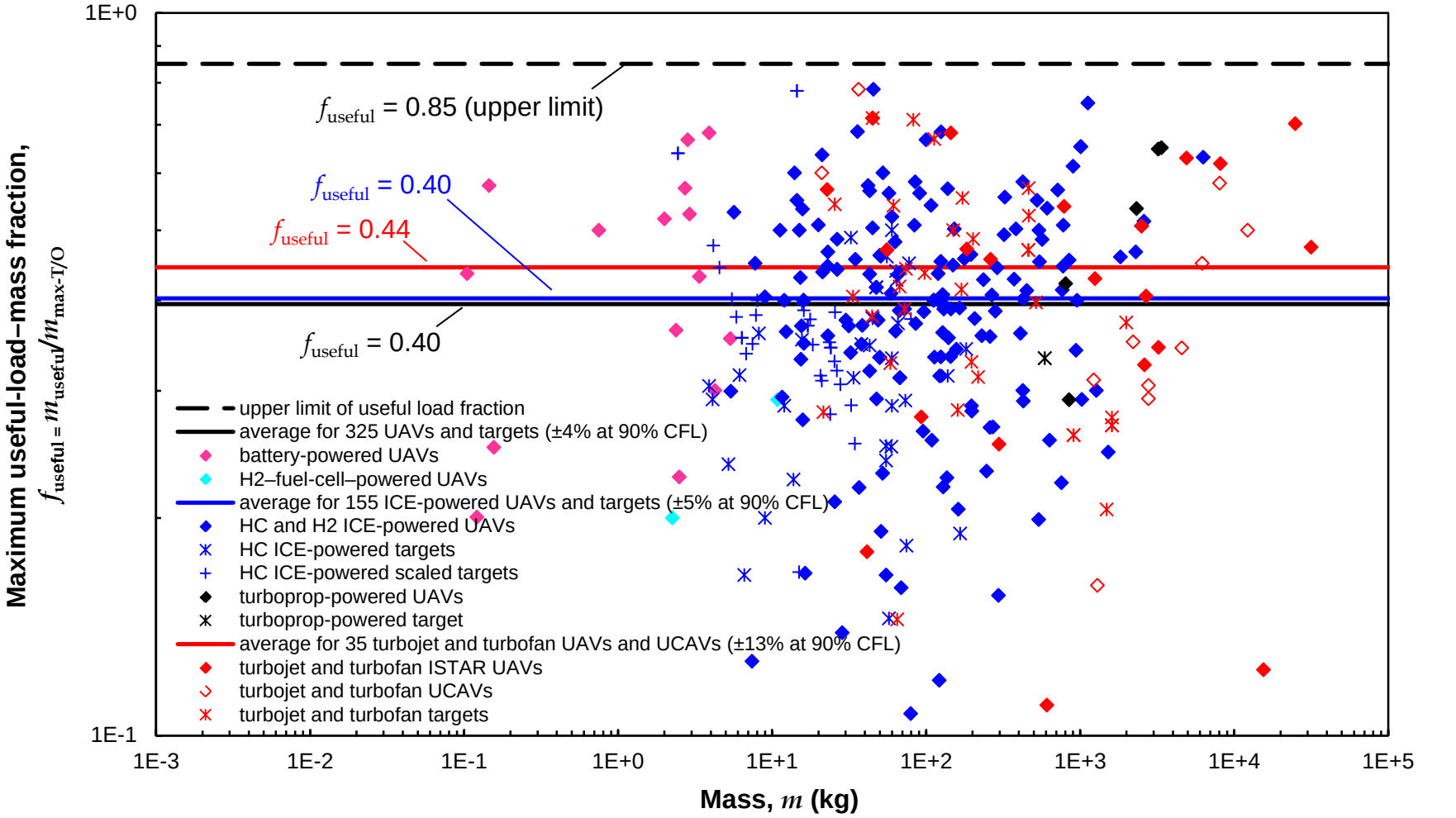

Figure 25 Maximum useful-load–mass fraction (i.e. *maximum payload plus fuel- or battery-mass fraction)* vs. *mean mass for all UAVs in the* Database. *The solid lines show the means for all types of UAVs, ICE-powered UAVs, and turbojet- or turbofan-powered UAVs; and the dashed black line shows an estimate of the upper limit of useful-load fraction for aircraft.*

and UCAVs display a mean payload-mass fraction that is lower than the other types of UAVs and decreases with m at a faster rate than is seen for ICE-powered UAVs.

Conversely, the fuel-mass fraction for turbojet- and turbofan-powered UAVs is on average greater than the battery- or fuel-mass fractions for other types of UAVs, indicating that their designers tend to sacrifice payload to permit higher fuel capacity. This is explained by the greater rate of fuel consumption required to achieve the high airspeeds exhibited by turbojet- and turbofan-powered UAVs (Figure 9). The mean fuel-mass fraction for turboprop-powered UAVs is also greater than that for the 'average' UAV, though to a lesser extent than was found for turbojet- and turbofan-powered UAVs. The differences are particularly observable at the upper end of the weight range (10^3 kg < m < 10^5 kg), where most UAVs designed for HALE ISTAR operation are found. The need for extended endurance explains the differences. Confirming this observation is the fact that the relative load-carrying capacity of turbojet- and turbofan-powered UAVs is actually greater (on average) than that of ICE- and battery-powered UAVs, as evidenced by the data for useful-load–mass fraction given in Figure 25 and Table 9.

An examination of the data for targets shown in Figures 23–25 indicates that their load-carrying capabilities are reasonably similar to those of ISTAR UAVs with the same propulsion systems, with the exception of scaled targets, which carry relatively higher payloads and lower fuel masses than do other targets or ISTAR UAVs. The mean useful-mass fraction of scaled targets is also significantly lower than that for other targets and ISTAR UAVs.

A value of the MTOM–to–mean-mass ratio was also computed from the mean of useful-load–mass fraction for all UAVs in the *Database* to verify its consistency with the value obtained previously. With the definitions of m and useful-load–mass fraction in Table 2, one may obtain a relationship between the MTOM–to–mean-mass ratio and the useful-load–mass fraction ($m_{\text{max-T/O}} / m = \left[1 - f_{\text{useful}} / 2\right]^{-1}$) that yields a MTOM–to–mean-mass ratio of 1.25 with a relative uncertainty of ±4% at 90% CFL, when the average value of the useful-load–mass fraction (0.40) is used. The uncertainty was estimated by error propagation [37]. This MTOM–to–mean-mass ratio is identical to the value obtained from the data shown in Figure 22, which yielded an average MTOM–to–mean-mass ratio of 1.25, which has a relative uncertainty of ±1.4% at 90% CFL.

The other values of useful-load–mass fraction given in Table 9 imply that the mean values of the MTOM–to–mean-mass ratio for ICE-powered UAVs are similar to the mean value for all UAVs; whereas the higher mean value of useful-load–mass fraction for turbojet- and turbofan-powered UAVs implies a higher value of MTOM–to–mean-mass ratio, 1.28. This is in good agreement with the mean value computed for the 35 (ISTAR UAVs or UCAV) turbojet- or turbofan-powered UAVs for which both payload- and fuel-mass fractions were known: 1.30, with a relative uncertainty of ±3.6% at 90% CFL. However, it is difficult to see from the data displayed in Figure 22 because UAVs for which MTOM or m was estimated with incomplete data for payload- and fuel-mass fraction are also plotted.

3.4.3 Payload–Range Product

The product of payload mass and range was examined as a figure of merit for surveillance systems, and the available data for this quantity are displayed as a function of m in Figure 26. However, the payload-mass–range product cannot be used exclusively to represent UAS performance because, in many cases, a value of payload mass (Figure 23) or range (Figure 14) is known, but not both. Therefore, many more data points are presented in Figures 14 and 23 than in Figure 26. Best-fit power laws for the payload-mass–range product have been obtained using exponents based on those used to represent range as a function of m (*i.e.* $\frac{2}{3}$ and $\frac{5}{6}$), increased by one to yield $\frac{5}{3}$ and $\frac{11}{6}$, respectively, to account for the approximate proportionality of payload mass to m (Table 7 and Figure 23).

3.4.4 Payload Types

The payload-type categorisation scheme given in Table 1 was used to create one or more entries describing the possible payloads (if any) for each UAS in the *Database* according to information in published accounts. The payload categories include:

- sensors, each of which is numbered separately, including
  - EO (daylight, low-light, or multi-spectral)
  - IR (or forward-looking IR)
  - radars (*e.g.* synthetic-aperture radar systems)
  - environmental (*e.g.* meteorological)
  - CBRN
  - acoustic
  - ELINT
  - geophysical sensors (*e.g.* magnetometers and terrain sensors)
- communications relay systems
- targeting systems (*e.g.* laser rangefinders or illuminators)
- EW devices (*e.g.* jammers)
- munitions or other weapons
- smoke generators, chaff, flares, sub-targets, and other devices associated with aerial targets
- cargo for transport or aerial release, including
  - safety equipment (*e.g.* buoyancy aids, telephones, strobes, transponders)
  - buoys, sonar sensors, and unmanned underwater vehicles
  - searchlights and megaphones
  - agricultural chemicals.

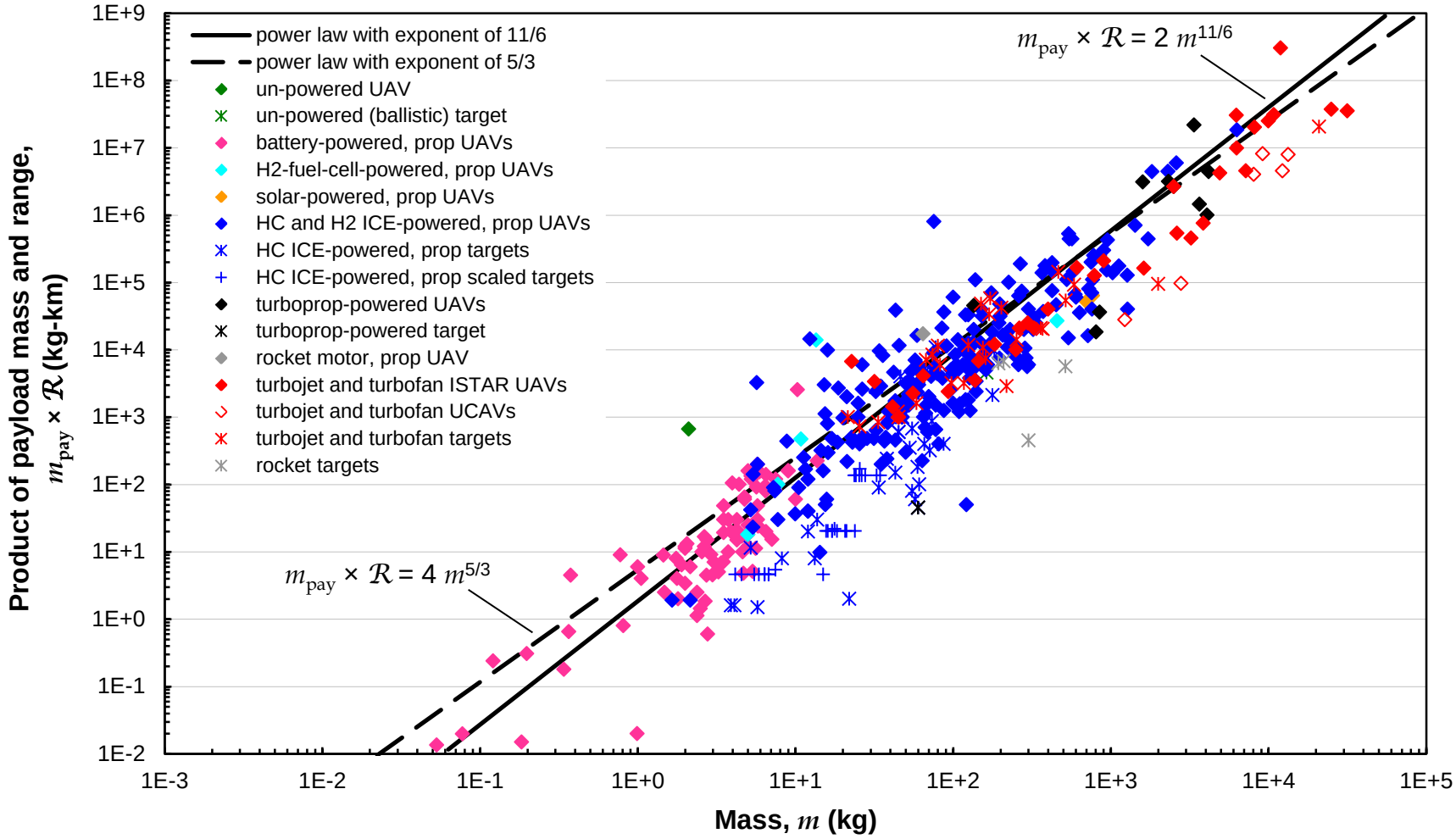

Figure 26 Payload–range product vs. *mean mass for all UAVs in the* Database. *Also shown are power laws with exponents of ⅝ and ¹¹⁄₆, which illustrate the approximate (purely empirical) dependence of* $m_{pay} \times \mathcal{R}$ *on* m.

Up to five entries were made in the *Database* for each UAS, depending on the payloads or payload types given in published descriptions. Up to four payload types were converted, in order of appearance, to numerical codes and entered as the primary, secondary, tertiary, or quaternary payload type for the UAS. If more than four payload types were given, those above four were enumerated in an entry called 'other payloads'.

The number of UAS in the *Database* with each payload option listed in Table 1 is displayed in Figure 27; and the spread of each option across the weight range of all UAS in the *Database* is illustrated in Figure 28. For ~30% of the entries in the *Database*, no payload option is specified in the literature; and another 11% carry no payload. The majority of these entries represent experimental or developmental UAS. The data in Figure 27 indicate that the most common type of payload is an EO sensor. Indeed 44% of the entries in the *Database* indicate that the primary payload is an EO sensor, and 47% have the option of an EO sensor. The data in Figure 28 show that EO sensors are used (or available for use) in UAVs spanning nearly the entire weight range contained in the *Database*.

The most common secondary payload is an IR sensor. EO and IR sensors are often available for the same UAV, with 249 entries in the *Database* (28%) indicating that the primary payload for a given UAS is an EO sensor and its secondary option is an IR sensor (frequently packaged with the EO sensor in a single unit). Only 12% of the entries in the *Database* list an EO sensor as the sole option. Another common payload option is a synthetic-aperture radar, with 8% of *Database* entries including the option of a radar unit. In total, sensors are the only payload types for 30% of the UAS in the *Database*.

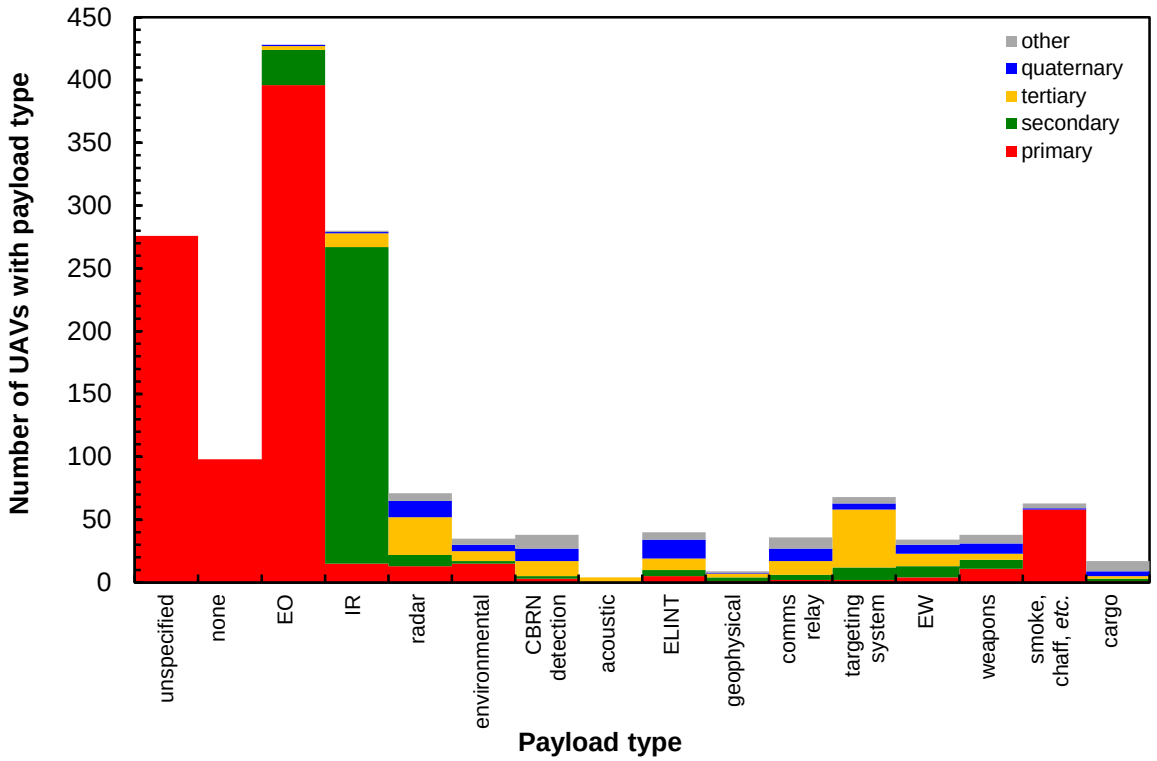

Figure 27 Number of UAVs in the Database *with each payload type*

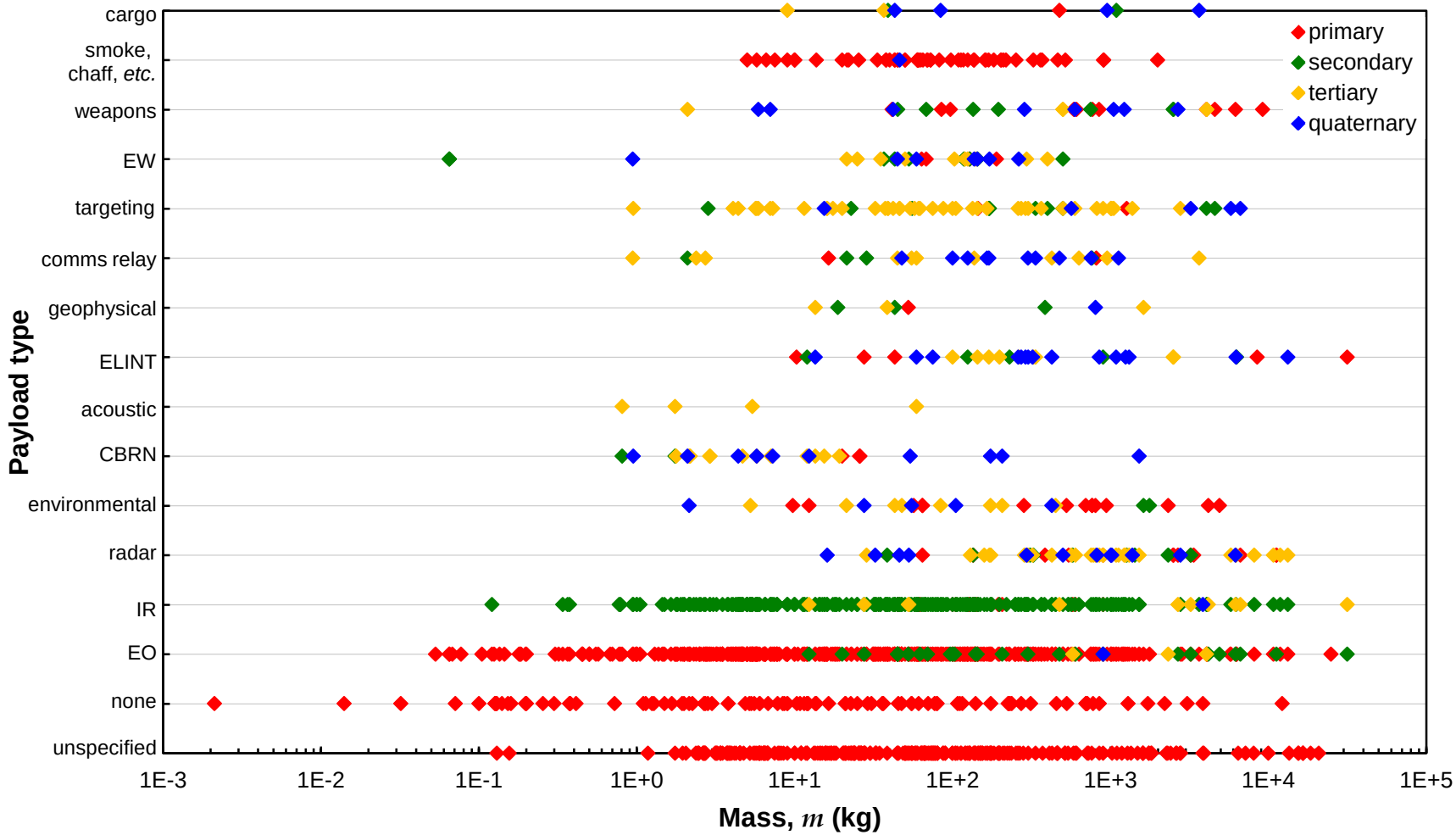

Figure 28 Payload type vs. *mean mass for all UAVs in the* Database. *The primary method is the first or only one listed in descriptions of each UAS. If any other method was mentioned, it is denoted as the secondary, tertiary, or quaternary method, depending on its order of appearance.*

Significant numbers of UAVs (8% of the entries in the *Database*) can carry targeting systems (laser designators or rangefinders); and such systems are often a third option in conjunction with ISR payloads, making a given UAS suitable for ISTAR missions. Smaller numbers of UAS carry cargo or serve as communications-relay platforms, and these are rarely primary or secondary payload options. The carriage of weapons is usually associated with UCAVs; however, published information on most UCAVs included in the *Database* does not specify a payload or no payload is included because the UCAV is in development, rather than being a marketable platform. In fact, most of the UAS in the *Database* with a claimed ability to carry weapons are ISTAR UAS that carry weapons as a non-primary payload option. The same is true for EW payloads, which are mostly carried by platforms with nominally ISTAR missions.

As shown in Table 6, nearly 180 targets are included in the *Database*, representing 20% of the entries. Equipment associated with targets, such as smoke generators, flares, towed targets, miss-distance indicators, chaff dispensers, and IR and radar augmenters, is listed as a payload option for 7% of the UAS entered in the *Database*. As target platforms are typically dedicated to a single mission, in most cases such equipment is the primary (and sole) payload on the air vehicle.

3.5 Launch and Recovery Methods

The numbers of UAVs employing each of the launch methods listed in Table 1 are displayed in Figure 29(a); and Figure 30 shows the launch methods for each UAS in the *Database* (where available), plotted against W to indicate their ranges of applicability. One may observe that wheeled, runway launches, typical of large ISTAR UAVs, targets, and UCAVs, are most common. This is followed by various mechanical (elastic, pneumatic, hydraulic rail) launchers, manual launch, and rocket-assisted launchers. Alternate (*i.e.* secondary or tertiary) methods typically utilise mechanical launchers or rocket boosters and occasionally air deployment or a wheeled undercarriage and a runway. Also found in the *Database* are a few un-powered, ballistic targets and VTOL UAVs that function as fixed-wing UAVs after launch. Launches from submarines, from the roof of a moving ground vehicle, and from a wheeled trolley, usually anchored at the centre of a circular track are equally rare. As shown in Figures 29(a) and 30, the latter two methods are not the primary means by which UAVs are launched, instead being alternative methods for specialised applications.

Figure 29(b) shows the number of UAVs employing each of the recovery methods listed in Table 1, and Figure 31 shows the distribution of each method as a function of the mean weight of the UAS. One may observe that skid, parachute or parafoil, and wheeled, runway landings are by far most common, both as primary and as secondary or tertiary recovery methods. A significant number of ISTAR UAVs are recovered from flight with a net or hook system or captured by a helicopter. Several rely on deep stall for an essentially vertical landing, as distinct from the VTOL UAVs, which are capable of controlled vertical landings and are labelled 'vertical' in Figures 29(b) and 31.

(a)

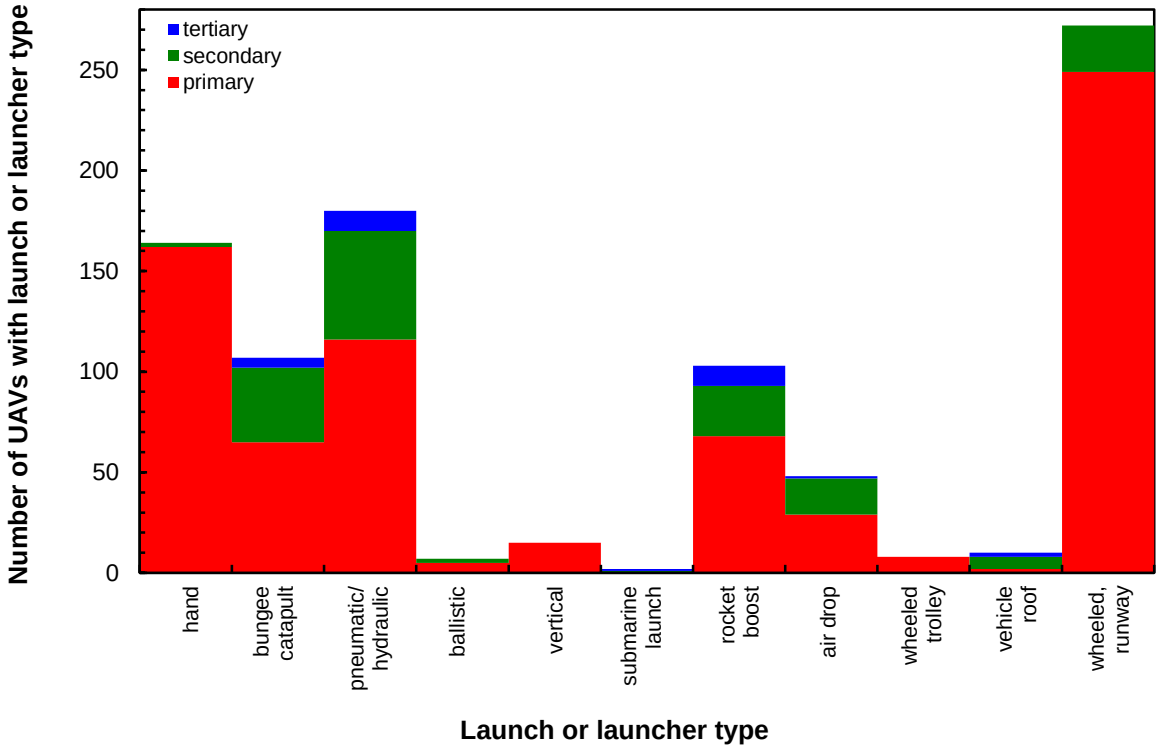

(b)

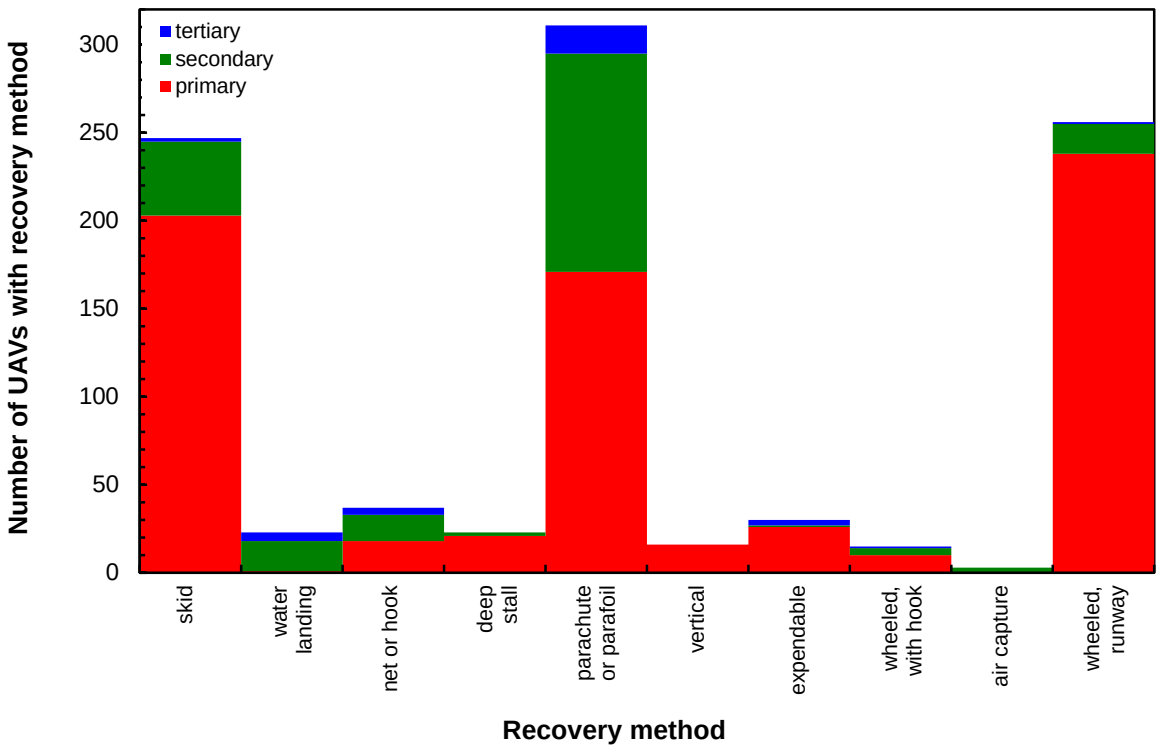

Figure 29 (a) Number of UAVs in the Database *with each launch or launcher type; and (b) number of UAVs in the* Database *with each recovery method*

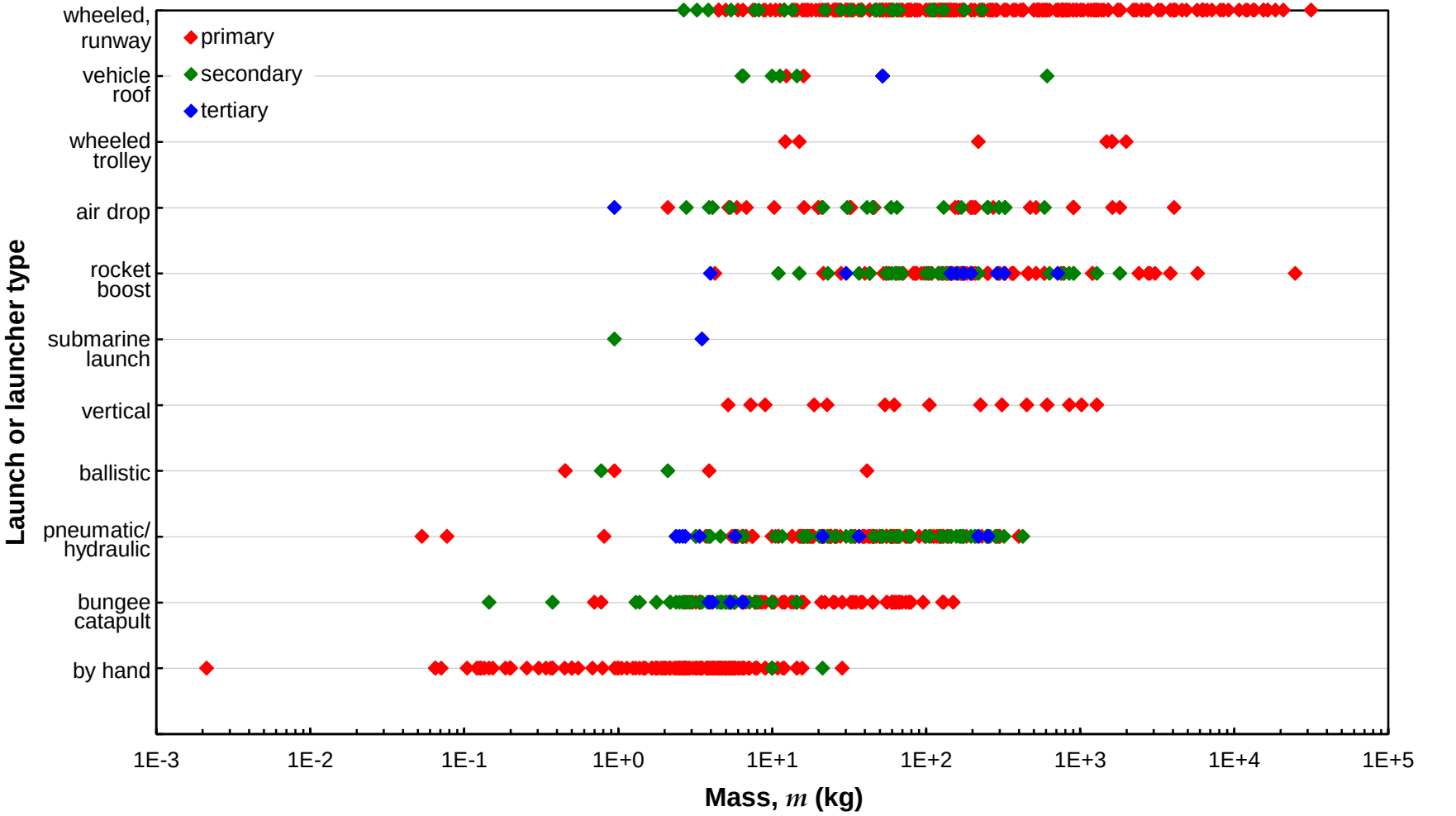

Figure 30 Launch method or launcher type vs. *mean mass for all UAVs in the* Database. *The primary method is the first or only one listed in descriptions of each UAS. If any other method was mentioned, it is denoted as the secondary or tertiary method, depending on its order of appearance.*

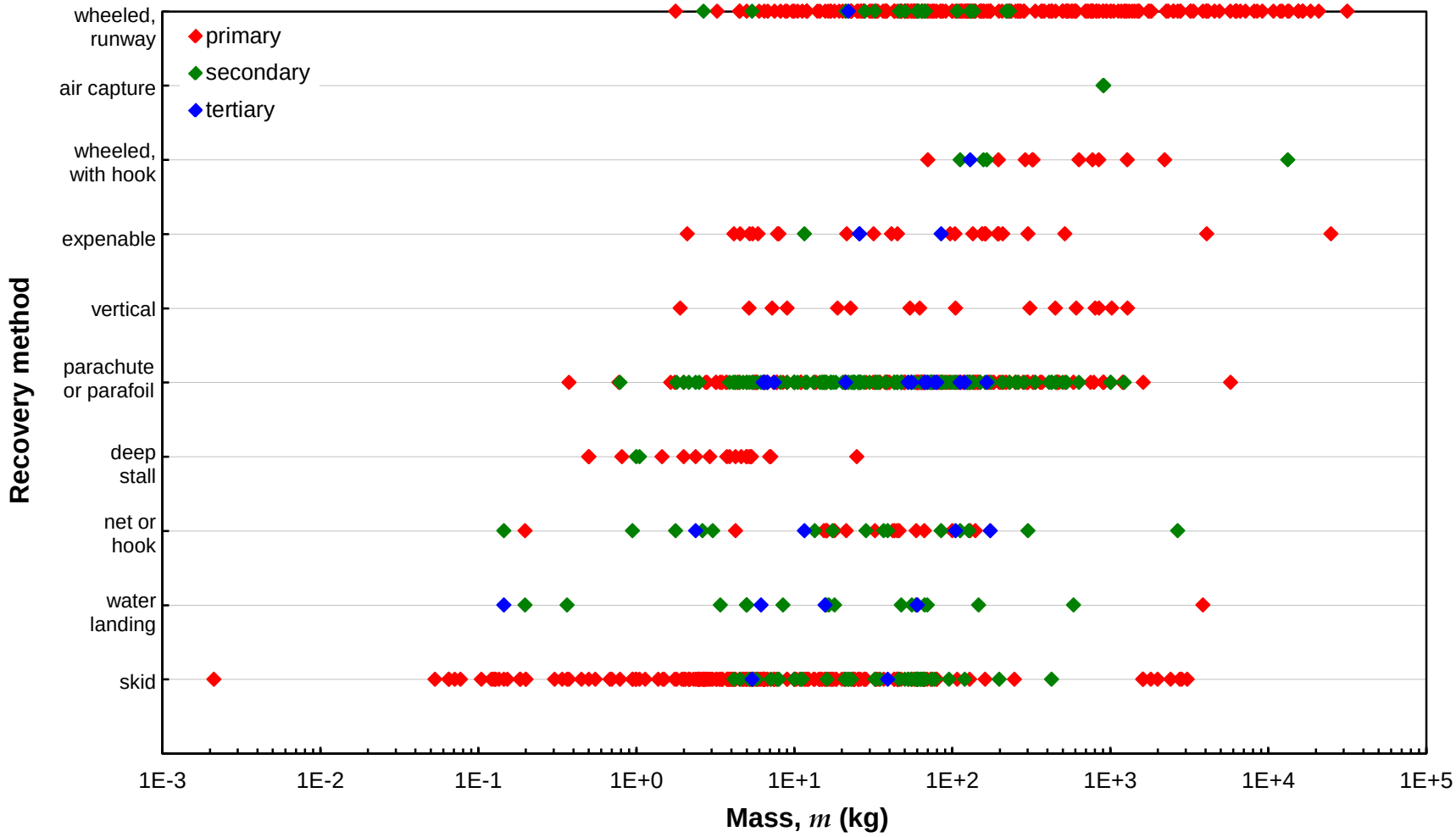

Figure 31 Recovery method vs. *mean mass for all UAVs in the* Database. *The primary method is the first or only one listed in descriptions of each UAS. If any other method was mentioned, it is denoted as the secondary or tertiary method, depending on its order of appearance.*

4 Comparative UAS Analysis

The relatively large spread of the UAS data around the scaling laws for manned aircraft and birds in Figures 2–12, when compared with the RMS errors associated with the best-fit power laws, suggests that UAVs have a broader range of geometric and aerodynamic characteristics than do the other categories of flyers. This greater observed variability is probably explained by their having a greater level of mission diversity and by the availability of alternative propulsion systems (*e.g.* electric systems). For example, UCAVs were included, but the scaling laws were derived from data for manned civil aviation and transport aircraft, rather than the (perhaps) more appropriate manned aircraft: tactical fighters and trainers. Another explanation is the diversity of propulsive methods. For instance, UAVs powered by solar and fuel cells have relatively low power available for propulsion (compared with UAVs equipped with liquid-fuelled or rocket engines) and thus are designed to be as efficient as possible.

In combination with the scaling laws derived for manned aircraft, the aggregated aerodynamic and performance data for UAS reveals areas in which technological advances may lead to significantly improved system performance. One example of this is the use of fuel cells as power sources for electric propulsion on UAVs; the points representing fuel-cell–powered UAVs on the performance plots (*e.g.* Figure 13), though small in number, indicate that such systems may offer significant advantages and enable the use of electric propulsion for larger size UAVs than do batteries. As noted in Section 3, a great deal of research is underway globally to develop fuel-cell–powered propulsion for manned and unmanned aircraft [6, 25, 38, 39].

At present, most UAS research and development efforts fall into three categories: (1) efforts to create operationally useful MAVs for missions in confined spaces (*e.g.* indoors and in urban canyons); (2) efforts to increase the range and endurance of ISTAR missions by small (*e.g.* hand-launched and tactical) and large (*e.g.* HALE) UAVs; and (3) efforts to create low-observable UAVs or UCAVs for penetrating, long-range strike missions and air combat. Each of these areas may be analysed through the use of the *UAS Database*; and examples of the first two are discussed below.

4.1 MAVs and NAVs

MAV technologies represent one area of UAS development that may be studied through comparative analysis. MAV research began with the Black Widow and Microbat projects, both of which were funded by the US Defense Advanced Research Projects Agency (DARPA) in the late-1990's, with the goal of demonstrating small, low-cost air vehicles with practical ISR capabilities [30, 40, 41]. Since then, developments have continued worldwide with many university groups building MAV-class fixed-, flapping-, and rotary-wing vehicles [9, 42-44]. DARPA also announced a 'nano' air vehicle (NAV) program in 2005, seeking the development of an ISR platform with a maximum dimension (and wingspan or rotor diameter) of 0.075 m and a mass of less than 0.01 kg [45, 46]. NAVs are also required to carry a payload of at least 0.002 kg and to have an endurance of 20 min.

In addition to the UAS data shown in this report, data on the characteristics of many unmanned rotary-wing vehicles (*e.g.* helicopters and ducted fans) has been gathered for comparison with those of the fixed-wing UAS and to enable the development of scaling laws for other classes of air vehicle, should such relationships prove descriptive and useful. The relative advantages of fixed- and rotary-wing MAVs were examined in detail by Palmer [9], in terms of their compactness, payload or useful-load capacity, and endurance for a given vehicle mass, features that determine the suitability of a platform for a given surveillance mission, along with its covertness and portability, among other features. The primary goal of the study was an exploration of MAVs and candidate solutions for DARPA's NAV program.

Of the seven rotary-wing UAVs that satisfy the MAV requirement for a rotor diameter of 0.15 m or less, only one potentially meeting NAV size and mass constraints was identified [9]; although, in that case, the MAV is a small experimental helicopter with a total length over the 0.075-m limit for a NAV. No fixed-wing platform smaller than the original MAV specification (*i.e.* having a maximum dimension of 0.15 m or less) has been described in the open literature, with the exception of a 0.1-m–wingspan, 0.002-kg glider that, even if scaled to a larger size and mass to meet the 0.002-kg payload specification, would likely be unable to meet other NAV requirements. However, based on the range of rotary-wing MAVs developed and tested worldwide, it would appear likely that a design meeting the size, mass, and payload requirements for a NAV is feasible.

Those considerations aside, a much more severe challenge for NAV designers is the required endurance of 20 min. While fixed-wing MAVs are typically capable of flying for 30 min, rotary-wing MAVs of the same mass achieve roughly 40% of the endurance of their fixed-wing counterparts. This fraction varies somewhat over the range of UAV mass considered [9], from ~30% at $W = 0.001$ kg to ~50% at 10 kg. At the maximum mass for a NAV, 0.01 kg, rotary-wing platforms are currently capable of flights of only ~3-min endurance. Attempts to increase their endurance by substituting additional batteries for payload would only achieve an endurance of ~5 min, because the typical payloads and useful loads of UAVs, whether fixed- or rotary-wing, are ~20% and ~50% of W, respectively. If batteries comprising 30% of W provide 3-min endurance, then added batteries that replace the payload and comprise 20% of W would provide an additional 2 min of endurance, for a total of 5 min.

Needless to say, eliminating all payload in favour of additional batteries would render the platform unusable for ISR missions. Additionally, this computation represents an optimistic estimate of the endurance gained by replacing the payload of a NAV-scale rotary-wing platform with batteries, because (based on the very small sample of data available) MAVs at the lower end of the mass range tend to have smaller payload capacity relative to their useful loads, meaning that payload has likely already been sacrificed for battery capacity.

Another option is the use of batteries with higher specific energy (and presumably energy density) than the rechargeable lithium-ion or -polymer cells currently employed in most portable electric devices. An energy-storage device with 6–7 (≈ 20 min/3 min) times more energy per unit mass (and volume) would be necessary for a NAV-scale rotary-wing

platform to obtain the required endurance. Research on existing batteries and comparisons with other forms of energy storage (*e.g.* primary Li-ion cells and supercapacitors) indicate that an improvement of almost a factor of three is likely possible with current technologies [6], meaning that the endurance of a rotary-wing MAV would still fall at least a factor of 2 short of the NAV goal.

Flapping-wing platforms may hold promise for greater flight efficiency and thus greater endurance with the same battery capacity, as suggested by data indicating that, at best-range conditions, birds use only ~¾ of the propulsive power required by a manned aircraft scaled to the same mass [19], affirming the general principle that biological systems are more strongly driven to higher efficiency than are their man-made counterparts [47], which often sacrifice energy efficiency for airspeed or other performance characteristics. An empirical exploration of the characteristics of entomopters and ornithopters (*i.e.* insect- and bird-like flyers, respectively) through comparisons with insects, birds, and bats, similar to that presented in Reference [9] for fixed- and rotary-wing MAVs, is thus warranted, as is a comparative analysis of fixed-, rotary-, and flapping-wing MAVs.

4.2 HALE UAVs and Other Efficient Flyers

The *UAS Database* provides many opportunities to examine the development of the characteristics of a particular UAS or of a class of UAS and to study the effects of various design drivers. For example, the history and design influences of the Predator family of tactical UAS have been documented [11], and the same may be done for HALE UAS. The latter are important because of the strategic advantages they can provide as re-taskable 'pseudo-satellites' [48]. In brief, the international research and development of HALE UAS may be traced back to the Compass Cope project, a 1960's US Air Force competition for the development of a high-altitude, long-range remotely piloted vehicle (RPV) for long-endurance photographic-reconnaissance and electronic-surveillance missions, through the 1980's with Boeing's Condor [34], and to the present deployments of Global Hawk by the US Air Force and Navy [49].

One of the chief design and technology drivers for HALE UAS has been the need to maximise propulsive efficiency to increase endurance and power availability for payload, communications, *etc.* At its most extreme, HALE research has taken the form of efforts to develop extremely lightweight, flexible airframes that incorporate solar power, for instance, in NASA's Environmental Research Aircraft and Sensor Technology (ERAST) project. Similarly novel aircraft have also been developed in more recent projects sponsored by the US Air Force and DARPA [50]. Solar power is attractive for HALE UAVs because of the possibility it presents for endurance limited only by maintenance requirements and reliability; however, its use imposes strict limits on energy consumption over the course of a mission and hence the need for designs fully optimised for that requirement [51]. Research on solar HALE UAVs originated from the development of manned solar-powered aircraft, which in turn may be traced back to experiments with human-powered aircraft [32]. In each case, successful designs were optimised for minimum power consumption, rather than for maximum efficiency *per se* [33].

In contrast, the designers of traditionally powered HALE UAVs, which must cruise and loiter efficiently to maximise endurance and other performance parameters, aim for a combination of propulsive, aerodynamic, and structural characteristics that maximise overall efficiency [52, 53]. Maximum aerodynamic efficiency (*i.e.* maximum lift-to-drag ratio, which equates to high flight efficiency for powered aircraft and a minimum sink rate for un-powered aircraft [54]) is also of primary concern in the design of un-powered ISTAR UAVs and manned gliders and sailplanes, as well as for biological species that use gliding or soaring as a strategy for energy conservation and endurance maximisation, as do birds of prey *i.a.* [22, 23] and some bats [55]. The same can be said of truly marginal natural flyers, such as large pterosaurs and archaic birds [23, 56, 57], which are thought to have been incapable of powered take-off and to have used thermal and ridge soaring almost exclusively.

Thus, meaningful comparisons may be made amongst: (1) traditionally powered HALE UAVs and manned HALE aircraft, such as Scaled Composites' Global Flyer and Lockheed's U-2 [20, 35]; (2) other efficient aircraft, including ultralights [20], manned gliders, and un-powered UAVs; (3) power-limited designs, such as UAVs and manned aircraft (HALE or low-altitude) powered by solar and fuel cells and human-powered aircraft; and (4) soaring natural flyers. Systematic differences between the characteristics common to very efficient flyers and those common amongst equivalents that have not necessarily been optimised primarily for flight efficiency (*e.g.* non-HALE UAVs and manned aircraft with traditionally fuelled propulsion systems and small birds with excess power, which frequently exhibit bounding flight [58]) may aid in the identification of design features that maximise flight efficiency as functions of the size, mass, and type of flyer. The features utilised by long-endurance flyers are explored further in Reference [10], where UAVs designed for minimal power requirements are compared with less-optimised versions and their similarities to soaring birds, bats, and pterosaurs are discussed.

One example of this type of comparative analysis is also possible using only the plots provided in Section 3, where the reader may observe that solar- and fuel-cell–powered UAVs generally have much higher values of wingspan and wing area (Figs. 2 and 5, respectively) and lower values of wing loading and best-range airspeed (Figs. 8 and 9, respectively) than do battery-, ICE-, turboprop-, turbojet-, and turbofan-powered UAVs of the same mass, as noted in Section 3.2.1. The relationship between wing loading and best-range airspeed for solar-powered UAVs, in contrast, is similar to that for other UAVs, as well as manned aircraft and birds, implying that the lift coefficient at best-range conditions varies only moderately amongst the different classes of aircraft (with the exception of MAVs) and even birds [19, 54]. Also obvious from this preliminary comparison is the fact that the scaling laws for manned general aviation and transport aircraft, while adequately describing the characteristics of many UAVs, do not adequately reflect the characteristics of those utilising solar power; however, a simple change in the magnitude of the relation for a particular aerodynamic characteristic (*i.e.* a change in the coefficient of the scaling law) can produce a new scaling law descriptive of the data for solar-powered UAVs.

Consider the solar-powered UAVs in two groups: those with $m \lesssim 10$ kg and those with $m > 10$ kg, which happen to roughly represent low- and high-altitude (*i.e.* HALE) designs,

respectively (with a small amount of intermixing). Fitting the data for the wingspans of low-altitude solar-powered UAVs yielded an expression for wingspan, $2.0\,m^{1/3}$, with a relative uncertainty of ±13% at 90% CFL; while the data for solar-powered HALE UAVs yielded $6.2\,m^{1/3}$, which has a relative uncertainty of ±15% at 90% CFL. The coefficients associated with these scaling laws are 2.1 and 6.3 times larger, respectively, than that of the scaling law for manned aircraft derived by Liu [19]: $0.989\,m^{1/3}$, which has a relative uncertainty of ±4% at 90% CFL and represents the wingspans of battery-, ICE-, and turboprop-powered UAVs reasonably well over the range of $1\text{ kg} < m < 10^3\text{ kg}$. The magnitudes of the coefficients and relative uncertainties indicate that the differences observed amongst the scaling laws are not merely the result of the scatter in the data, but rather represent systematic differences amongst these classes of very efficient UAVs and traditionally powered UAVs of the same mass. Similar analyses of the data for wing area and wing loading yielded similar findings: significantly higher values of wing area and lower values of wing loading than other UAVs of the same mass.

The departures of the scaling-law coefficients for solar-powered HALE UAVs from the baseline values applicable to other UAVs and to manned aircraft is reminiscent of the change over the past 100 years of the Gabrielle—von Karman limit-line describing the maximum efficiency of various modes of natural and mechanical locomotion as a function of speed. As discussed by McMasters [47], technological breakthroughs that increase the performance of ground, sea, and air vehicles have monotonically increased the upper limit of efficiency achievable at a given speed, but the slope of the limit-line (*i.e.* the variation of efficiency with speed) remains unchanged. By analogy, applications of new technologies on aircraft may result in changes of the coefficients of the scaling laws describing their characteristics, but the values of the exponents (*i.e.* the dependencies of the scaling laws on mass) are invariant because they are governed by the laws of physics.

An implication of the low wing loadings and high aspect ratios of solar-powered HALE UAVs, and their precursors, human-powered and manned, solar-powered aircraft, is very large wings, often with a high degree of flexibility [32] or, in any case, with minimal structural integrity [51, 59]. This creates fragile aircraft, as evidenced by NASA's Helios UAV, which was lost due to a combination of gusting winds in the lower atmosphere and control problems [60]. Such features are attractive, however, if transits of the lower atmosphere can be avoided or carefully managed [51]. The former is the goal of the Very-high-altitude, Ultra-Long-endurance Theater Reconnaissance Element (VULTURE) program recently undertaken by DARPA [61, 62]. After initial take-off and positioning in high-altitude flight, fragile aircraft would be relatively safe. Additional requirements are then imposed, including most importantly high reliability, which may require the use of space-grade materials.

5 Conclusions and Recommendations

Aerodynamic and performance data for UAS are available from a wide range of sources, including many publications and on-line sources. Collation of a *Database* was found to be necessary because none of the existing sources provides the information in a form that permits detailed mathematical and historical or developmental analyses. A large number of UAS was included both for completeness and, where possible, to permit systematic analyses of UAS characteristics. This also permits meaningful comparison between classes of vehicles (*e.g.* MALE *vs.* HALE) and comparison with the characteristics of natural flyers and manned aircraft.

While the *Database* is useful for examining trends in classes of UAS and identifying candidates with desired characteristics, the reader is reminded that the entries are from published sources and in some cases represent estimated, assumed, or inferred values. The data may also be obsolete, if a manufacturer has, for example, modified or eliminated a design. Performance and other data must be verified directly with the manufacturer or supplier of a given UAS before it is deemed accurate and trustworthy. Independent verification is recommended before acquisition decisions are made.

The *Database* provides a source of data that may be used in historical or developmental studies and empirical analyses, just two of which are described in Section 4. Documented applications include comparisons of fixed and flapping-wing UAVs with birds and comparisons of long-endurance UAVs with ultra-efficient manned aircraft (*e.g.* human-powered aircraft) and natural flyers (*e.g.* soaring birds and bats). The aim of exploring the extremes made possible by the absence of a human pilot has been pursued, beginning with the most obvious: small size and long endurance. Similarly, one could compare and contrast manned tactical fighter aircraft with UCAVs to examine how design changes with the removal of the aircrew (*e.g.* because higher manoeuvre rates are permissible).

As noted previously, the dataset in the original Excel® *Database* has been imported into an Access® *Database* by TTCP AER TP-6. The payload and datalink categories have been expanded by AER TP-6, and the new version of the *Database* is available to the wider DSTO and TTCP communities. It is recommended that researchers wishing to utilise the *Database* employ the Access® version. Maintenance, further validation of the data (on an as-needed basis), and on-going additions may be undertaken by AER TP-6.

References

1. Executive Overview: Unmanned aerial vehicles. *Jane's Unmanned Aerial Vehicles and Targets*, 11 April 2011. Available from: http://catalog.janes.com/catalog/public/index.cfm?fuseaction=home.ProductInfoBrief&product_id=98136 [cited 18 August 2011].

2. United States Department of Defense, *Unmanned systems roadmap 2007–2032*. 10 December 2007, The Office of the Secretary of Defense: Washington, DC, USA.

3. US Department of Defense, *Unmanned systems integrated roadmap, FY2011–2036*. 2011, Washington, DC, USA. Available from: http://www.acq.osd.mil/sts/docs/Unmanned%20Systems%20Integrated%20Roadmap%20FY2011-2036.pdf [cited 8 October 2013].

4. Spreadsheet: Unmanned aerial vehicles and targets contractors *Jane's All the World's Aircraft: Unmanned*, 21 October 2011. Available from: http://www.ihs.com/products/janes/defence/det-products/worlds-aircraft-unmanned.aspx [cited 8 October 2013].

5. Worldwide UAV operators. *Jane's Unmanned Aerial Vehicles and Targets* 2009. Available from: http://www.janes.com/products/janes/defence/air/unmanned-aerial-vehicles-targets.aspx?pu=1&rd=janes_com [cited 6 October 2009].

6. Palmer, J.L., Energy alternatives for unmanned aerial vehicles in *Land Warfare Conference Proceedings*, Puri, V.P., and D. Filippidis, eds., 27–31 October 2008, Brisbane, QLD, Australia. Commonwealth of Australia: Canberra, ACT, Australia, pp. 161–183. Available from: http://dspace-dsto.dsto.defence.gov.au/dspace/handle/dsto/6703 [cited 12 December 2011].

7. Wharington, J.M., and J.L. Palmer, UAV performance improvement through autonomous soaring in *13th Australian International Aerospace Congress, 3rd Australasian Unmanned Air Vehicles Conference*, 9–12 March 2009, Melbourne, VIC, Australia. Defence Science and Technology Organisation: Port Melbourne, VIC, Australia. Available from: http://dspace-dsto.dsto.defence.gov.au/dspace/handle/dsto/6820 [cited 28 October 2013].

8. Harvey, J.R., and J.L. Palmer, *The characterisation of a PEM fuel-cell system with a focus on UAS applications*, November 2013, Report DSTO-TR-2934, Aerospace Division, Defence Science and Technology Organisation: Fishermans Bend, VIC, Australia, p. 58. Available from: http://dspace-dsto.dsto.defence.gov.au/dspace/handle/dsto/24198 [cited 11 June 2014].

9. Palmer, J.L., Aerodynamic and performance characteristics of small unmanned aerial vehicles compared with those of manned aircraft in *13th Australian International Aerospace Congress, 3rd Australasian Unmanned Air Vehicles Conference*, 9–12 March 2009, Melbourne, VIC, Australia. Defence Science and Technology Organisation: Port Melbourne, VIC, Australia. Available from: http://dspace-dsto.dsto.defence.gov.au/dspace/handle/dsto/6821 [cited 28 October 2013].

10. Palmer, J.L., Comparative analysis of long-endurance UAVs and aircraft with soaring birds and bats in *AUVSI Unmanned Systems North America Conference*, Vol. 2, 11–13 August 2009, Washington, DC, USA. Curran Associates, Inc.: Red Hook, NY, USA, pp.

852–870. Available from: http://dspace-dsto.dsto.defence.gov.au/dspace/handle/dsto/6821 [cited 28 October 2013].

11. Blake, B., *The development of the General Atomics unmanned aerial vehicle Predator*, 15 February 2008, ADFA Student Project Report, Air Vehicles Division, Defence Science and Technology Organisation: Fishermans Bend, VIC, Australia.

12. Stagg, A., *The development of BAE Systems unmanned aerial vehicle program*, 29 February 2008, ADFA Student Project Report, Air Vehicles Division, Defence Science and Technology Organisation: Fishermans Bend, VIC, Australia.

13. Clothier, R.A., J.L. Palmer, R.A. Walker, and N.L. Fulton, Definition of airworthiness categories for civil unmanned aircraft systems (UAS) in *27th International Congress of the Aeronautical Sciences (ICAS)*, Vol. 6, 19–24 September 2010, Nice, France. Curran Associates, Inc.: Red Hook, NY, USA, pp. 4611–4622. Available from: http://eprints.qut.edu.au/32789/ [cited 28 August 2013].

14. Clothier, R.A., J.L. Palmer, R.A. Walker, and N.L. Fulton, Definition of an airworthiness certification framework for civil unmanned aircraft systems. *Safety Science*, **49**(6): pp. 871–885, July 2011. Available from: www.sciencedirect.com/science/article/pii/S0925753511000270 [cited 8 May 2012].

15. *Jane's All the World's Aircraft: Unmanned*, 2013. Available from: http://catalog.janes.com/catalog/public/index.cfm?fuseaction=home.ProductInfoBrief&product_id=98136 [cited 23 August 2009].

16. Unmanned aerial vehicles and drones. *Aviation Week & Space Technology*, **168**(1): pp. 114–122, 28 January 2008.

17. *Shephard UVOnline UAV DataSource*, 2008. Available from: http://www.shephard.co.uk/UVonline/UVSpecs.aspx [cited 14 July 2008].

18. *AUVSI's Online Guide to Unmanned Systems*, 2010. Available from: http://guide.auvsi.org/auvsi/index.form [cited 7 January 2011].

19. Liu, T., Comparative scaling of flapping- and fixed-wing flyers. *AIAA Journal*, **44**(1): pp. 24–33, January 2006.

20. *Jane's All the World's Aircraft*, 2010. Available from: http://catalog.janes.com/catalog/public/index.cfm?fuseaction=home.ProductInfoBrief&product_id=96083 [cited 7 January 2011].

21. Tennekes, H., *The simple science of flight: from insects to jumbo jets*. 1st MIT Press paperback ed. 1997, MIT Press: Cambridge, MA, USA.

22. Alerstam, T., M. Rosén, J. Bäckman, P.G.P. Ericson, and O. Hellgren, Flight speeds among bird species: Allometric and phylogenetic effects. *PLoS Biology*, **5**(8): p. e197, 1 August 2007. Available from: http://dx.doi.org/10.1371%2Fjournal.pbio.0050197 [cited 8 October 2013].

23. Chatterjee, S., R.J. Templin, and K.E. Campbell, Jr., The aerodynamics of *Argentavis*, the world's largest flying bird from the Miocene of Argentina. *Proceedings of the National Academy of Sciences of the United States of America*, **104**(30): pp. 12398–12403, 24 July 2007.

24. Devore, J.L., *Probability and statistics for engineering and the sciences*. 1982, Brooks/Cole Publishing Company: Monterey, CA, USA.

25. Verstraete, D., J.R. Harvey, and J.L. Palmer, Hardware-in-the-loop simulation of fuel-cell-based hybrid-electrical UAV propulsion. Paper ICAS2012-4.5.2 in *28th International Congress of the Aeronautical Sciences (ICAS)*, Vol. 4, Grant, I., ed., 23–28 September 2012, Brisbane, QLD, Australia. Curran Associates, Inc.: Red Hook, NY, USA, pp. 2662–2674. Available from: www.icas.org/ICAS_ARCHIVE/ICAS2012/PAPERS/656.PDF [cited 23 August 2013].

26. Verstraete, D., J.R. Harvey, and J.L. Palmer, Analysis of the performance of fuel-cell-based hybrid-electrical UAV propulsion through hardware-in-the-loop simulation. Paper ISABE-2013-1706 in *21st International Symposium on Air-Breathing Engines (ISABE)*, 9–13 September 2013, Busan, Korea. Available from: http://dspace-dsto.dsto.defence.gov.au/dspace/handle/dsto/17919 [cited 14 January 2014].

27. Harvey, J.R., R.L. Bagg, D. Honnery, and J.L. Palmer, An investigation into the influence of environmental conditions on the performance of a hybrid-electric unmanned aircraft in *15th Australian International Aerospace Congress*, 25–28 February 2013, Melbourne, VIC, Australia. Royal Aeronautical Society (Australian Division) and Engineers Australia: Mascot, NSW, Australia, pp. 161–172. Available from: http://search.informit.com.au/fullText;dn=352650170047569;res=IELENG [cited 14 January 2014].

28. Templin, R.J., The spectrum of animal flight: Insects to pterosaurs. *Progress in Aerospace Sciences*, **36**(5): pp. 393–436, May–June 2000.

29. Michelson, R.C., Novel approaches to miniature flight platforms. *Proceedings of the Institution of Mechanical Engineers, Part G: Journal of Aerospace Engineering*, **218**(6): pp. 363–373, 2004.

30. Grasmeyer, J.M., and M.T. Keennon, Development of the Black Widow micro air vehicle, Paper AIAA-2001-0127. Presented at *Technical Papers — 39th AIAA Aerospace Sciences Meeting and Exhibit*, 8–11 January 2001, Reno, NV, USA: American Institute of Aeronautics and Astronautics, Inc.: New York, NY, USA.

31. Hale, F.J., *Introduction to Aircraft Performance, Selection, and Design*. 1984, John Wiley & Sons, Inc.: New York, NY, USA. p. 290.

32. MacCready, P.B., P.B.S. Lissaman, W.R. Morgan, and J.D. Burke, Sun powered aircraft design. Paper AIAA-81-0916 in *Technical Papers — Frontiers of Achievement*, 12–14 May 1981, Long Beach, CA, USA. American Institute of Aeronautics and Astronautics, Inc.: New York, NY, USA, p. 13.

33. The Open University, *Conceptual design for human powered flight: A comparison of two design spaces*, 2009. Available from: http://openlearn.open.ac.uk/mod/resource/view.php?id=211299 [cited 15 May 2009].

34. Henderson, B.W., Boeing Condor raises UAV performance levels. *Aviation Week & Space Technology*, **132**(1): pp. 36–38, 23 April 1990.

35. Scaled Composites, *Virgin Atlantic Global Flyer*, 2006. Available from: http://www.scaled.com/projects/globalflyer.html [cited 8 February 2009].

36. Official records. *Jane's All the World's Aircraft* 28 February 2013. Available from: http://www.janes.com/?fromBanner=true [cited 8 October 2013].

37. Winzer, P.J., Accuracy of error propagation exemplified with ratios of random variables. *Review of Scientific Instruments*, **71**(3): pp. 1447–1454, March 2000. Available from: http://link.aip.org/link/?RSI/71/1447/1 [cited 8 October 2013].

38. Verstraete, D., K. Lehmkuehler, A.T.Y. Gong, J.R. Harvey, G. Brian, and J.L. Palmer, Characterisation of a hybrid, fuel-cell-based propulsion system for small unmanned aircraft. *Journal of Power Sources*, **250**: pp. 204–211, 15 March 2014. Available from: http://www.sciencedirect.com/science/article/pii/S0378775313018430 [cited 5 December 2013].

39. Verstraete, D., A.T.Y. Gong, D. Lu, and J.L. Palmer, Experimental investigation of the role of the battery in the AeroStack hybrid, fuel-cell-based propulsion system for small unmanned aircraft systems. *International Journal of Hydrogen Energy (accepted)* 2014.

40. Hewish, M., A bird in the hand. *Jane's International Defence Review*, **32**(11) 1 November 1999. Available from: https://janes.ihs.com/CustomPages/Janes/DisplayPage.aspx?DocType=News&ItemId=+++1099348&Pubabbrev=IDR [cited 23 August 2013].

41. Pornsin-sirirak, T.N., Y.-C. Tai, C.-M. Ho, and M.T. Keennon, Microbat: A palm-sized electrically powered ornithopter in *NASA/JPL Workshop on Biomorphic Robotics*, 14–16 August 2001, Pasadena, CA, USA. Jet Propulsion Laboratory: Pasadena, CA, USA.

42. Tanaka, H., K. Hoshino, K. Matsumoto, and I. Shimoyama, Flight dynamics of a butterfly-type ornithopter in *Proceedings of the IEEE/RSJ International Conference on Intelligent Robots and Systems*, 2–6 August 2005, Edmonton, Alberta, Canada. IEEE: Piscataway, NJ, USA, pp. 310–315.

43. Zdunich, P., D. Bilyk, M. MacMaster, D. Loewen, J.D. DeLaurier, R.D. Kornbluh, T.P. Low, S.E. Stanford, and D. Holeman, Development and testing of the Mentor flapping-wing micro air vehicle. *Journal of Aircraft*, **44**(5): pp. 1701–1711, September–October 2007.

44. Wood, R.J., Liftoff of a 60mg flapping-wing MAV in *Proceedings of the IEEE/RSJ International Conference on Intelligent Robots and Systems*, 29 October – 2 November 2007, San Diego, CA, USA. IEEE: Piscataway, NJ, USA, pp. 1889–1894.

45. Pines, D.J., *BAA 06-06, Proposer Information Pamphlet (PIP) for Defense Advanced Research Projects Agency (DARPA) Defense Sciences Office (DSO) Nano Air Vehicle (NAV) Program*, December 2005. Available from: www.darpa.mil/dso/solicitations/BAA06-06_sect2.pdf [cited 11 November 2008].

46. Hylton, T., *Nano Air Vehicle*, 2008. Available from: http://www.darpa.mil/dso/thrusts/materials/multfunmat/nav/index.htm [cited 18 October 2008].

47. McMasters, J.H., Reflections of a paleoaerodynamicist. *Perspectives in Biology and Medicine*, **29**(3, Part 1): pp. 331–384, Spring 1986.

48. Executive Overview: IHS Jane's All the World's Aircraft: Unmanned. *Jane's Unmanned Aerial Vehicles and Targets* 2012. Available from: http://www.janes.com/products/

janes/defence/air/unmanned-aerial-vehicles-targets.aspx?pu=1&rd=janes_com [cited 8 May 2012].

49. Northrop Grumman RQ-4 Global Hawk. *Jane's Unmanned Aerial Vehicles and Targets* 2010. Available from: http://www.janes.com/products/janes/defence/air/unmanned-aerial-vehicles-targets.aspx?pu=1&rd=janes_com [cited 17 May 2010].

50. Palmer, J.L., Addressing energy as a military cost. *Australian Defence Force Journal*, **178**: pp. 91–116, May 2009. Available from: http://www.adfjournal.adc.edu.au/UserFiles/issues/178%202009%20Mar_Apr.pdf [cited 8 May 2012].

51. Laurenzo, R., Soaring on a Solar Impulse. *Aerospace America*: pp. 32–36, May 2009. Available from: http://www.aiaa.org/aerospace/images/articleimages/pdf/32%20-%20Solar%20Impulse_MAY2009.pdf [cited 7 February 2012].

52. Reed, R.D., High-flying Mini-Sniffer RPV: Mars bound? *Astronautics and Aeronautics*, **16**(6): pp. 26–39, June 1978.

53. Johnstone, R., and N.J. Arntz, CONDOR — High altitude long endurance (HALE) automatically piloted vehicle (APV), Paper AIAA-90-3279. Presented at *Technical Papers — AIAA/AHS/AESS Aircraft Design, Systems, and Operations Conference*, 17–19 September 1990, Dayton, OH, USA: American Institute of Aeronautics and Astronautics, Inc.: New York, NY, USA.

54. Lan, C.-T.E., and J. Roskam, *Airplane Aerodynamics and Performance.* 1980, Roskam Aviation and Engineering Corporation: Ottawa, KS, USA.

55. Lindhe-Norberg, U.M., A.P. Brooke, and W.J. Trewhella, Soaring and non-soaring bats of the family Pteropodidae (flying foxes, *Pteropus* spp.): Wing morphology and flight performance. *Journal of Experimental Biology*, **203**(3): pp. 651–664, 1 February 2000. Available from: http://jeb.biologists.org/cgi/reprint/203/3/651.pdf [cited 8 October 2013].

56. Chatterjee, S., and R.J. Templin, eds. *Posture, locomotion, and paleoecology of pterosaurs, Special paper 376*. 2004, The Geological Society of America: Washington, DC, USA. p. 64.

57. Alexander, D.E., Ancient *Argentavis* soars again. *Proceedings of the National Academy of Sciences of the United States of America*, **104**(30): pp. 12233–12234, 24 July 2007. Available from: http://www.pnas.org/content/104/30/12233.full.pdf+html?sid=af70e026-79c2-4d98-9a6a-866c9094640c [cited 8 October 2013].

58. Keating, H.A., *A literature review on bounding flight in birds with applications to micro uninhabited air vehicles*, March 2002, Report DSTO-GD-0320, AR-012-173, Aeronautical and Maritime Research Laboratory, Defence Science and Technology Organisation: Fishermans Bend, VIC, Australia, p. 10. Available from: http://dspace-dsto.dsto.defence.gov.au/dspace/handle/dsto/3226 [cited 8 October 2013].

59. *Inventing the future*, 2008. Available from: http://www.solarimpulse.com/en/index.php [cited 26 August 2008].

60. Ehernberger, L.J., C. Donohue, and E.H. Teets, Jr., A review of solar-powered aircraft flight activity at the Pacific Missile Range Test Facility, Kauai, Hawaii. Paper P8.3 in *11th Conference on Aviation, Range, and Aerospace Meteorology*, 4–8 October 2004,

Hyannis, MA, USA. American Meteorological Society: Boston, MA, USA, pp. 1063–1069.

61. Davis, S., *The VULTURE air vehicle program*, 16 May 2007. Available from: http://www.arpa.mil/baa/SN07-38.html [cited 30 October 2007].

62. Newman, D., *VULTURE*, 19 February 2008. Available from: http://www.darpa.mil/ucar/Programs/Vulture.htm [cited 15 October 2008].

63. ESDU International, *ESDU 77022, Equations for calculation of International Standard Atmosphere and associated off-standard atmospheres*, 1986. Available from: http://www.esdu.com/cgi-bin/ps.pl?sess=unlicensed_1130814010556bzh&t=doc&p=di_77022c [cited 23 August 2013].

Acknowledgements

I would like to thank my colleagues Mr Howard Quick and Dr John Wharington for their assistance with the power-requirement computations discussed in this report. Howard Quick also researched and entered many of the values for power-plant mass in the *UAS Database*. My thanks go as well to Pilot Officer Brendan Blake and Cadet Officer Andrew Stagg, Australian Defence Force Academy students who undertook periods of work experience with me in early 2008, during which they verified portions of the *Database* and made additions to it. Mr James R. Harvey is thanked for his additions as well. Mr Geoff Brian and Mr Stephen Kracinovich (US NAVAIR) are thanked for their assistance with editing the report. I am particularly grateful to Prof Tianshu Liu of Western Michigan University, who provided me with extensive data for manned aircraft and birds that he assembled for an article cited in this report. The idea for this project originated with Dr Simon Henbest.

Appendix A Detailed Description of UAS Data Entry

A.1 Masses and Weights

As described in Section 2, an entry for a given UAS was made in the *UAS Database* only if the maximum take-off mass of the UAV and its wingspan were available or calculable. If the 'empty' or 'dry' aircraft mass (*i.e.* the mass without payload or fuel) was unknown, it was estimated from the value of maximum take-off mass with any values given for payload and fuel masses subtracted. Alternatively, if the empty, payload, and fuel masses were known, the maximum take-off mass was estimated by summing those quantities; and the UAS was entered in the *Database*. The empty mass of battery-powered UAVs normally includes the battery pack; and information about the battery mass is sometimes provided by the manufacturer. If an 'empty' mass not including a battery was provided, the battery mass was added to the empty mass before the latter was entered; and the maximum take-off mass (if not stated) was computed by summing the empty and payload masses.

Table 2 lists the masses and weights entered or computed for each UAS in the *Database*. Values of maximum take-off and empty mass for each UAV were entered as described above, the input method was recorded with a code, the mean mass, m, was computed, and the masses were converted to equivalent weights. The values of payload, fuel or battery, and the airframe mass (if given) were entered and used to compute mass fractions. In many cases, the permitted maximum mass of payload plus fuel was less than the sum of payload and fuel masses (*i.e.* payload may be traded for fuel by the operator, if desired). Therefore, the maximum useful load was input separately (if available) or estimated (from the payload and fuel or battery mass) and used to compute a useful-load–mass fraction.

A.2 Geometric and Aerodynamic Characteristics

The input geometric parameters, listed in Table 3, included the total length and height of the aircraft and the length and maximum width of the aircraft fuselage. If the UAV has no fuselage (*e.g.* it is a flying wing), the values for fuselage length and maximum width were set to 0. The span, planform area, and aerofoil profile of the main wing were input; and the mean wing chord, aspect ratio, and mean wing loading were calculated from these values. The span and area of any horizontal fore-plane and tail-unit surfaces were also recorded (if they exist and their lengths were known). In some cases, the wing area was computed from a published value of wing loading and the maximum take-off or mean mass for the UAV or estimated from the published vehicle geometry (*i.e.* images or drawings) and known values of wingspan and/or total aircraft or fuselage length.

A.3 Performance Characteristics

As indicated in Table 4, whenever possible, several performance characteristics were entered, including the stall, best-loiter (minimum-power), best-range (maximum-range or cruise), maximum, never-exceed, and launch or take-off speeds of the UAV. If a value for

loiter airspeed was provided, but no best-range airspeed was given, a value equal to 1.32 times the loiter airspeed was input for best-range airspeed [54]; and, conversely, if only best-range airspeed was given, the loiter airspeed was estimated from it. The maximum vertical climb rate (usually specified at sea level) was also entered, as were the altitudes at which the given best-range and maximum airspeeds were applicable, along with the minimum and maximum operating altitudes of the UAV and its ceiling.

The ceiling value is simply the stated maximum useable altitude of the UAV, rather than strictly its service ceiling, a term commonly used to describe manned aircraft, denoting 'the density altitude at which flying in a clean configuration, at the best rate of climb airspeed for that altitude and with all engines operating and producing maximum continuous power, will produce a 100 feet per minute climb' [31]. In some cases, published sources provided a true service ceiling (*e.g.* for large ICE-, turboprop-, turbojet-, or turbofan-powered UAVs); while, in many others (*e.g.* small, battery-powered UAVs), the UAV is incapable of climbing at 100 ft/min (*i.e.* 30 m/min), so the reported 'ceiling' corresponds to the upper limit its operation or (often) to its absolute ceiling [31].

The various airspeeds are often published in the form of Mach numbers. If so, then the speed of sound at the given loiter, best-range, or maximum altitude (or at the average operating altitude, if no specific altitude is given) was computed using relations for the International Standard Atmosphere (ISA) [63]; and the product of the sound speed and Mach number was input to the *Database*.

For turbojet- or turbofan-propelled UAVs (and manned aircraft), the value provided for best-range airspeed in published reports was often more accurately interpreted as an operating airspeed, rather than as the maximum-range airspeed for the airframe, as evidenced by the fact that the stated 'cruise speed' was often significantly higher than 1.32 times the loiter airspeed. Therefore, for turbojet- and turbofan-powered UAVs, the published best-range airspeed was usually entered in the *Database* as the operating speed, V_{op}, and the 'cruise altitude' as the operating altitude. The published 'cruise' values were entered as maximum-range conditions only if the speed is termed an 'economy cruising' speed or some other indication was given that it represented the maximum-range airspeed.

Frequently, only a maximum airspeed is provided for turbojet- or turbofan-propelled UAVs. In that case, a value equal to 92% of the maximum airspeed was input for the operating airspeed for relatively large, turbojet- or turbofan-powered UAVs (with $W_{max\text{-}T/O} > 10^4$ N). This estimate was based on the finding, described in Section 3.2.1, that the mean operating-to-maximum airspeed ratio for turbojet- and turbofan-powered UAVs in this mass class is ~92%, with a relative RMS error of ±2%. For smaller UAVs, the maximum and operating airspeeds are not strongly coupled and the operating-to-maximum airspeed ratio varies from 0.5 to 1, likely due to mismatches between the power requirements of the given UAV and the limited selection of small turbojet and turbofan engines available for use. For this reason, if no published value of operating airspeed was available for UAVs with $W < 10^4$ N, none was input to the *Database*. Conversely, if only an operating airspeed was provided, an estimate of the maximum airspeed obtained by di-

viding that value by 0.92 was input for UAVs with $W > 10^4$ N. As indicated in Table 4, the Reynolds number based on the mean wing chord and best-range speed, which indicates the relative magnitudes of the inertial and viscous forces in the flow over the wings of an air vehicle, was computed using the value of air viscosity at standard conditions, 1.46×10^{-5} m^2/s [63]. For turbojet- and turbofan-powered UAVs, a Reynolds number based on operating airspeed was similarly computed for comparison.

The remaining performance parameters input were the ferry (one-way) range or mission radius, from which a total range value was computed, as indicated in Table 4, and a code signifying whether the datalink range or on-board energy (*i.e.* fuel or battery capacity) limits the total mission range. If a UAV is controlled by a line-of-sight (LOS) datalink (as most small UAVs are), the distance over which LOS control can be maintained usually limits its range; whereas if a UAV is controlled via satellite (as is the case for large UAVs, such as Predator and Global Hawk [15]), then on-board fuel capacity will be the range limiter.

A.4 Propulsion System and Power Requirements

The last category of data entered for each UAV describes its propulsion system and source of power, as shown in Table 5. A description of the power plant was entered, along with a code signifying the type of propulsion system (if any) used, as was the mass of the power plant, from which a mass fraction was evaluated.

For propeller-driven UAVs, the rated power of the electrical motor(s), piston or turboprop engine(s), or rocket motor (in a single case) was entered into the *Database* as the supplied power of the plant; and a supplied power-to-mass ratio was evaluated. Also entered was the estimated or measured efficiency of the propulsion system, which indicates the fraction of the supplied electrical or mechanical power converted to propulsive power. This value was sometimes provided by the designer or manufacturer of the UAS (in which case it was entered directly), or an assumed value based on empirical data for similar systems was input [54]; and a code identifying the entry method was recorded. Most often, the propulsive efficiency was assumed to be 0.4 for electrically driven propellers and 0.8 for propellers driven by piston engines or turboprops.

In some cases, the power required at best-range conditions was provided by the manufacturer and was entered into the *Database*. The maximum propulsive power available from the propulsion system was obtained from the product of supplied power and the stated or assumed value of propulsive efficiency (see Table 5). Occasionally, the maximum thrust provided by the propulsion system (*i.e.* the power plant coupled with the propeller) was also given, in which case that value was entered as the supplied thrust of the power plant. Rarely, the thrust of the power plant at the best-range condition was stated, in which case it too was entered. Alternatively, if values of maximum propulsive power and maximum-range airspeed were provided, the maximum-range thrust was computed from their ratio.

For turbojet-, turbofan-, or rocket-propelled UAVs, the rated thrust of the engine(s) or rocket motor was input to the *Database* as the supplied thrust of the power plant. If the thrust required at best-range conditions was provided, its value was input. The propulsive power supplied by turbojet or turbofan engines or rocket motors was estimated from the product of the rated thrust and the maximum or, in its absence, operating airspeed of the UAV; and, as for propeller-driven UAVs, a supplied-power–to–mass ratio was computed.

The maximum available thrust of whatever propulsion system is used was then computed by dividing $P_{\text{av,max}}$ by $V_{\max}$; and the maximum thrust-to-weight ratio, $T_{\text{av,max}}/W$, was computed. For turbojet-, turbofan-, and rocket-propelled UAVs, this is simply the rated thrust and thrust-to-weight published for the system, T_{supp} and T_{supp}/W, respectively; while, for propeller-driven UAVs, a value that can be used for comparison with other systems and with any published thrust values was obtained.

Also for comparison with published values entered in the *Database*, the propulsive power required at the best-range condition was estimated when values of maximum available power and maximum climb rate were available for propeller-driven UAVs or from the product of supplied thrust and best-range airspeed for turbojet- or turbofan-driven UAVs, as indicated in Table 5. The computation for propeller-driven UAVs relies on the analytical methods employed by Lan and Roskam [54] for manned aircraft and is outlined in Appendix B. From the values of $W_{\text{max–T/O}}$, $V_{\text{max-}\mathcal{R}}$, and $P_{\text{max-}\mathcal{R}}$ (if available), the maximum flight efficiency ($\eta_{\text{flight,max}}$, defined in Table 5), an approximation of the maximum lift-to-drag ratio was evaluated. It could then be compared with any published values.

Appendix B Estimation of Best-Range Power for Propeller-Driven Aircraft

The best-range (*i.e.* cruise) power of an aircraft ($P_{\text{max-}\mathcal{R}}$) may be estimated from known values of maximum available propulsive power ($P_{\text{av,max}}$), best-range airspeed ($V_{\text{max-}\mathcal{R}}$), and maximum vertical climb rate ($(R/C)_{\text{max}}$) by use of the simplified analytical methods described in Chapters 5 and 9 of Lan and Roskam [54]. The values of $P_{\text{max-}\mathcal{R}}$ provided in the *Database* were obtained by the method outlined here. *N.B.* All variables in the following analysis are those at sea level.

At an aircraft's maximum-climb condition, its full propulsive power ($P_{\text{av,max}}$, as defined in Table 5) is assumed to be utilised to provide the power required to overcome drag (P_{req}) and that required purely for the vertical climb. Therefore,

$$P_{\text{av,max}} = P_{\text{req},(R/C)_{\text{max}}} + W(R/C)_{\text{max}}, \tag{B.1}$$

where $P_{\text{req},(R/C)_{\text{max}}}$ is the propulsive power required at the airspeed at which the maximum climb rate is achieved and W is the weight of the aircraft. The required power at any steady flight condition is given by the general relation:

$$P_{\text{req}} = DV, \tag{B.2}$$

where V is the speed of the aircraft. The drag force (D) is balanced by the thrust of the aircraft's propulsion system and is given by:

$$D = \frac{1}{2}\rho S_{\text{wing}} V^2 C_D, \tag{B.3}$$

where ρ is the density of air [63], S_{wing} is the wing area, and C_D is the drag coefficient. If a parabolic approximation is used for the drag polar, one may write:

$$C_D = C_{D,0} + \frac{C_L^2}{\pi e AR}, \tag{B.4}$$

where $C_{D,0}$ is the 'parasitic drag' coefficient, C_L is the lift coefficient, e is Oswald's span efficiency factor, and AR is the wing aspect ratio. In steady flight, when the lift balances the weight of the aircraft, one may also write:

$$W = \frac{1}{2}\rho S_{\text{wing}} V^2 C_L. \tag{B.5}$$

It may be shown that for propeller-driven aircraft at the maximum-climb condition [54], Equation B.4 yields:

$$C_D = C_{D,(R/C)_{\text{max}}} = 4C_{D,0}. \tag{B.6}$$

Evaluating Equations B.2 and B.3 at the maximum-climb condition and substituting the results, along with $C_{D,(R/C)_{\max}}$ from Equation B.6, into Equation B.1 yields:

$$P_{\text{av,max}} - W(R/C)_{max} = 2\rho S_{\text{wing}} V^3_{(R/C)_{\max}} C_{D,0}\,. \tag{B.7}$$

The lift and drag coefficients and forward speed of the aircraft at the maximum-climb condition ($C_{L,(R/C)_{\max}}$, $C_{D,(R/C)_{\max}}$, and $V_{(R/C)_{\max}}$ respectively) may be related to the lift and drag coefficients and speed at the best-range condition ($C_{L,\text{max-}\mathcal{R}}$, $C_{D,\text{max-}\mathcal{R}}$, and $V_{\text{max-}\mathcal{R}}$, respectively) to permit $C_{D,0}$ to be obtained from Equation B.7. At best-range conditions, it may be shown that [54]:

$$C_D = C_{D,\text{max-}\mathcal{R}} = 2C_{D,0}\,. \tag{B.8}$$

Combining Equations B.6 and B.8 with evaluations of Equation B.5 at the best-range and maximum-climb conditions yields:

$$\frac{V_{(R/C)_{\max}}}{V_{\text{max}-\mathcal{R}}} = \sqrt{\frac{C_{L,\text{max-}\mathcal{R}}}{C_{L,(R/C)_{\max}}}} = \frac{1}{\sqrt[4]{3}}\,. \tag{B.9}$$

Substituting $V_{(R/C)_{\max}}$ from Equation B.9 into Equation B.7 and solving for $C_{D,0}$ then gives:

$$C_{D,0} = \frac{3^{3/4}}{2}\frac{P_{\text{av,max}} - W(R/C)_{max}}{\rho S_{\text{wing}} V^3_{max-\mathcal{R}}}\,. \tag{B.10}$$

Finally, the power required at the best-range condition may be obtained by evaluating Equations B.2, and B.3 at the best-range condition and employing Equation B.8. Thus,

$$\begin{aligned} P_{\text{max-}\mathcal{R}} &= \rho S_{\text{wing}} V^3_{\text{max-}\mathcal{R}} C_{D,0} \\ &= \frac{3^{3/4}}{2}\left[P_{\text{av,max}} - W(R/C)_{max}\right], \end{aligned} \tag{B.11}$$

where the expression for $C_{D,0}$ given in Equation B.10 has been used. To assess the reasonableness of the data used in the computation and the result, one may determine e and from Equations B.4 (in combination with Equations B.5 and B.8) and B.10 and compare their values with published data for similar aircraft [54].

Appendix C Scaling Laws for the Characteristics of Manned Aircraft and Birds

Scaling laws for the characteristics of manned aircraft and birds have been presented alongside the data from the *UAS Database* to illustrate the expected dependence of vehicle characteristics on m, based on the assumption of geometric and aerodynamic similarity (*i.e.* characteristic lengths scale as $m^{1/3}$ and C_L is constant) and to demonstrate how the characteristics of UAVs compare with those of other flyers. From data published in *Jane's All the World's Aircraft* [20], Liu [19] derived these scaling laws and empirically based power laws for manned propeller-driven (*i.e.* piston-engine and turboprop) and turbofan-powered transport aircraft, which describe their geometric, aerodynamic, and propulsive characteristics. For convenience, they are provided in Table C.1.

The entry in Table C.1 for the mean wing loading, W/S_{wing}, of manned aircraft differs from the one given by Liu, as he provided a scaling law for the maximum wing loading, $W_{\text{max-T/O}}/S_{\text{wing}}$, rather than for W/S_{wing}. The newly derived relation for W/S_{wing} as a function of m was obtained through least-squares fitting of the data for manned aircraft supplied by Liu, as was the relation for the best-range airspeed, $V_{\text{max-}\mathcal{R}}$, of propeller-driven aircraft as a function of W/S_{wing}. Empirically based best-fit power laws for the installed engine thrust, T_{supp}, were obtained similarly; however, the exponents were not fixed and were products of the linear-regression analyses. *N.B.* The term P_{supp} is used here to represent the total power supplied to the aircraft (or bird) by its engine(s), also sometimes termed installed power; whereas Liu used the term 'available power', P_A, to represent this quantity.

Shown in parentheses with each entry in Table C.1 is the relative uncertainty (at 90% CFL) associated with the best-fit power law. For the scaling laws with fixed exponents (*e.g.* ⅓ for length scales, as dictated by the assumption of geometric similarity), the value represents the relative uncertainty associated with the power-law coefficient. Liu [19] provided mean relative error values; whereas the relative uncertainty values presented here were computed using the raw data supplied by Liu.

Based largely on the biometric data published by Tennekes [21], Liu [19] also provided a similar set of scaling laws and empirical best-fit power laws for birds. Several of these are listed in Table C.1 (where noted), along with a scaling law for the length of a bird's body provided by Templin [28] (and also used by Liu). Additional data for birds was sourced from Alerstam *et al.* [22] and Chatterjee *et al.* [23]; and it, along with the geometrical data provided by Tennekes (via Liu), was regressively fitted to obtain several of the scaling laws given in Table C.1. Because the data for the best-range airspeed, $V_{\text{max-}\mathcal{R}}$, of birds provided by Tennekes was itself the product of an estimation based on a scaling law for $V_{\text{max-}\mathcal{R}}$ in terms of W/S_{wing}, the scaling law for $V_{\text{max-}\mathcal{R}}$ provided by Liu was not used. Instead, it was replaced with the power law for best-range airspeed as a function of m derived by Alerstam *et al.* Likewise, the scaling law for the chord-based Reynolds number associated with fixed-wing cruising flight, $Re_{\text{max-}\mathcal{R}}$, for birds provided by Liu was

Table C.1 Scaling laws and empirical best-fit power laws for manned aircraft and birds that permit estimation of the aerodynamic and geometric characteristics of a flyer given its mean mass, m. The scaling laws for aircraft were derived by Liu [19] or obtained through least-squares fitting or averaging of the data provided by Liu. The scaling laws for birds were obtained by use of data provided by Liu, Alerstam et al. *[22], and Chatterjee* et al. *[23]. Listed in parentheses with each entry is the relative uncertainty at 90% CFL.*

parameter	manned propeller-driven aircraft	manned turbofan-powered aircraft	birds
maximum mass, $m_{\text{max-T/O}}$ or m_{max} (N)	$1.282\ m$ (±1.2%) [a]		$1.242\ m$ (±3.1%) [a]
length, l_{total} (m)	$0.878\ m^{1/3}$ (±2.8%) [a]		$0.306\ m^{1/3}$ (N/A) [b]
maximum fuselage width, d_{fuse} (m)	$0.103\ m^{1/3}$ (±3.2%) [a]		N/A
wingspan, b (m)	$0.989\ m^{1/3}$ (±4.0%) [a]		$1.10\ m^{1/3}$ (±2.5%) [c]
wing area, S_{wing} (m^2)	$0.120\ m^{2/3}$ (±8.6%) [a]		$0.160\ m^{2/3}$ (±5.0%) [c]
mean chord, $\bar{c}$ (m)	$0.121\ m^{1/3}$ (±9.6%) [a]		$0.146\ m^{1/3}$ (±5.2%) [d]
wing aspect ratio, AR	8.15 (±10%) [a]		7.55 (±5.7%) [d]
mean wing loading, m/S_{wing} (kg/m^2)	$9.02\ m^{1/3}$ (±5.3%) [e]		$7.73\ m^{1/3}$ (±6.5%) [c]
best-range airspeed, $V_{\text{max-}\mathcal{R}}$ (m/s)	$22.7\ m^{1/6}$ (±8.0%) [a] $2.70\ (W/S_{\text{wing}})^{1/2}$ (±4.9%) [e]	236 (±2.8%) [f]	$16.0\ m^{0.13}$ (±4.5%) [g] $4.7\ (W/S_{\text{wing}})^{0.28}$ (±2.9%) [g]
Reynolds number, $Re_{\text{max-}\mathcal{R}} = V_{\text{max-}\mathcal{R}}\bar{c}/\nu$	$194 \times 10^3\ m^{1/2}$ (±7.6%) [a]	$315 \times 10^3\ m^{1/2}$ (±5.9%) [a]	$157 \times 10^3\ m^{0.463}$ (±4.6%) [h]
best-range power, $P_{\text{max-}\mathcal{R}}$ (W)	$24.0\ m^{7/6}$ (±9.4%) [a]		$17.7\ m^{7/6}$ (±18%) [a]
maximum flight efficiency, $\eta_{\text{flight,max}}$	11.9 (±11%) [a]		$11\ m^{-0.037}$ (±22%) [d]
supplied power, P_{supp} (W)	$69.3\ m^{1.13}$ (±7.2%) [a]	$1190\ m^{0.977}$ (±7.9%) [e]	$31\ m^{0.9675}$ (±16%) [a]
supplied thrust, T_{supp} (N)	$5.28\ m^{0.884}$ (±18%) [e]	$8.93\ m^{0.924}$ (±3.2%) [e]	N/A

[a] Derived by Liu [19].
[b] Derived by Templin [28].
[c] Obtained through least-squares fitting of data provided by Liu, Alerstam *et al.* [22], and Chatterjee *et al.* [23].
[d] Based on other scaling laws (using definitions given in Tables 1–5); error estimated by propagation [37].
[e] Obtained through least-squares fitting of data provided by Liu.
[f] Obtained by averaging the data provided by Liu.
[g] Derived by Alerstam *et al.*
[h] Obtained through least-squares fitting of the data provided by Alerstam *et al.*

replaced with a newly derived expression for $Re_{\max\text{-}\mathcal{R}}$ based on the relation for $V_{\max\text{-}\mathcal{R}}$ given by Alerstam *et al.* and the scaling law for mean wing chord, $\bar{c}$, derived here; and Liu's scaling law for maximum flight efficiency, $\eta_{\text{flight,max}}$, was replaced with a newly derived expression based on the relation for $V_{\max\text{-}\mathcal{R}}$ given by Alerstam *et al.* and those for $W_{\max\text{-T/O}}$ and $P_{\max\text{-}\mathcal{R}}$ given by Liu. The substitutions were made because the extensive experimental data used by Alerstam *et al.* is likely to be significantly more accurate than that from many other sources, as all bird species were evaluated in cruising, migratory flight, rather than under laboratory conditions (*e.g.* in wind tunnels). The relation for $V_{\max\text{-}\mathcal{R}}$ as a function of W/S_{wing} given by Alerstam *et al.* is also presented in Table C.1.

The scaling laws and empirically based best-fit power laws for the various aircraft parameters are presented in Table C.2 as functions of $W_{\max\text{-T/O}}$. In several cases, new best-fit power laws for the data for manned aircraft provided by Liu were derived to obtain these relations; while in others (where noted), the scaling laws given in Table C.1 were re-cast from dependence on m to dependence on $m_{\max\text{-T/O}}$ by use of the relation between W and $W_{\max\text{-T/O}}$ given by Liu: $W_{\max\text{-T/O}} = 1.282\,W$, which implies that $m_{\max\text{-T/O}} = 1.282\,m$. This was done when the data needed to fit a given parameter as a function of $m_{\max\text{-T/O}}$ was unavailable. The scaling laws for birds presented in Table C.1 were re-cast in terms of $m_{\max}$ by use of a similar relation derived by Liu for birds: $W_{\max} = 1.242\,W$ (or $m_{\max} = 1.242\,m$). Re-casting was necessary because the biometric data for birds was given by Tennekes [21], Alerstam *et al.* [22], and Chatterjee *et al.* [23] as a function of m alone.

Table C.2 Scaling laws and empirical best-fit power laws for manned aircraft and birds that permit the characteristics of a flyer to be estimated given its maximum mass ($m_{\text{max-T/O}}$ or m_{max} (kg) for aircraft or birds, respectively). The scaling laws for aircraft were obtained by fitting the data provided by Liu [19] or (when insufficient data were available) by re-casting Liu's scaling laws from dependence on m to dependence on $m_{\text{max-T/O}}$. The scaling laws for birds were obtained by re-casting those given in Table C.1 in terms of m_{max}. Listed in parentheses with each entry is the relative uncertainty at 90% CFL.

parameter	manned propeller-driven aircraft	manned turbofan-powered aircraft	birds
length, l_{total} (m)	$0.814\ m_{\text{max-T/O}}^{1/3}$ (±3.0%) [a]		$0.285\ m_{\text{max}}^{1/3}$ (N/A) [b]
maximum fuselage width, d_{fuse} (m)	$0.0948\ m_{\text{max-T/O}}^{1/3}$ (±3.4%) [b]		N/A
wingspan, b (m)	$0.924\ m_{\text{max-T/O}}^{1/3}$ (±3.8%) [a]		$1.02\ m_{\text{max}}^{1/3}$ (±2.6%) [b]
wing area, S_{wing} (m^2)	$0.103\ m_{\text{max-T/O}}^{2/3}$ (±7.7%) [a]		$0.139\ m_{\text{max}}^{2/3}$ (±5.1%) [b]
mean chord, $\bar{c}$ (m)	$0.112\ m_{\text{max-T/O}}^{1/3}$ (±8.9%) [c]		$0.136\ m_{\text{max}}^{1/3}$ (±5.0%) [c]
wing aspect ratio, AR	8.29 (±10%) [c]		7.55 (±5.7%) [c]
max wing loading, $W_{\text{max}}/S_{\text{wing}}$ (N/m^2)	$109\ m_{\text{max-T/O}}^{1/3}$ (±5.3%) [a]		$81.6\ m_{\text{max}}^{1/3}$ (±7.4%) [b]
best-range airspeed, $V_{\text{max-}\mathcal{R}}$ (m/s)	$22.7\ m_{\text{max-T/O}}^{1/6}$ (±7.7%) [a] $3.53\ (W_{\text{max-T/O}}/S_{\text{wing}})^{1/2}$ (±5.2%) [a]	236 (±2.8%) [d]	$15.6\ m_{\text{max}}^{0.13}$ (±4.5%) [b] $8.4\ (W_{\text{max}}/S_{\text{wing}})^{0.28}$ (±3.5%) [b]
Reynolds number, $Re_{\text{max-}\mathcal{R}} = V_{\text{max-}\mathcal{R}}\bar{c}/\nu$	$184\times10^3\ m_{\text{max-T/O}}^{1/2}$ (±7.1%) [a]	$272\times10^3\ m_{\text{max-T/O}}^{1/2}$ (±6.2%) [a]	$142\times10^3\ m_{\text{max}}^{0.463}$ (±4.7%) [b]
best-range power, $P_{\text{max-}\mathcal{R}}$ (W)	$21.0\ m_{\text{max-T/O}}^{7/6}$ (±10%) [a]		$13.7\ m_{\text{max}}^{7/6}$ (±19%) [b]
maximum flight efficiency, $\eta_{\text{flight,max}}$	10.6 (±12%) [c]		$11\ m_{\text{max}}^{-0.037}$ (±22%) [c]
supplied power, P_{supp} (W)	$40.4\ m_{\text{max-T/O}}^{1.16}$ (±8.3%) [a]	$1910\ m_{\text{max-T/O}}^{0.924}$ (±4.6%) [a]	$25\ m_{\text{max}}^{0.9675}$ (±17%) [b]
supplied thrust, T_{supp} (N)	$3.97\ m_{\text{max-T/O}}^{0.896}$ (±18%) [a]	$8.62\ m_{\text{max-T/O}}^{0.906}$ (±3.2%) [a]	N/A

[a] Obtained through least-squares fitting of data provided by Liu [19].
[b] Obtained by re-casting the scaling law given in Table C.1 by use of Liu's relations: $W_{\text{max-T/O}} = 1.282\ W$ (±12%) for aircraft and $W_{\text{max}} = 1.242\ W$ (±9%) for birds; error estimated by propagation [37].
[c] Based on other scaling laws (using definitions given in Tables 1–5); error estimated by propagation [37].
[d] Obtained by averaging the data provided by Liu [19].

DISTRIBUTION LIST

Assembly and Initial Analysis of a Database of the Characteristics of Fixed-Wing Unmanned Aircraft Systems

Jennifer L Palmer

AUSTRALIA

DEFENCE ORGANISATION	**No. of copies**
Task Sponsor	
Dr Ken Anderson, Chief of Aerospace Division	1
S&T Program	
Chief, Projects and Requirements Division DG Science Strategy and Policy	Doc Data Sht & Exec Summary (Shared)
Counsellor Defence Science, London	Doc Data Sheet
Counsellor Defence Science, Washington	Doc Data Sheet
Scientific Adviser Intelligence and Information	1
Navy Scientific Adviser	1
Scientific Adviser – Army	1
Air Force Scientific Adviser	1
Scientific Adviser – VCDF	Doc Data Sht & Dist List
Scientific Adviser – CJOPS	Doc Data Sht & Dist List
Scientific Adviser – Strategy	Doc Data Sht & Dist List
Dr Alex Zelinsky, Chief Defence Scientist	Doc Data Sht & Dist List
Dr Ian Sare, Deputy Chief Defence Scientist Platform and Human Systems	Doc Data Sht & Exec Summary
Mr Jan Drobik, Research Leader, Aerospace Division	Doc Data Sht & Dist List
Dr Lynn Booth, Research Leader, Aerospace Division	Doc Data Sht & Dist List
Dr Simon Ng, Group Leader, Aerospace Division	1
Mr David Holmes, Group Leader, Aerospace Division	1
Dr Michael Skinner, Acting Group Leader, Aerospace Division	1
Dr Jennifer Palmer, Aerospace Division	1
Mr Geoff Brian, Aerospace Division	1
Mr Kent Rosser, Aerospace Division	1
Dr John Wharington, Maritime Division	1

Dr Karl Pavey, Land Division	1
Dr Malcolm Alderton, Land Division	1
Dr Jason Scholz, Joint Operations and Analysis Division	1
Mr Phillip Gowlett, Joint Operations and Analysis Division	1

DSTO Library and Archives

Library Fishermans Bend	1 Printed
Library Edinburgh	1 Printed
Library, Sydney	Doc Data Sheet
Library Canberra	Doc Data Sheet

Capability Development Group

Director General Maritime Development	Doc Data Sheet
Director NCW Development	Doc Data Sheet
Assistant Secretary Investment Analysis	Doc Data Sheet
RPDE Liaison Officer	Doc Data Sht & Exec Summary & Dist List
Dr Peter Maguire, Director Emerging and Integrated Systems, Lead–Unmanned Aerial Systems Planning Team	1

Chief Information Officer Group

DICTF	Doc Data Sheet

Strategy Executive

Policy Officer, Counter-Terrorism and Domestic Security	Doc Data Sheet

Vice Chief of the Defence Force Group

Director, Chemical, Biological, Radiological and Nuclear	1
SO (Science) – Counter Improvised Explosive Device Task Force	Doc Data Sht & Exec Summary & Dist List

Joint Logistics Command

Directorate of Ordnance Safety	1
Head Engineering Systems	
Director General Strategic Logistics	Doc Data Sheet

Military Strategic Commitments

Director General Military Strategic Commitments	Doc Data Sheet

Navy

Australian Maritime Warfare Centre	Doc Data Sht & Dist List
CAPT Peter Scott – Commander , AMWC	
Mr Kenneth James – Deputy Director AMWC	
Director General Navy Capability Plans & Engagement	Doc Data Sheet
Director General Navy Communications & Information Warfare	Doc Data Sheet
Director General Navy Certification and Safety	Doc Data Sheet
Director General Submarine Capability Management	Doc Data Sheet
Director General Technical Seaworthiness	Doc Data Sheet

Australian Hydrographer	Doc Data Sheet
Director General Logistics – Navy	Doc Data Sheet
Head Navy Engineering	Doc Data Sheet
Commodore Training	Doc Data Sheet
Commander Surface Force	Doc Data Sheet
Commander Mine Warfare, Hydrographic, and Patrol Force	Doc Data Sheet
Commander Fleet Air Arm	Doc Data Sheet
Commander Submarine Force	Doc Data Sheet
Commodore War	Doc Data Sheet
Commodore Support	Doc Data Sheet
SO Science Fleet Headquarters	1

Army

Australian National Coordination Officer ABCA (AS NCO ABCA), Land Warfare Development Centre, Puckapunyal	Doc Data Sheet
SO(Science) Forces Command	1
Director Special Operations Science and Technology	Doc Data Sht & Exec Summary & Dist List
SO(Science) 1st Division	Doc Data Sheet
SO2 S&T FDG LWDC – (Staff Officer for Science and Technology, Force Development Group)	Doc Data Sheet
SO(Science) 1Bde	Doc Data Sheet
SO(Science) 3Bde	Doc Data Sheet
SO(Science) 17 CSS Bde	Doc Data Sheet
J86 (TCS GROUP), DJFHQ	Doc Data Sheet
LT COL Nathan Loynes, Commander – 20th Surveillance and Target Acquisition Regiment	Doc Data Sheet
MAJ Keirin Joyce, JP129 (Tactical UAV) Capability Implementation Team	Doc Data Sheet

Air Force

SO (Science) – Headquarters Air Combat Group, RAAF Base, Williamtown NSW 2314	Doc Data Sht & Exec Summary
Staff Officer Science Surveillance and Response Group	Doc Data Sht & Exec Summary
SO (Science) Combat Support Group	Doc Data Sht & Exec Summary
Staff Officer Science HQ Air Lift Group	Doc Data Sht, Exec Summary & Dist List
GPCAPT Alan Clements, Director of Defence Aviation and Air Force Safety (DDAAFS)	1

Australian Defence Simulation Office

Dr Mike Brennan, Director General – Simulation	1

Intelligence and Security Group

AS Transnational and Scientific Intelligence, DIO	Doc Data Sheet
Manager, Information Centre, Defence Intelligence Organisation	1

Director Advanced Capabilities, DIGO	Doc Data Sheet

Defence Materiel Organisation

CoS GM Systems	Doc Data Sheet
Program Manager Air Warfare Destroyer	Doc Data Sheet
Guided Weapon & Explosive Ordnance Branch (GWEO)	Doc Data Sheet
Director Engineering Operations; Land Engineering Agency (Michael Yates)	Doc Data Sheet
CSIO	Doc Data Sheet
Deputy Director Joint Fuel & Lubricants Agency	Doc Data Sheet
Systems Engineering Manager	Doc Data Sheet
CBRNE Program Office, Land Systems Division	

OTHER ORGANISATIONS

National Library of Australia	1
NASA (Canberra)	1

UNIVERSITIES AND COLLEGES

Australian Defence Force Academy

Library	1
Head of Aerospace and Mechanical Engineering	1
Hargrave Library, Monash University	Doc Data Sheet

OUTSIDE AUSTRALIA

INTERNATIONAL DEFENCE INFORMATION CENTRES

US Defense Technical Information Center	1
UK Dstl Knowledge Services	1
Canada Defence Research Directorate R&D Knowledge & Information Management (DRDKIM)	1
NZ Defence Information Centre	1

ABSTRACTING AND INFORMATION ORGANISATIONS

Library, Chemical Abstracts Reference Service	1
Engineering Societies Library, US	1
Materials Information, Cambridge Scientific Abstracts, US	1
Documents Librarian, The Center for Research Libraries, US	1
International Technology and Science Center (ITSC) Library	1

INFORMATION EXCHANGE AGREEMENT PARTNERS

National Aerospace Laboratory, Japan	1
National Aerospace Laboratory, Netherlands	1

Total number of copies: **PDF: 41**

DEFENCE SCIENCE AND TECHNOLOGY ORGANISATION
DOCUMENT CONTROL DATA

1. PRIVACY MARKING/CAVEAT (OF DOCUMENT)
Public Release

2. TITLE

Assembly and Initial Analysis of a Database of the Characteristics of Unmanned Aircraft Systems

3. SECURITY CLASSIFICATION (FOR UNCLASSIFIED REPORTS THAT ARE LIMITED RELEASE USE (L) NEXT TO DOCUMENT CLASSIFICATION)

Document	(U)
Title	(U)
Abstract	(U)

4. AUTHOR(S)

Jennifer L Palmer

5. CORPORATE AUTHOR

DSTO Defence Science and Technology Organisation
506 Lorimer St
Fishermans Bend Victoria 3207 Australia

6a. DSTO NUMBER	6b. AR NUMBER	6c. TYPE OF REPORT	7. DOCUMENT DATE
DSTO-TR-2952	AR-015-904	Technical Report	November 2014

8. FILE NUMBER	9. TASK NUMBER	10. TASK SPONSOR	11. NO. OF PAGES	12. NO. OF REFERENCES
2008/1096712/1	07/250	Chief, Aerospace Division	79	63

13. DSTO Publications Repository

http://dspace.dsto.defence.gov.au/dspace/

14. RELEASE AUTHORITY

Chief, Aerospace Division

15. SECONDARY RELEASE STATEMENT OF THIS DOCUMENT

Approved for public release

OVERSEAS ENQUIRIES OUTSIDE STATED LIMITATIONS SHOULD BE REFERRED THROUGH DOCUMENT EXCHANGE, PO BOX 1500, EDINBURGH, SA 5111

16. DELIBERATE ANNOUNCEMENT

No Limitations

17. CITATION IN OTHER DOCUMENTS Yes

18. DSTO RESEARCH LIBRARY THESAURUS

Unmanned aircraft, UAV, UAS, Performance, Characteristics, Database

19. ABSTRACT

The *DSTO UAS Database* contains geometric, aerodynamic, and performance data for nearly nine hundred semi-autonomous and remotely piloted unmanned aircraft systems (UAS) utilising fixed-wing unmanned aerial vehicles (UAVs). The *Database* has been created using information from a variety of public sources and is intended to serve as a repository and as a source of data for analysis of the various systems. Here, the characteristics of fixed-wing UAVs are examined as functions of their weight. Where appropriate, fixed-wing UAVs are compared with manned aircraft and birds to provide the reader with an overview of the contents of the *Database* and to indicate some of its possible uses. Other demonstrated applications include historical analyses. The *Database* has recently been converted from its original Microsoft Excel® spreadsheet format to a structured database format to make it more widely available to and searchable by potential users. Periodic maintenance, further validation of the data, and on-going additions are planned.